การสังเคราะห์และสมบัติของอะคริโลไนไทรล์-บิวทาไดอีน-สไตรีนโคพอลิเมอร์ที่มีอนุภาคนาโนซิลิกา

นายจรุงกิจ ใจแก้ว



วิทยานิพนธ์นี้เป็นส่วนหนึ่งของการศึกษาตามหลักสูตรปริญญาวิทยาศาสตรดุษฎีบัณฑิต
สาขาวิชาวัสดุศาสตร์ ภาควิชาวัสดุศาสตร์
คณะวิทยาศาสตร์ จุฬาลงกรณ์มหาวิทยาลัย
ปีการศึกษา 2560

# SYNTHESIS AND PROPERTIES OF ACRYLONITRILE-BUTADIENE-STYRENE COPOLYMER CONTAINING SILICA NANOPARTICLES

Mr. Charungkit Chaikaew



A Dissertation Submitted in Partial Fulfillment of the Requirements
for the Degree of Doctor of Philosophy Program in Materials Science
Department of Materials Science
Faculty of Science
Chulalongkorn University
Academic Year 2017

| | |
|---|---|
| Thesis Title | SYNTHESIS AND PROPERTIES OF ACRYLONITRILE-BUTADIENE-STYRENE COPOLYMER CONTAINING SILICA NANOPARTICLES |
| By | Mr. Charungkit Chaikaew |
| Field of Study | Materials Science |
| Thesis Advisor | Associate Professor Kawee Srikulkit, Ph.D. |

Accepted by the Faculty of Science, Chulalongkorn University in Partial Fulfillment of the Requirements for the Doctoral Degree

.....Dean of the Faculty of Science

(Associate Professor Polkit Sangvanich, Ph.D.)

THESIS COMMITTEE

.....Chairman

(Assistant Professor Dujreutai Pongkao Kashima, Ph.D.)

.....Thesis Advisor

(Associate Professor Kawee Srikulkit, Ph.D.)

.....Examiner

(Associate Professor Pranut Potiyaraj, Ph.D.)



.....Examiner

(Assistant Professor Kanoktip Boonkerd, Ph.D.)

.....External Examiner

(Associate Professor Pranee Phinyocheep, Ph.D.)

จรุงกิจ ใจแก้ว : การสังเคราะห์และสมบัติของอะคริโลไนไทรล์-บิวทาไดอีน-สไตรีนโคพอลิเมอร์ที่มีอนุภาคนาโนซิลิกา (SYNTHESIS AND PROPERTIES OF ACRYLONITRILE-BUTADIENE-STYRENE COPOLYMER CONTAINING SILICA NANOPARTICLES) อ.ที่ปรึกษาวิทยานิพนธ์หลัก: รศ. ดร. กาวี ศรีกูลกิจ, 129 หน้า.

งานวิจัยนี้มีจุดประสงค์เพื่อพัฒนาอะคริโลไนไทรล์ บิวตะไดอีน สไตรีนคอมพอสิตที่เสริมแรงด้วยอนุภาคนาโนซิลิกาโดยเทคนิคการสังเคราะห์ที่เกิดขึ้นภายในแหล่งกำเนิด (in-situ) ของอนุภาคยางอะคริโลไนไทรล์ บิวตะไดอีน สไตรีนซึ่งประกอบด้วยอนุภาคนาโนของซิลิกาที่มีโครงสร้างแบบไม่ชอบน้ำ ขั้นแรกทำการดัดแปรอนุภาคนาโนซิลิกาด้วยเฮกซะเดซิลไตรเมทอกซีไซเลน (HDTMS-Silica) ด้วยอัตราส่วนเฮกซะเดซิลไตรเมทอกซีไซเลนต่ออนุภาคนาโนซิลิกา หนึ่งต่อหนึ่ง (HDTMS-silica1) สองต่อหนึ่ง (HDTMS-silica2) และสามต่อหนึ่ง (HDTMS-silica3) ในระบบอิมัลชันด้วยกระบวนการไซเลนไนเซชั่น จากนั้นจึงเติมสารผสมระหว่างอนุภาคนาโนซิลิกาที่ดัดแปรด้วยเฮกซะเดซิลไตรเมทอกซีไซเลนในสไตรีนมอนอเมอร์และอะคริโลไนไทรล์มอนอเมอร์ลงในพอลิบิวทาไดอีนเลเท็กซ์และเติมสารริเริ่มปฏิกิริยาที่อุณหภูมิ 65°C เป็นเวลา 3.5 ชั่วโมง จะทำให้เกิดพอลิเมอร์ร่วมแบบต่อกิ่งขึ้นจากนั้นจึงทำการเตรียมวัสดุเชิงประกอบอนุภาคนาโนอะคริโลไนไทรล์ บิวตะไดอีน สไตรีนคอมพาวนด์ด้วยการหลอมเหลวยางอะคริโลไนไทรล์ บิวตะไดอีน สไตรีนที่ประกอบด้วยอนุภาคนาโนซิลิกาที่ดัดแปรด้วยเฮกซะเดซิลไตรเมทอกซีไซเลนเข้ากับสไตรีน อะคริโลไนไทรล์โคพอลิเมอร์ จากการทดสอบคุณสมบัติเชิงกลของวัสดุเชิงประกอบอนุภาคอนุภาคนาโนอะคริโลไนไทรล์ บิวตะไดอีน สไตรีนคอมพาวด์ โดยพบว่าอนุภาคนาโนซิลิกาที่ถูกดัดแปรด้วยเฮกซะเดซิลไตรเมทอกซีไซเลนสามารถแสดงคุณสมบัติความไม่ชอบน้ำและกระจายตัวในโทลูอีนได้เป็นอย่างดีในทุกๆอัตราส่วนการผสมระหว่างเฮกซะเดซิลไตรเมทอกซีไซเลนและอนุภาคนาโนซิลิกา และจากการสังเกตุปรากฏของแถบที่เกิดจากการดูดกลืนแสงของซิลานอลสามารถบอกได้ว่าอนุภาคนาโนซิลิกาที่ถูกดัดแปรด้วยเฮกซะเดซิลไตรเมทอกซีไซเลนในอัตราส่วนสามต่อหนึ่งเป็นอัตราส่วนที่แสดงคุณสมบัติความไม่ชอบน้ำได้สมบูรณ์ที่สุด อย่างไรก็ตามคุณสมบัติเชิงกลจะเกิดขึ้นได้ดีที่สุดของอนุภาคนาโนซิลิกาที่ถูกดัดแปรด้วยเฮกซะเดซิลไตรเมทอกซีไซเลนในอัตราส่วนสองต่อหนึ่ง ในปริมาณ 2 เปอร์เซ็นต์โดยน้ำหนักเนื่องจากในอัตราส่วนของอนุภาคนาโนซิลิกาที่ถูกดัดแปรด้วยเฮกซะเดซิลไตรเมทอกซีไซเลนเฮกซะเดซิลไตรเมทอกซีไซเลนที่ต่ำกว่าสองต่อหนึ่งจะทำให้เฮกซะเดซิลไตรเมทอกซีไซเลนไม่เพียงพอที่จะทำให้คุณสมบัติความไม่ชอบน้ำเกิดขึ้นได้อย่างเต็มที่ และในอัตราส่วนที่มากกว่านี้ปริมาณเฮกซะเดซิลไตรเมทอกซีไซเลนที่มากเกินจะทำให้ปริมาณของอนุภาคนาโนซิลิกาลดลง สังเกตุได้จากการดูดกลืนพลังงานและสมบัติด้านการเสริมแรงลดลง อัตราส่วนของอนุภาคนาโนซิลิกาที่ถูกดัดแปรด้วยเฮกซะเดซิลไตรเมทอกซีไซเลนที่เหมาะสมที่สุดที่ทำให้เกิดคุณสมบัติเชิงกลที่ดีที่สุดคือที่อัตราส่วนสองต่อหนึ่งในปริมาณ 2 เปอร์เซ็นต์โดยน้ำหนัก และในปริมาณของอนุภาคนาโนซิลิการที่ถูกดัดแปรด้วยเฮกซะเดซิลไตรเมทอกซีไซเลนที่มากกว่า 2 เปอร์เซ็นต์โดยน้ำหนักจะส่งผลในทางตรงกันข้ามเนื่องจากการรวมตัวกันของอนุภาคนาโนซิลิกา

ภาควิชา วัสดุศาสตร์ ลายมือชื่อนิสิต .....

สาขาวิชา วัสดุศาสตร์ ลายมือชื่อ อ.ที่ปรึกษาหลัก .....

ปีการศึกษา 2560

# # 5572804023 : MAJOR MATERIALS SCIENCE

KEYWORDS: IN SITU SYNTHESIS / ABS/HYDROPHOBIC SILICA NANOCOMPOSITE

CHARUNGKIT CHAIKAEW: SYNTHESIS AND PROPERTIES OF ACRYLONITRILE-BUTADIENE-STYRENE COPOLYMER CONTAINING SILICA NANOPARTICLES. ADVISOR: ASSOC. PROF. KAWEE SRIKULKIT, Ph.D., 129 pp.

The aim of this research is to develope acrylonitrile butadiene styrene composite reinforced with hydrophobic silica nanoparticles. In this study, in-situ synthesis of ABS rubber particles containing hydrophobic silica nanoparticles (HDTMS-silica) was carried out. Firstly, three of HDTMS-silicas (HDTMS-silica1, HDTMS-silica2, and HDTMS-silica3) were prepared by silanization of $SiO_2$ nanoparticle with hexadecyltrimethoxysilane (HDTMS : $SiO_2$ wt ratios of 1 : 1, 2 : 1, and 3 : 1) in an emulsion system. Then, HDTMS-silica/styrene and acrylonitrile mixture was fed into a polybutadiene latex reactor. Following that, graft copolymerization was carried out using persulfate initiator at temperature of 65 oC for 3.5 h. Thus obtained ABS rubber containing HDTMS-silica was melt extruded with styrene-acrylonitrile (SAN) to prepare ABS nanocomposite compound. Mechanical properties of ABS nanocomposite compounds were evaluated. It was found that all of HDTMS : $SiO_2$ wt ratios produced hydrophobic $SiO_2$ nanoparticles exhibiting good dispersibility in toluene test. In fact, 3 :1 HDTMS : $SiO_2$ showed the complete hydrophobicity modification, judged by the absence of silanol absorption band. However, the optimum mechanical properties were achieved at 2 wt% loading of 2 : 1 HDTMS : $SiO_2$. Below 2 : 1 ratio, the HDTMS ratio was not enough to obtain the fully hydrophobic surface modification. Above 2: 1 ratio, the excessive HDTMS ratio led to a decrease in $SiO_2$ content judged by Si EDX mapping, causing a gradual decrease in its energy absorption and reinforcement performance. In case of 2 : 1 HDTMS : $SiO_2$, optimum mechanical properties were achievable at 2 wt% HDTMS-$SiO_2$ loading, resulting from the optimum dispersibility of HDTMS-SiO2 nanoparticles. Further increase in HDTMS-$SiO_2$ loading resulted in a reverse effect due to agglomeration problem.



Department: Materials Science Student's Signature .....

Field of Study: Materials Science Advisor's Signature .....

Academic Year: 2017

# ACKNOWLEDGEMENTS

I would like to express my gratitude to my thesis advisor, Associate Professor Kawee Srikulkit, Ph.D., for his encouraging guidance, supervision and helpful suggestion throughout this research as well as his tireless reviews and corrections of the thesis writing. In addition, I am also grateful to thank my thesis committee sincerely, Assistant Professor Dujreutai Pongkao Kashima, Ph.D., the chairman of thesis committee for her valuable advice, and also would like to express my appreciation to the thesis committee members, Associate Professor Pranut Potiyaraj, Ph.D., Assistant Professor Kanoktip Boonkerd, Ph.D. and Associate Professor Pranee Phinyocheep, Ph.D., for the detailed review, invaluable suggestion, constructive criticism and excellence guidance.

I would like to thank and acknowledge Thailand Research Fund (RRi, grant No.-PHD56I0033) for financial support.

Besides, I am also thanks for the research materials support from IRPC Public Company. Many thanks are going to Mr. Phayom Boonyoung and Mr. Ronnapa Phonthong for their assistance during the period of this research.

Thanks are going towards my friends whose names are not mentioned here but and contributed their assistance, suggestion, advice concerning the experimental techniques and the encouragement during the period of this work.

Finally, I would like to express a deep sense of gratitude to my mother and my parents who always stand by my side and believe in me. I owe my life for their constant love, encouragement, supports and blessing.

**CONTENTS**

Page

Page

Page

Page

Page

Page

# LIST OF TABLES

# LIST OF FIGURES

# CHAPTER I
# INTRODUCTION

## 1.1 Purpose of investigation

Acrylonitrile-butadiene-styrene (ABS) is a copolymer exhibiting an effective capability of toughness and dimensional stability due to the fact that ABS particle behaves like a rubber which acts as an impact strength modifier [1]. Industrially, ABS is produced by graft copolymerization of acrylonitrile and styrene onto polybutadiene backbone. The nitrile groups from neighboring chains attract each other by polar force and bind the chains together, rendering ABS strong while the polybutadiene elastomeric component provides resilience [2-4]. In industrial application, ABS rubber is compounded with styrene-acrylonitrile copolymer (SAN), hence providing impact resistance and toughness. These properties could further be enhanced by the addition of nanosized particles including silica nanoparticles, naming nanocomposite materials [5].

Nanocomposites are promising materials due to their superior properties including mechanical properties. Well dispersed nanoparticles play an important role in absorbing and then transferring energy to other nanoparticles in their vicinity [6-18]. However, the most difficult task of nanocomposite preparation is how to achieve the optimum dispersibility of nanoparticles in an ABS rubber particle.

In this research, ABS rubber particles containing nanosized silica particles were in-situ synthesized. Firstly, hydrophobicity surface modification of colloidal silica nanoparticles (commercial silica colloid) was carried out in an emulsion system [19-26]. Thus obtained hydrophobic nanosilica powder was well dispersed in styrene monomer prior to graft copolymerization. Then, ABS rubber particles containing nanosized silica were compounded with styrene-acrylonitrile (SAN) to prepare ABS/silica nanocomposite. Mechanical properties of ABS/silica nanocomposite including impact strength, tensile properties, and flexural strength were evaluated.

In addition, effects of ABS rubber on properties improvement of poly(lactic acid), PLA, were investigated. Poly(lactic acid)/ABS-*g*-MAA blends were prepared using an internal mixer. Then, mechanical properties of PLA/ABS-*g*-MAA including impact strength, tensile properties, and flexural strength were evaluated.

**1.2 Research objectives**

The main purpose of this study is to focus on the preparation of ABS/silica nanocomposites. Morphological behavior, impact strength, tensile properties, flexural strength, and thermal properties of the resulting ABS/silica nanocomposites are investigated. In part II, effects of ABS rubber on properties improvement of poly(lactic acid), PLA, were investigated.

**1.3 Scope of the research**

The scope of this research work is divided into two parts as follows:

**Part I: synthesis of ABS rubber containing $SiO_2$ nanoparticle and properties investigation of ABS containing $SiO_2$ nanoparticle**

1. Literature survey and in-depth study of this research work.

2. Synthesis of hydrophobic silica nanoparticle (HDTMS-silica) ratios HDTMS:silica (1:1, 2:1 and 3:1) using high speed homogenizer.

3. In-situ preparation of styrene/HDTMS-silica dispersion at various HDTMS-silica (0.5, 1, 2, 3, 4 and 5 wt%) using high speed homogenizer.

4. In-situ synthesis of ABS/HDTMS-silica nanocomposite using 20L reactor.

5. Preparation of ABS/HDTMS-silica nanocomposite compound.

6. Measurement of particle size distribution of HDTMS-silicas using particle size analyzer.

7. Evaluation of thermal stability of HDTMS-silicas using TA instrument.

8. Observation of the morphological structures of the HDTMS-silicas using transmission electron microscopic (TEM) technique.

9. Investigation of FT-IR spectra to the functional group of HDTMS-silicas.

10. Observation of the morphological structure of the ABS/HDTMS-silica nanocomposites using scanning electron microscopic (SEM-EDS) technique.

11. Evaluation of thermal stability of ABS/HDTMS-silica nanocomposites using TA instrument.

12. Measurement of tensile properties, flexural strength, and izod impact strength of the ABS/HDTMS-silica nanocomposites.

13. Synthesis of $SiO_2$ nanoparticles by precipitation technique.

14. In-situ preparation of styrene/HDTMS-$SiO_2$ dispersion at various HDTMS-$SiO_2$ (0.5, 1, 2, 3, 4 and 5 wt%) using high speed homogenizer.

15. In-situ synthesis of ABS/HDTMS-$SiO_2$ nanocomposite using 20L reactor.

16. Preparation of ABS/HDTMS-$SiO_2$ nanocomposite compound.

17. Observation of the morphological structure of the ABS/HDTMS-$SiO_2$ nanocomposites using Transmission electron microscopic (TEM) technique.

18. Measurement of izod impact strength of the ABS/HDTMS-$SiO_2$ nanocomposites.

**Part II: Preparation of PLA/ABS-*g*-MAA and PLA/ABS$^{Si}$-*g*-MAA blends and properties investigation**

1. Literature survey and in-depth study of this research work.

2. Synthesis of PMAA-*g*-ABS rubber at various MAA content (10 and 20 wt%) using 20L reactor.

3. Preparation of PLA/ABS-*g*-MAA and PLA/ABS$^{Si}$-*g*-MAA blends at blend ratio 90/10, 80/20 and 70/30 using an internal mixer.

4. Measurement of izod impact strength, tensile properties and percent elongation of the blends.

5. Evaluation of thermal properties of the blends using differential scanning calorimetry (DSC).

6. Measurement of heat distortion temperature (HDT) for evaluate the thermal properties.

7. Observation of the morphological structures of the PLA/ABS-*g*-MAA blends using scanning electron microscopic (SEM) technique.

# CHAPTER II

# THEORY AND LITERATURE REVIEWS

## 2.1 Acrylonitrile Butadiene Styrene terpolymer (ABS)

ABS (acrylonitrile-butadiene-styrene) terpolymer are elastomeric and thermoplastic composites, which exhibit excellent toughness and good dimensional stability. The elastomeric component, usually polybutadiene, exists as a discrete phase dispersed in the thermoplastic component, a copolymer of styrene and acrylonitrile (SAN). In industrial, ABS is a synthetic rubber made by graft copolymerization of acrylonitrile and styrene onto polybutadiene. The nitrile groups from neighboring chains, being polar, attract each other and bind the chains together, making ABS rubber stronger than pure polystyrene. ABS has become the largest selling engineering thermoplastic because of its broad properties balance and the processing options. The range of properties typically available for ABS is illustrated in Table 2.1.

Table 2.1 Properties of ABS and related products

| Properties | ASTM method | Units | Low impact | High impact | Heat resistant | Flame retardant | Plating |
|---|---|---|---|---|---|---|---|
| Izod impact | D256 | J/m | 105-215 | 375-440 | 120-320 | 185-280 | 265-375 |
| Tensile strength | D638 | Mpa | 41-52 | 33-44 | 41-52 | 40-50 | 38-40 |
| Tensile elongation | D638 | % | 5-30 | 15-70 | 5-20 | 5-25 | 10-30 |
| Flexural modulus | D790 | Gpa | 2.3-2.6 | 1.8-2.2 | 2.1-2.8 | 2.3-2.8 | 2.3-2.7 |
| Rockwell hardness | D785 | R | 105-110 | 88-100 | 100-112 | 97-111 | 103-110 |
| Heat deflection temperature | D648 | ℃ | 94-100 | 98-104 | 105-121 | 90-107 | 95-100 |



All properties cannot be maximized simultaneously, thus each grade is designed to meet specific product requirements from customer.

2.1.1 Polymerization of ABS

The development of ABS products were based on the physical blend of ungrafted polybutadiene with a copolymer of styrene and acrylonitrile. Incompatibility between the ungrafted polybutadiene and the glassy matrix limits the effectiveness of polybutadiene as an impact modifier because of the formation of large nonuniformly dispersed aggregates of the rubber and the reduction of adhesion of rubber particles to the matrix during fracture. The use of acrylonitrile-butadiene copolymer that increase compatibility with the matrix adversely effects hear distortion hardness, and tensile properties. On the other hand, the compatibility achieved by grafting a styrene and acrylonitrile copolymer onto the rubber particles provides optimal impact properties with minimal adverse effects on heat distortion, hardness and tensile strength. Therefore, most commercially significant ABS products are now comprised of grafted rubber dispersed in a glassy matrix of styrene-acrylonitrile copolymer.

*2.1.1.1 The mechanism of ABS polymerization*

The polymerization of ABS start with the polymerization of butadiene monomer to be polybutadiene. Whereat, grafting of the styrene-acrylonitrile copolymer onto polybutadiene achieved by copolymerization in the presence of the polybutadiene. Possible mechanism of ABS polymerization is illustrated in equation (1, 2, 3, 4, 5, 6, and 7).



Radical abstraction from the polybutadiene.

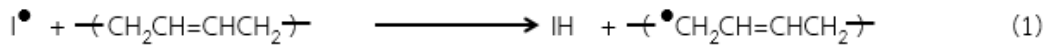

(1)

Radical addition from the polybutadiene.

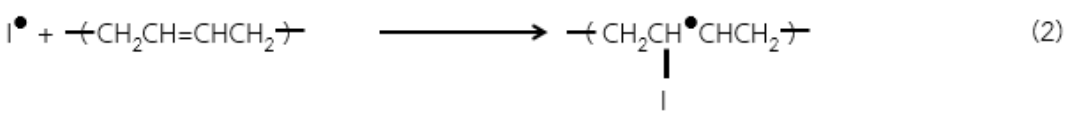

(2)

$I^{\bullet}$ is an initiator radical. Radical attack on the substrate polybutadiene competes with formation of styrene-acrylonitrile copolymer.

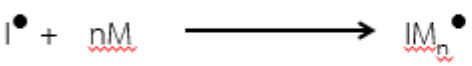

(3)

M is styrene or acrylonitrile monomer and $Mn^{\bullet}$ is a growing linear styrene-acrylonitrile polymer radical. The polybutadiene radical $P^{\bullet}$ formed in equations 1 and 2, where P* is $-(CH_2CH=CHCH_2)-$ or $-(CH_2\underset{I}{CH^{\bullet}}CHCH_2)-$ can now alternatively iniate polymerization, combine with a growing linear copolymer radical, induce cross-linking, or undergo chain transfer.

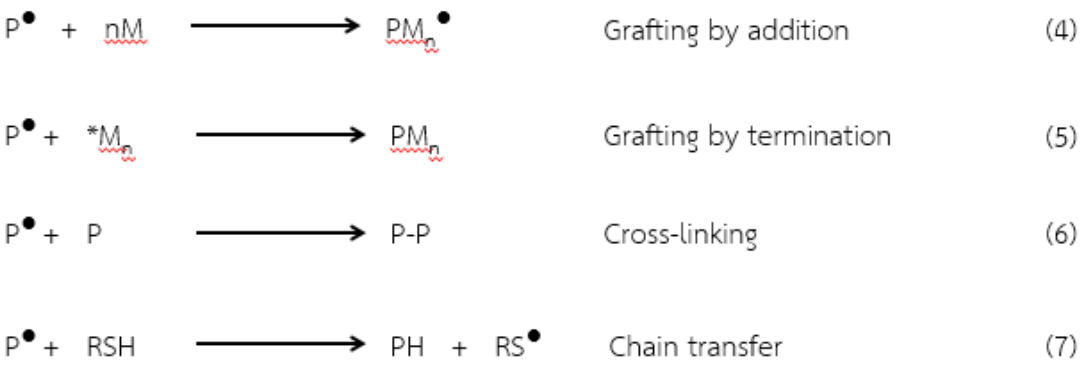

| | | |
|---|---|---|
| $P^{\bullet} + nM \longrightarrow PM_n^{\bullet}$ | Grafting by addition | (4) |
| $P^{\bullet} + {}^*M_n \longrightarrow PM_n$ | Grafting by termination | (5) |
| $P^{\bullet} + P \longrightarrow P\text{-}P$ | Cross-linking | (6) |
| $P^{\bullet} + RSH \longrightarrow PH + RS^{\bullet}$ | Chain transfer | (7) |

where RSH is a chain transfer agent.



2.1.2 The ABS commercial process

*2.1.2.1 Emulsion process*

Emulsion polymerization is a complex process in which the radical addition polymerization proceeds in a heterogeneous system. This process involves emulsification of the relatively hydrophobic monomer in water by an oil-in-water emulsifier, followed by the initiation reaction with either a water-soluble or an oil-soluble free radical initiator. At the end of the polymerization, a milky fluid called latex is obtained. Latex is defined as colloidal dispersion of polymer particles in an aqueous medium. The ABS emulsion process involves a two-step polymerization, the polybutadiene main chains latex produced, and then styrene and acrylonitrile are

grafted onto the polybutadiene main chains and the grafted latex is obtained. The grafted latex is coagulated and the resin is separately from the water, washed and dried. A typical emulsion process is shown in Figure 2.1.

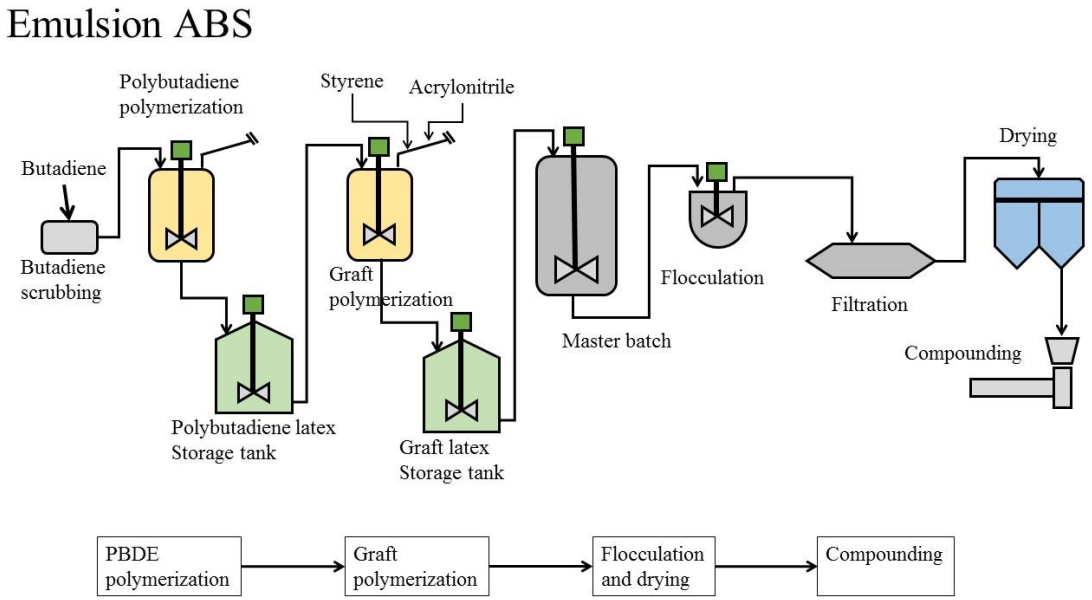


Figure 2.1 Emulsion ABS process

The first step of emulsion ABS is the production of polybutadiene. The water, emulsifiers and chain transfer agent are added to the reactor and the temperature is controlled at 10-85 °C. The butadiene and the initiator are then added. When the desired conversion is reached, the polybutadiene latex is stripped or any residual monomer. The second step is the reaction of styrene and acrylonitrile in the presence of polybutadiene. The rubber proportion and range from 12 to 30% and monomers proportion range from 20 to 50%. Latex produced in the second step reaction is coagulated and the resin recovered. ABS resins can be sold in the uncompounded form as an impact modifier for alloys with Polycarbonate and other plastics, or compounded with additive and pigments.

*2.1.2.2 Bulk process*

In bulk ABS process, all polymerization is completed in a monomer-polymer medium. A schematic for bulk ABS process is shown in Figure 2.2.

Bulk ABS

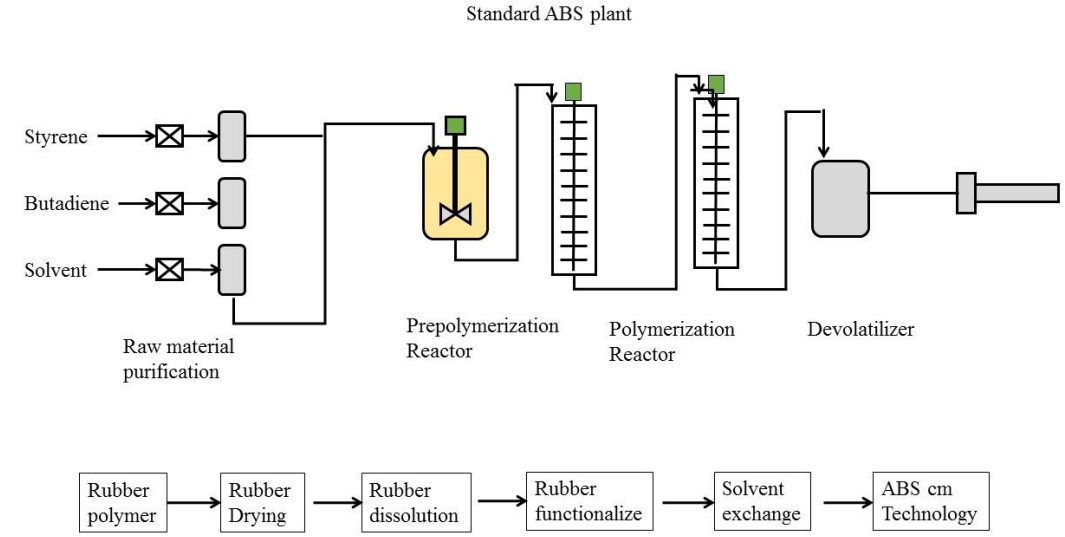


Figure 2.2 Bulk ABS process

In this process, a butadiene rubber is dissolved in styrene and acrylonitrile to a continuous prepolymerizer. Monomer conversion in prepolymerizer is usually from 10-40%. The prepolymer from the first reactor is continuously to one or more polymerization reactors in series, where the monomer conversion is increased to 50-90%. Reaction temperature in bulk ABS process are usually 90-150 ℃ in the prepolymer and 110-180 ℃ in the polymerization reactor. The polymer melt is pumped to devolatilization equipment. The bulk process is limited to a percentage of rubber up to approximately 15%, above this concentration, melt viscosity is very high and processing is difficult.

*2.1.2.3 Suspension process*

The suspension process is two part process in which a bulk polymerized prepolymer is made and then conversion is completed in a suspension reaction. The polybutadiene is solute in the styrene-acrylonitrile mix-monomer. The styene/acrylonitrile ratio can be varied from 80/20 to 60/40. The monomer ratio 75/25 to 70/30 is preferred for optimum color, tensile strength and chemical resistance. The portion of polybutadiene can be varied between 4 to 15%. The suspension ABS process is shown in Figure 2.3.

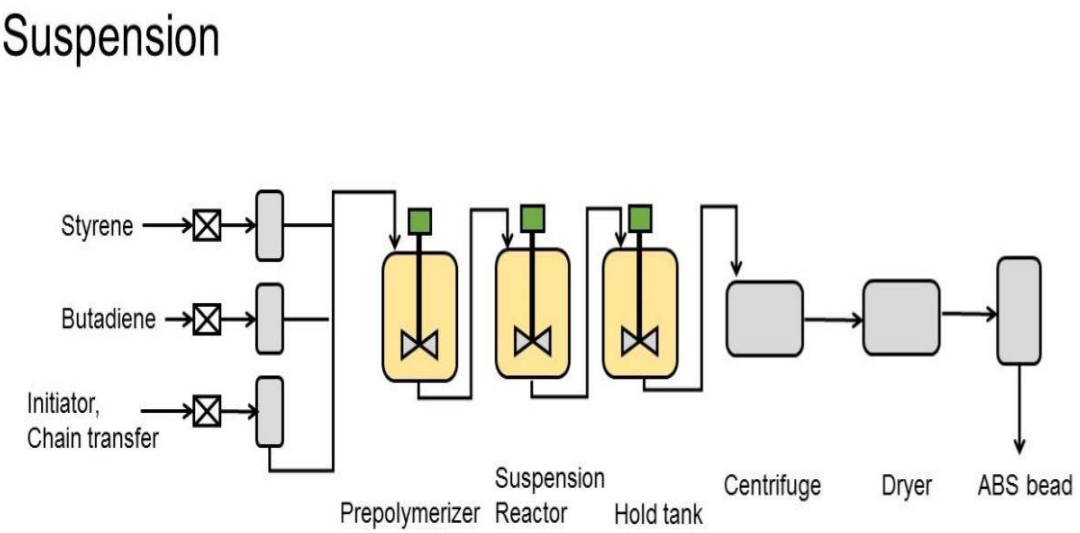


Figure 2.3 Suspension ABS process

2.1.3 The applications of ABS

The largest market for ABS in 2017 was the appliance market, which 35% market share. Within this market, the largest applications were refrigerator doors and tank liners. Others applications include injection molded housings for kitchen appliances, vacuum sweepers, sewing machines and hair dryers.

Electronics and electrical applications are the second largest market, which 30% market share, for ABS terpolymer. Performance needs in the business machine and consumer electronics markets vary considerable, as a result, general purpose grades of ABS are suitable for applications such as telephone, whereas others require specialty flame retardant grades.

The automotive applications, which are included in the transportation market are in the fourth largest market, which 11% market share, for ABS. High heat grades have been developed for instrument panels, light housings, pillar post moldings and other interior trim parts.

Other applications for ABS include luggage, bathtub and shower surrounds, toys. ABS grades are also used as impact modifier for rigid PVC and PC. The ABS market share in 2017 is shown in Figure 2.4.

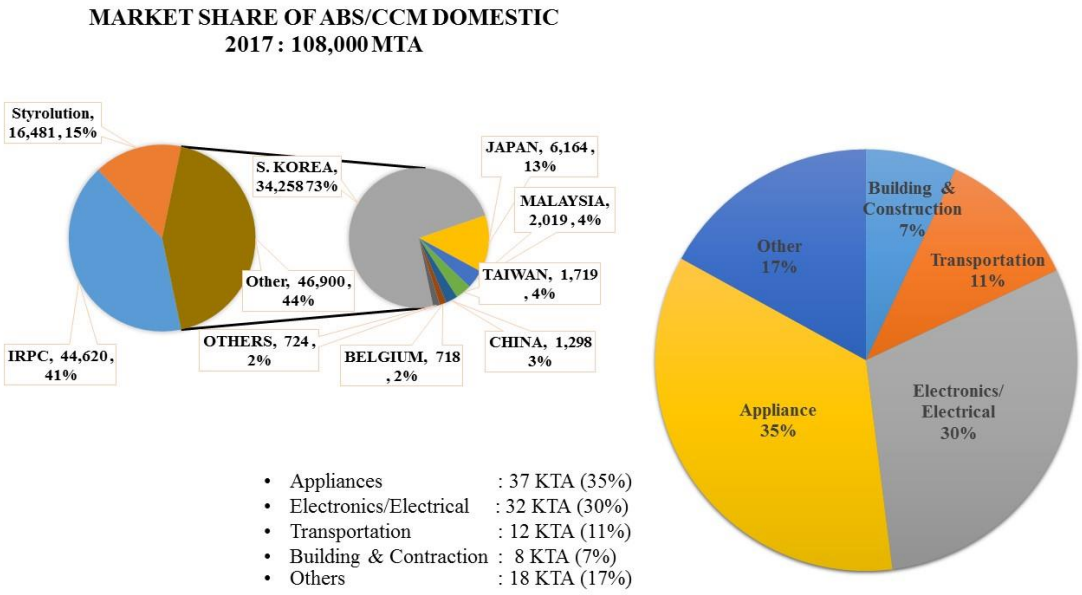


Figure 2.4 ABS market share in 2017 (Petrochemical business, IRPC Public Company)

2.3.4 ABS market outlook

The global demand of ABS terpolymer is slightly growth in the next three years and depended on the global GDP. However, the top three regions, in order of the additional demand, are China, Middle East, and Europe. Figure 2.5 showed the additional demand growth of ABS from 2010 to 2020.

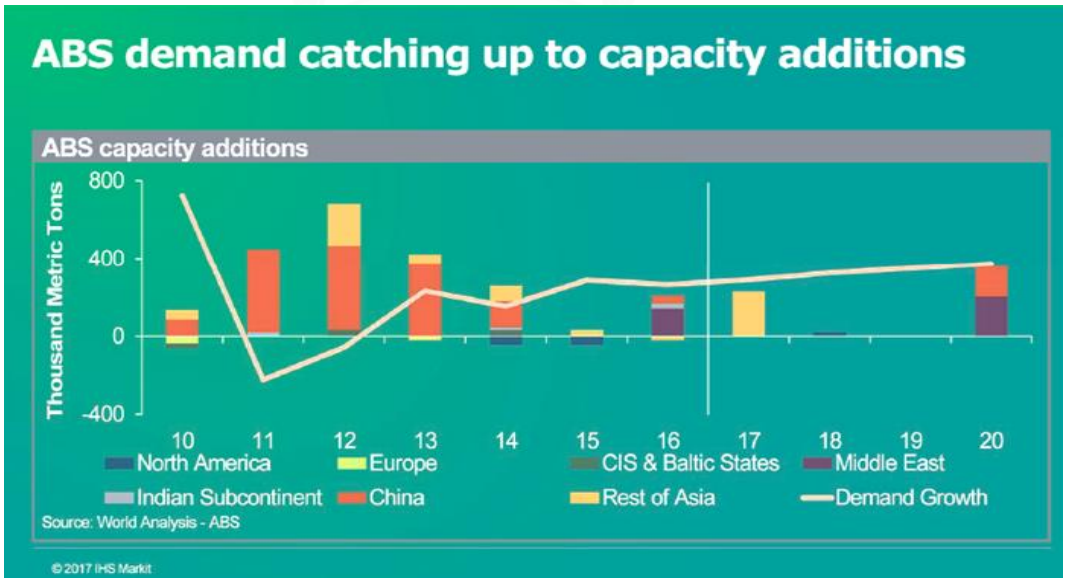


Figure 2.5 The additional demand growth of ABS from 2010 to 2020 (HIS 2017)

The ABS market by volume and value on 2013 to 2025 is shown in Figure 2.6.

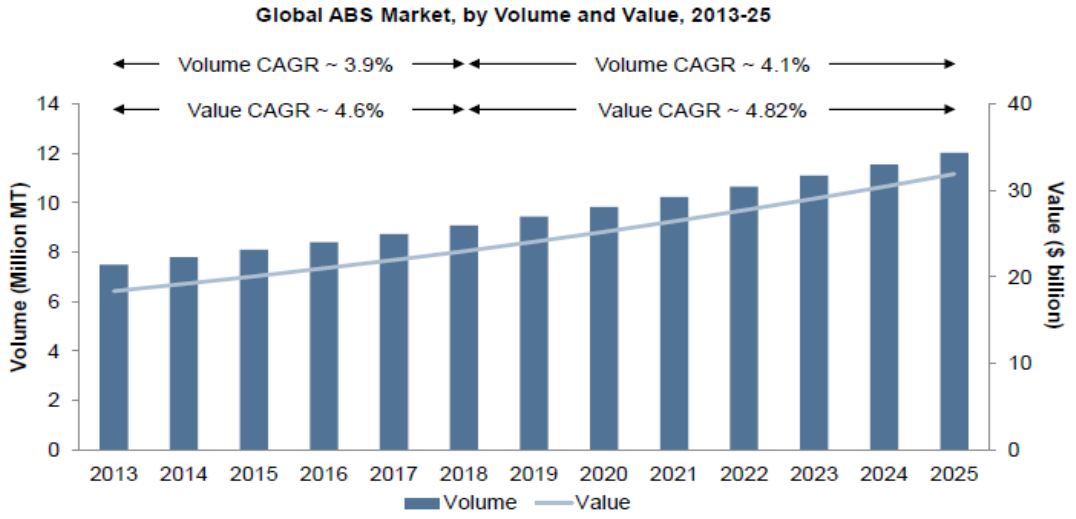


Figure 2.6 The ABS market by volume and value on 2013 to 2025 (Frost & Sullivan analysis)

The Global ABS market was around 7.5 million tons in 2013, and is expected to increase to around 9 million tons by 2018, and to 12 million tons by 2025.

Industrially, ABS is produced by graft copolymerization of acrylonitrile and styrene onto polybutadiene backbone. The nitrile groups from neighboring chains attract each other by polar force and bind the chains together, rendering ABS strong while the polybutadiene elastomeric component provides resilience [2-4]. In industrial application, ABS rubber is compounded with styrene-acrylonitrile copolymer (SAN), hence providing impact resistance and toughness. These properties could further be enhanced by the addition of nanosized particles including silica nanoparticles, naming nanocomposite materials [5]. Nanocomposites are promising materials due to their superior properties including mechanical properties. Well dispersed nanoparticles play an important role in absorbing and then transferring energy to other nanoparticles in their vicinity [6-18]. However, the most difficult task of nanocomposite preparation is how to achieve the optimum dispersibility of nanoparticles in an ABS rubber particle.

## 2.2 Silica nanoparticle

In the field of inorganic/organic nanocomposites is growing rapidly due to such hybrid materials can possess combined properties of both the incorporated inorganic materials and base polymers. A wide variety of colloidal inorganic materials has been used in polymer nanocomposites, including silica [27], titanium dioxide [28], copper oxide [29], magnetic oxide [30], aluminum hydroxide [31], silver [32], clay [33] and carbon black [34]. Among them, silica is the most studied material, due to hybrid structures of silica and polymer have an excellent physical reinforcement, high thermal resistance, high flexibility, high gas permeability and low surface energy, because the incorporation of silica. Silica nanoparticles have been used as a filler in the manufacture of paints, rubber products and plastic binder.

Silica is the most abundant material on earth covering 75 wt% of the Earth's surface as bound silicates and 12-14 wt% as free silica as quartz. The building block of silica and silicate structures is the $SiO_4$ tetrahedron, four oxygen atoms at the corners of a regular tetrahedron with silicon ion at the center (Figure 2.7)

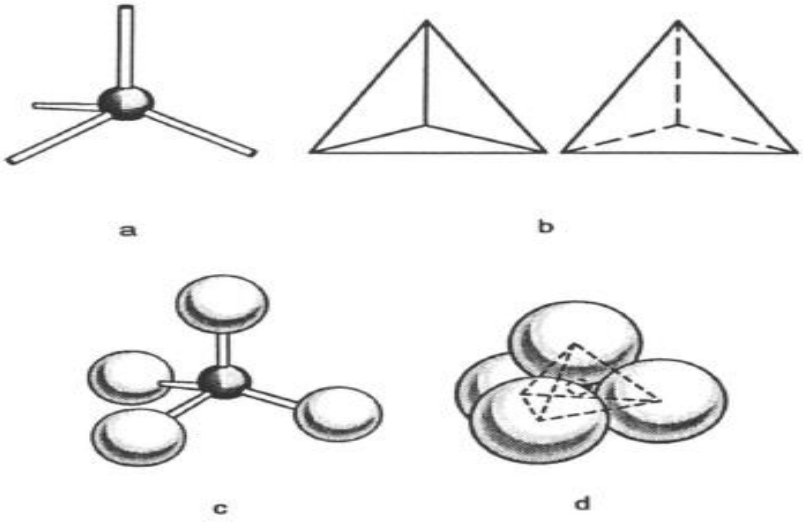


Figure 2.7 The tetrahedral coordination of oxygen ions with silicon

Silica structure is contain the Si-O bond, which is the most stable of all Si-X element bonds. The Si-O bond length is about 0.162 nm, which is smaller than the sum of the covalent radii of silicon and oxygen atoms (0.191 nm).

The Silanols group (Si-OH) mostly covering the surface of silica nanoparticles (some can exist in the inner part) enables surface modifications. The Si-O bond length, and Si-O-Si bond angle in crystalline and amorphous silicas have been studied by X-ray diffraction and infrared spectroscopy. Three strong absorption bands at 1250, 1100 and 800 $cm^{-1}$ measured by infrared transmission technique are attributed to Si-O vibrations and do not difference in the various silica modifications, whereas in the high frequency region at 2800-4000 $cm^{-1}$ certain distinct differences are observed.

Silica sol, also known as colloidal silica is a dispersed system, where $SiO_2$ is forming the discontinuous phase in continuous dispersion medium, such as water (hydrosols or aquasols). The particle diameters have to be between 1 nm and 100 nm by definition. The appearance depends on the particle size and also concentration.

A stable dispersion of solid colloidal particles in a liquid is called a sol. Stable in this case means that the solid particles do not settle or agglomerate at a significant rate. If the liquid is water, the dispersion is known as an aquasol or hydrosol. If the liquid is an organic solvent, the dispersion is called an organosol. A gel consists of a three dimensional continuous network of the sol particles, which encloses a liquid phase. Drying a gel by evaporation under normal conditions results in a dried gel called a xerogel. An aerogel is a special type of xerogel from which the liquid has been removed by drying a wet gel in an autoclave above the critical point of the liquid so that there is no capillary pressure and therefore relatively little shrinkage.

Commercial colloidal silicas are in form of sols or powders. The powder can be xerogels, dry precipttates, aerogels, and aerosils or dried. Figure 2.8 shows the formation of silica sols, gels, and powder.

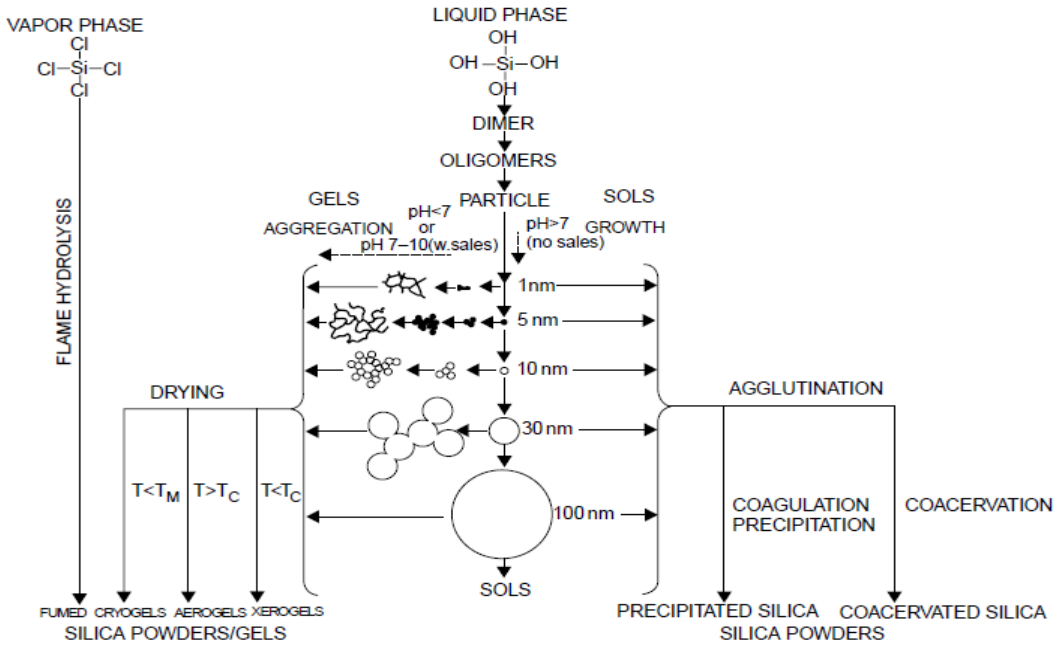


Figure 2.8 Formation of silica sols, gels, and powders by silica monomer condensation-polymerization followed by aggregation or agglutination and drying

The Stöber process is a sol-gel approach to preparing monodisperse (uniform) spherical silica ($SiO_2$) materials. The synthesis proceeds with the hydrolysis and condensation of tetraethyl orthosilicate (TEOS) in a mixer of alcohol, water and amnonia (catalyst). The hydrolysis and condensation reactions provide precursor species and the necessary supersaturation for the formation of particles. During the hydrolysis reaction, the ethoxy group of TEOS reacts with the water molecule to form the intermediate $[(OC_2H_5)_3Si(OH)]$ with hydroxyl group substituting ethoxy groups.

Ammonia works as a basic catalyst to this reaction. Following the hydrolysis reaction, the condensation reaction occurs immediately. Where the hydroxyl group of intermediate $[(OC_2H_5)_3Si(OH)]$ reacts with either the ethoxy group of other TEOS “alcohol condensation” or the hydroxyl group of another hydrolysis intermediate “water condensation” to form Si-O-Si bridges. The overall reaction is expressed in Scheme 2.1.

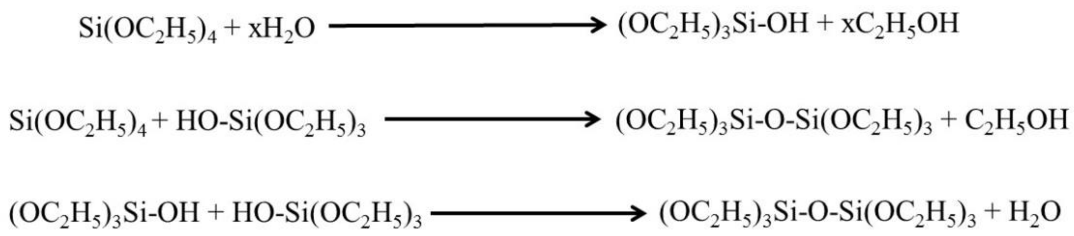


Scheme 2.1 Synthesis of Stöber spherical silica particles

The silica particles are stabilized by electrostatic repulsion due to the ions in the ammonia solution (Scheme 2.2).

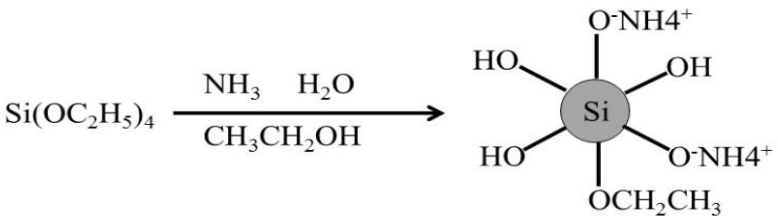


Scheme 2.2 Stabilization of the silica particles

**2.3 Surface modification of silica nanoparticles**

The properties of nanocomposites are greatly influenced by the dispersion degree of the inorganic components in the base polymer. The agglomeration and poor dispersion of the filler (such as silica) in the polymer matrix can reduce the enhancement of properties, the strength, adhesion, durability, and abrasion resistance of material. The chemical properties of the silica surface are determined by the silanol and siloxane groups are present on the external as well as the internal structure. The silica nanoparticles have negative surface charge, due to the existence of the silianol groups on the surface and make them highly hydrophilic, which causes their agglomeration during mixing. In addition, the incompatibility of the hydrophilic nanoparticles and the hydrophobic matrix causes in poor interfacial interaction and can weaken the mechanical properties.

2.3.1 Chemical treatment

The surface modification of silica nanoparticles by chemical treatments (such as the absorption of silane coupling agents) is a useful method to improve the dispersion stability of silica nanoparticles in various liquid media.

In order to achieve a good dispersion of the silica nanoparticles and to increase the interfacial adhesion with the polymer, physical and chemical methods have been used to modify the silica surface. The hydroxyl groups on the surface of silica nanoparticles can easily tailed with organic materials. Silanol groups can be easily functionalized by different chemical procedures. The most convenient method for surface modification of silica nanoparticle is treated with silane coupling agents to enhance the dispersibility (Scheme 2.3).

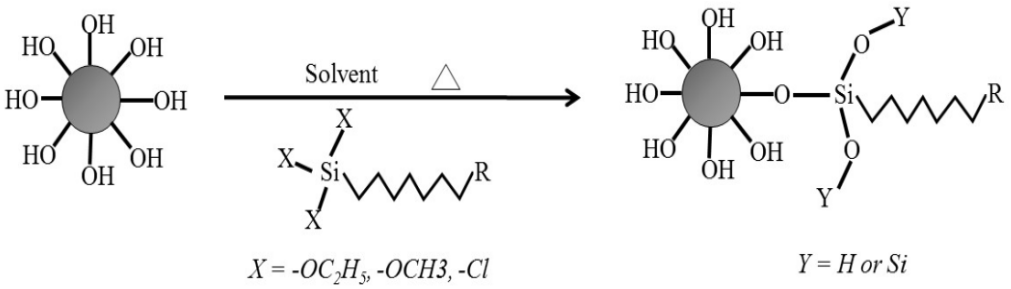


Scheme 2.3 Surface modification of silica nanoparticles



Sun et al. [20] prepared poly (vinyl chloride)-based composites by blending PVC with nano-$SiO_2$ particles, which were modified with dimethyl dichlorosilane (DMCS), ϒ-methylacryloxypropyl trimethoxy silane (KH570). From the SEM photography, it was found that the silica nanoparticles modified with DMCS had better dispersion and compatibility than the unmodified but worse than KHS in PVC matrix.

Zhang et al. [22] prepared the ultrafine precipitated silica modified by 3-methacryloxypropyltrimethoxysilane (KH570). It was found that the modification

degree of precipitated silica could be indicated by the activation index (following formula: h= (1-m) x 100%; where h is the average activation index of precipitated silica; m is the weight of silica (g)). The results showed that the average activation index of precipitated silica increased rapidly with the increasing KH570 when the KH570 dosage was less than 1% but after that, it increased slowly with increasing KH570 dosage. The average activation index reached 90% and most of precipitated silica has been modified when KH570 dosage was more than 1% that was, most of surface hydroxyl of precipitated silica has been replaced by organic groups of KH570.

He et al. [23] modified the colloidal silica nanoparticles (Acidic silica sol pH 2.6 and alkaline silica sol pH 9.0) by γ-aminopropyltrimethoxysilane (KH550) and γ-glycidoxypropyltrimethoxysilane (KH560) with different pH value (pH 2.6, 9.0). It was found that after the KH550 was added to silica sol, the solution changed from light blue to milky and some aggregates appeared but the KH560 did not induce the same phenomenon. For the acidic silica sol after modified with KH560, the nanoparticle size nearly unchanged because the acidity of KH560 did not disturbs the intermediate stable state of silica sol and the homocondensation was slower than the grafting process for the hydrolyzed KH560 and the silane molecules did not react with each other, forming aggregates.

Iijima et al. [25] modified silica nanoparticles by 3-glycidoxypropyltrimethosilane (GPS) or hexyltrimethoxysilane (C6S) in MEK. It was found that the generation of a steric repulsive force by the silane network as well as the reduction in the adhesion force between the silica nanoparticles decreased the viscosity of the silica MEK suspension and the surface interaction forces and the suspension viscosity were dependent on the silane network structure rather than the amount of coupling agent chemisorbed.

2.3.2 Grafting of synthetic polymers

Normally, the inorganic surfaces materials are functionalized with polymer chains either chemically (through covalent bonding) or physically (by physisorption) [38]. Covalent grafting method are preferred to maximize a stable interfacial

compatibility between the two phases. However, two methods for chemically attaching polymer chains to a solid state are the grafting to and the grafting from methods. In the grafting to technique, end functionalized polymer chains are reacted with a chemically activated substrate (Figure 2.9).

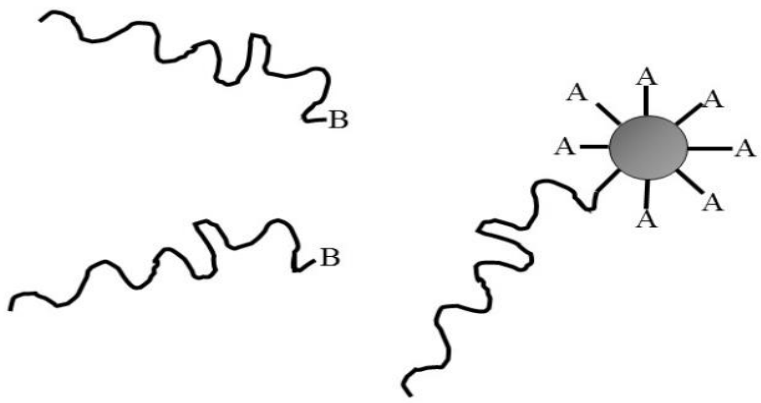


Figure 2.9 Grafting to approach of surface modification

The grafting from method involves formation of an initiator layer on the surface of silica followed by polymerization of monomer (Figure 2.10).

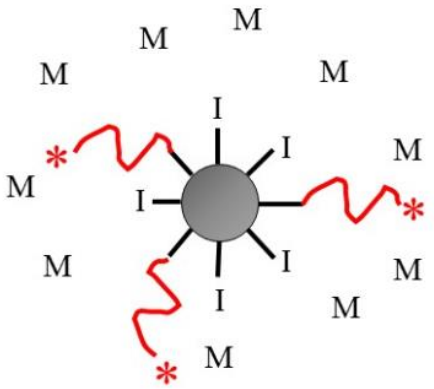


Figure 2.10 Grafting from approach for surface modification

Agudelo et al. [13] synthesized polystyrene-graft-silica particles based on styrene and triethoxyvinylsilane. It was found that increasing the amount of triethoxyvinysilane in the polymerization mixture decreased the molecular weight of

the copolymer indicating the occurrence of chain transference to the monomer. And the grafting density was depending on the molecular weight of the copolymers.

Suhendi et al. [14] prepared core-shell polystyrene/silica particles. The morphology observation by SEM and TEM images showed that the synthesized PS particles were coated by silica nanoparticles, spherical and well dispersed. And after electrospraying, the surface of the particles became rough.

Zhang et al. [16] prepared styrene butadiene rubber and used silane-grafted silica-covered kaolinite (SMKS), unmodified kaolinite (ORK), silane grafted kaolinite (SMK) and precipitate silica (PS) as fillers. SEM images showed that the SMKS particles were better compatible with the rubber matrix than SMK, and the rubber chains were attached to the SMKS particles. The thermal stability of SMKS filled SBR was greatly improved compared with that of PS filled SBR.

2.3.3 Other methods of surface modification

Other methods for surface modification of silica nanoparticles including adsorption of polymeric dispersants and in-situ surface modification. Surface modification by adsorption of polymeric dispersants is one of the simplest methods to improve the dispersion behavior of silica nanoparticles in aqueous systems. The hydrophilic silica nanoparticles can be dispersed in highly polar organic solvents by using anionic or cationic polymer dispersants. These dispersants generate steric repulsive forces among the polymer chains and increase the surface charge, which results in better dispersibility of the silica nanoparticles.



Lavorgna et al. [21] prepared the functionalization multiwalled carbon nanotubes (MWCNTs) with silica nanoparticles, obtaining silica enriched carbon nanotubes with the bunches morphology. It was found that the 3-amminopropryltriethoxy silane (APTES) functionalized and silica enriched carbon nanotubes were better dispersed within epoxy matrix, exhibiting smaller aggregate when compared with acid functionalized MWCNTs.

Shin et al. [24] modified silica nanoparticles with poly (ethylene glycol) methacrylate (PEGMA) or poly (propylene glycol) methacrylate (PPGMA). The size and

shape of the pure and modified silica particles was observed using SEM, the sample was prepared by placing a drop of suspension onto a glass plate and then drying under vacuum. It was found that the SEM images showed the pure and modified particles had a uniform size, spherical shape and no agglomeration of particles after surface modification. It was concluded that the surface modification of silica particles with polymer was successfully.

Xiao et al. [9] prepared cationic silica nanoparticles, chemical modification with cationic reagent (N-trimethoxysilylpropyl-N, N, N-trimethylammonium chloride) onto the surface of silica nanoparticles, used as flocculants for fine clay flocculation. It was found that under clay flocculation conditions, the cationic silica nanoparticles alone produced little effect. However, when used in conjunction with anionic polyacrylamide-based polymer, cationic silica nanoparticles/polymer system induced the clay flocculation effectively.

**2.4 Nanocomposites**

Recently, inorganic-organic composites including nanocomposites have been promising materials due to their superior properties including mechanical strengths, light weight and reinforcement properties. Nanocomposites can be described into a multiphase solid material where one of the phases has one, two or three dimensions of less than 100 nanometers (nm), or structures having nano-scale repeat distances between the different phases that make up the material. A strong and stiff component of composite, which called a reinforcement, will be dispersed in a softer component called a matrix.

The nanocomposites such as polymer nanocomposites obtained by incorporation of inorganic materials can lead to the improvement in several areas, such as optical, mechanical, and fire retardancy properties. Polymer nanocomposites containing inorganic nanoparticles exhibit the functionalities of polymer matrix (light weight and easy formability) combined with the unique features of the inorganic nanoparticles (impact resistance and toughness). Among numerous inorganic/organic

polymer nanocomposites, silica containing polymer nanocomposites are mostly studied and found in the research report. It has been widely accepted that silica nanoparticles have been used as fillers in the manufacture of paints, rubber products, and plastic binders.

Nanocomposite materials can be classified, according to their matrix materials, in three different categories.

1. Ceramic Matrix Nanocomposites (CMNC); Fe-Cr/$Al_2O_3$, Ni/ $Al_2O_3$, Co/Cr, Fe/MgO, Al/CNT, and Mg/CNT.

2. Metal Matrix Nanocomposites (MMNC); $Al_2O_3/SiO_2$, $SiO_2$/Ni, $Al_2O_3/TiO_2$, $Al_2O_3$/SiC, and $Al_2O_3$/CNT.

3. Polymer Matrix Nanocomposites (PMNC); Thermoplastic/thermoset polymer/layered silicates, polyester/$TiO_2$, polymer/CNT, polymer/layered double hydroxides.

3.1 Polymer matrix - discontinuous reinforcement (non-layered) nanocomposites

The reinforcment materials employed in the production of polymer nanocomposites can be classified according to their dimensions. The three dimensions are in the nanometre scale, they are called isodimensional nanoparticles, for examples include spherical silica, metal particles and semiconductor nanoclusters. The reinforcement material is distributed all over the polymer matrix, as illustrated in Figure 2.11 [35].

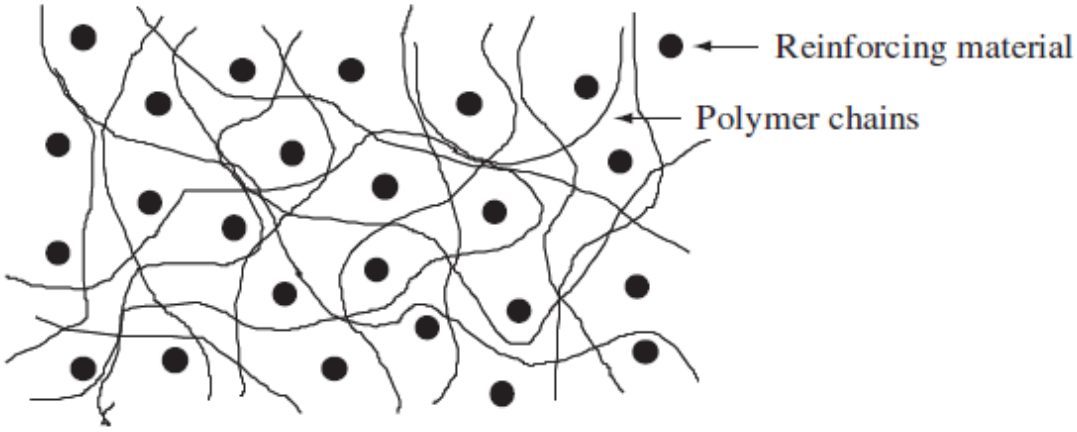


Figure 2.11 Typical structure of particle-reinforced polymer nanocomposites

Some examples will be given below in order to illustrate this statement.

Parvinzadeh et al. [7] prepared poly (ethylene terephthalate) (PET) based nanocomposites containing hydrophilic or hydrophobic nano-silica by melt compounding. SEM images showed that the neat PET had a relatively smooth and uniform surface. Additions of nano-silica particles to the PET matrix leads to various nano-silica particle-particle and nano-silica particle-PET chain interactions, enabling formations of aggregates and agglomerates on the surface of PET composites. Furthermore, the agglomerations of hydrophobic nano-silica/PET composites were smoother surfaces when compared with hydrophilic nano-silica/PET composites while hydrophobic nano-silica was more compatible with the molecular chains of PET.



Rostamiyan et al. [8] designed the optimized mixture proportions of epoxy-based hybrid nanocomposite with nano-silica as reinforcement, high-impact polystyrene as thermoplastic phase and hardener. It was found that the mixture design approach was fitting method to optimization of mentioned mechanical properties with an HIPS content of 2.67 wt%, a nano-silica content of 4.01 wt% and hardener content of 28 phr had best tensile, flexural, compression and impact strength.

Jumahat et al. [26] prepared nano-silica/epoxy nanocomposites. The morphology of the composites by TEM images showed that there was no agglomeration of the silica nanoparticles even at high volume fraction due to good

dispersion. It was found that the performance of the nanocomposites offers higher tensile stiffness and strength when compared to the neat epoxy.

Tianjin et al. [10] prepared silica-Polystyrene composite as a nucleating agent for PET. They modified silica nanoparticles with ϒ-methacrylic propyl trimethoxysilane (MPS) and dispersed silica modified into polystyrene. The result showed that modified silica particles could be successfully encapsulated with PS while the un-modified silica particles could not be encapsulated with it. It was found that the encapsulation of silica particles with PS effectively improved the dispersion of organic particles in PET.

Zhang et al. [11] prepared polystyrene/silica core-shell nano-composite with controllable size. It was found that at low ammonia concentration, small silica particles were found as a result of unsuppressed homogeneous nucleation. While, the ammonia concentration needs to be higher than 0.362 mol/L in order to obtain monodispersed PS/$SiO_2$ core-shell particles without small silica particles. Moreover, SEM images showed that the thickness of silica coating could be controlled in the range of 15-64 nm by adjusting the concentration of TEOS precursor.

Elias et al. [12] prepared an immiscible polymer blend polypropylene/polystyrene (PP/PS ratio 70/30) filled with silica nanoparticles. Two types of nanosilica were used, a hydrophilic silica and hydrophobic silica. It was found that the volume droplet radius decreased from 3.25 to 1 μm for filled blends with 3 wt% silica. In addition SEM images showed that the hydrophilic silica was tend to confine in the PS phase whereas hydrophobic was located in the PP phase.

Saavedra et al. [15] prepared fumed silica/epoxy composites and studied effect of silica loading at 10, 20, 30, 40 and 50 wt% on thermal stability and thermal degradation by TGA. It was found that the thermal degradation behavior of the resin was affected by the silica loading. Some thermal stability improvement was explained as silica layer formation. Some worsening of the thermal stability was probable due to the negative effect of the silica on the cure and to the small amount of silanol groups on the fume silica to create substantial hydrogen bonding between the organic and inorganic phases.

Chuayjuljit et al. [17] prepared nanocomposites of natural rubber (NR) and polystyrene (PS)-encapsulated nano-silica. It was found that the incorporation of an appropriate amount of PS-encapsulated nano-silica apparently improved the tensile strength (3 phr), modulus at 300% strain (9 phr optimal) and flammability (9 phr optimal) of the NR.

Liu et al. [18] prepared rubber (SBR, NR, BR and EPDM) nanocomposites filled with nanokaolin (NK) and precipitate silica (PS). It was found that the rubber composites filled by NK improved the operation security of rubbers in prophase vulcanization, had an excellent elasticity and improved thermal stability by the increase of onset weight loss temperature (T0) 50-90 ºC over that of a PS composite.

Jovanovic et al. [19] prepared the silica-reinforced nanocomposites based on EPDM and NBR rubbers and EPDM/NBR rubber blends. SEM images showed that the component dispersion nature in the blends was not uniform, which indicative of their heterogeneous nature. As the NBR rubber content increased, the tensile strength increases to its optimal value and then decreased. The tensile strength showed a maximum with the EPDM/NBR = 20/80 rubber blend when the EPDM content was above 20 phr, the tensile strength decreased. From DSC showed two separate T*g* values, first T*g* from the EPDM rubber with temperature range of -60 ºC to -52 ºC and second T*g* were produced by the NBR rubber with the temperature range of -30 ºC to -23 ºC. Therefore, as indicated that the EPDM/NBR polymer blends are immiscible.



Liu et al. [2] prepared immiscible PA6/ABS blends filled with hydrophobic nano-silica. SEM images showed that the 40/60 composition was the phase inversion composition for PA6/ABS blends. The hydrophobic nano-silica particles showed selective distribution in the blends, which was dependent on the blends composition. A nano-silica network-like structure was formed in the ABS phase when ABS was the matrix phase.

Wei et al. [3] synthesized mesoporous silica and surface modification with 9, 10-dihydro-9-oxa-10-phosphaphenanthrene-10-oxide (DOPO), used for flame retardant in polycarbonate (PC)/acrylonitrile-butadiene-styrene (ABS) compared with phosphoric

acid triphenylester (TPP). They found that in PC/ABS/6 wt% TPP/2 wt% DM system, the flame retardancy of the composite improved significantly with 28% LOI value and V0 rating in UL-94 test.

Kim et al. [4] synthesized ABS/silica hybrid nanocomposites. TEM images showed nanocomposite latexes with a rough surface due to the presence of small silica particle surrounding the PB-*g*-SAN beads. The impact strength, with increased silica nanoparticle content the impact strength of the nanocomposites increased first and then levels off up to 3 wt%.

3.2 Polymer nanocomposites with layered reinforcements

Polymer layered silicate (PLS) nanocomposites have attracted great interest because their improved properties compared with the pure polymer. Two characteristics of layered silicates are generally considered for PLS nanocomposites. The first is the ability of the silicate particles to disperse into individual layers. The second is the ability to fine-tune their surface chemistry through ion exchange reactions with organic and inorganic cations. The main reason for the remarkable improvements observed in polymer/layered-silicate nanocomposites is the stronger interfacial interaction between the matrix and the silicate, compared to conventional filler-reinforced systems. Some examples will be given below in order to illustrate this statement.



Hongbo et al. [36] studied the preparation and characterization of polyethylene modified with grafting MAH monomer on its backbone at first. Then two kinds of nanocomposites, polyethylene (PE)/organic montmorillonite (Org-MMT) and maleic anhydride-grafted-polyethylene (PE-*g*-MAH)/Org-MMT nanocomposites were prepared. The FT-IR spectroscopy, X-ray diffractometry (XRD), transmission electron microscopy (TEM), differential scanning calorimetry (DSC) and thermogravimetric analysis (TGA) of the nanocomposites were investigated. It was found that the FT-IR spectra of PE-*g*-MAH showed the characteristic bands of succinyl anhydride rings bonded to PE which proved the successful grafting reaction. The XRD and TEM micrographs showed that an intercalated structure would be acquired on mixing the PE and Org-MMT and an almost

exfoliated system would be obtained by mixing the PE-*g*-MAH and Org-MMT. The DSC and TGA thermogram showed that both nanocomposites had a higher thermal decomposition temperature and a higher crystallization temperature when compared to the original matrix.

Haiyun et al. [37] studied morphology, thermal stability and flammability properties of ABS-*g*-MAH/clay nanocomposites by melt blending. It was found that FTIR spectra confirmed that the MAH was successfully grafted onto butadiene chains of the ABS backbone in the molten state using dicumyl peroxide as an initiator and styrene as the comonomer and the relative grafting degree increased with increasing loading of MAH. TEM images indicated that the size of the dispersed rubber domains of ABS-*g*-MAH increased and the dispersion was more uniform than the neat ABS resin. XRD and TEM showed that intercalated/exfoliated structure was formed in ABS-*g*-MAH/OMT nanocomposites and the rubber phase intercalated into the clay layers. TGA showed that the intercalated/exfoliated structure of ABS-*g*-MAH/OMT nanocomposites had better barrier properties and thermal stability than did the intercalated ones of ABS/OMT nanocomposites. The T*g* of ABS-g-MAH resin was unchanged compared to the neat ABS but the addition of clay could improve T*g* of ABS-*g*-MAH/OMT and the Tg of ABS-g-MAH/OMT nanocomposites was higher than that of the neat ABS/OMT nanocomposites. The cone calorimetric measurement showed that ABS-*g*-MAH/OMT nanocomposites exhibit reduced flammability compared to ABS/OMT nanocomposites at the same clay content. The chars of ABS-*g*-MAH/OMT nanocomposites were tighter, denser, more integrated and fewer surface microcracks than those of the ABS/OMT nanocomposites.



**2.5 Polylactic acid**

Poly(lactic acid) (PLA) is one of important biopolymers derived from renewable resources such as sugar cane, corn or cassava. PLA offers interesting properties including transparency, good mechanical strength, low toxicity and good barrier properties [38]. Therefore, PLA has been intensively developed as a promising material

for various applications such as packaging (especially food packagings), films, biomedical materials, agriculture and engineering plastic applications.

PLA can be produced by several polymerization processes from both of D-lactic acid and L-Lactic acid including azeotropic dehydrative condensation, direct condensation polymerization, and polymerization through lactide formation as shown in Figure 2.12. Nowadays, the high molecular weight PLA is most synthesized by ring opening polymerization

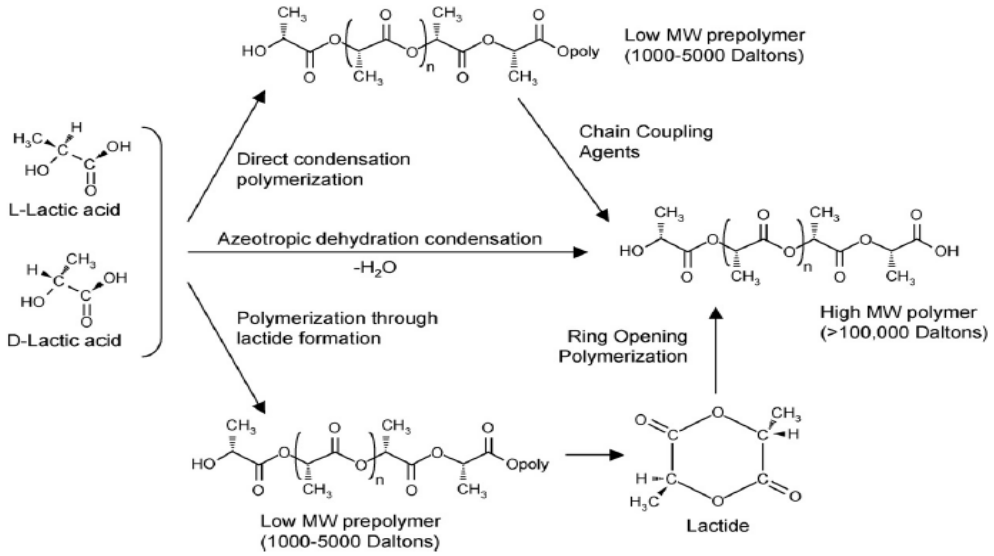


Figure 2.12 Synthesis of PLA from L- and D-lactic acids



Until now, the drawbacks of PLA are brittleness under tension and bending loads, low heat distortion temperature, processing difficulties due to low crystallization rate, and high price [39]. Therefore, many methods such as copolymerization, plasticization or blending with other polymer materials have been studied and developed to overcome the limitation of PLA [40-43]. Due to the chiral characteristic of lactic acid, various stereochemistry forms of poly(lactic acid) exist. Poly-L-lactide (PLLA) is a product resulting from polymerization of L,L-lactide having a crystallinity of about 37%, *Tg* between 60-65 °C, Tm between 170-178 °C and a tensile modulus between 2.7-16 GPa [1,2]. Poly-D-lactide (PDLA) exhibits semi-crystalline behavior while poly(DL-lactide) is an amorphous polymer [40]. Due to the presence of crystallinity as well as a compact structure, PLLA having the same molecular weight exhibits better mechanical properties and durability than poly(DL-lactide). However,

the degree of crystallinity depends on many factors such as annealing treatment, molecular weight, temperature and processing. PLA can be processed using industrial processing machines including injection, thermoforming and blown film [41]. Products from PLA can potentially be used in medical devices and packaging due to its good mechanical and physical properties, biocompatibility, non-toxic by-products and an ease of processability. However, PLA is considered a brittle polymer derived from low thermal stability occurring during heat processing, leading to its application restriction. Hence, attempts to toughen PLA have been in the spot light. Research focus could be divided into three routes as follows; copolymerization, plasticization and blending. Block copolymers of c-caprolactone and L-lactide can be achieved by ring-opening polymerization using stannous octoate/ethanol as an initiating system [42]. By incorporation of flexible units with low *Tg* into a polymer chain, copolymers were found to exhibit a lower tensile strength, an increased elongation and a higher impact strength [43, 44]. Multiblock copolymer such as polylactide-co-poly(glycolide-co-caprolactone) multiblock copolymers were synthesized, aiming at the development of biodegradable shape-memory polymers [45]. In the same manner, copolymerization of lactide with ethylene glycol to achieve triblock copolymer such as poly-DL-lactide-poly(ethylene glycol)-poly-D,L-lactide triblock copolymer results in a copolymer with flexibility and biodegradability suitable for biomedical applications [46]. The mechanical properties were found varied which was dependent on the flexible segments and the degree of crystallinity. Copolymerization of lactide and poly(ethylene glycol) to achieve polylactide-co-poly(ethylene glycol) copolymer was investigated, aiming at the desired result of a biodegradable polymer with flexibility properties and enhanced biodegradability. However, copolymers cannot be produced on an industrial scale for packaging applications. The plasticization of PLA by the addition of diglycerine tetraacetate was found to enhance plastic elongation and reduce brittleness [47]. Since PLA is a non-toxic polymer the plasticizing agents for PLA should be similar, limiting the suitable plasticizing agents to biodegradable and biocompatible groups. Another possibility to improve the properties of PLA is polymer blending. Blending of PLA with other biodegradable polymers such as polycaprolactone poly(butylene adipate-co-terephthalate) and polybutylene

succinate, polyethylene glycol, gelatinized starch and natural rubber is considered to be a relatively easy route to improve the toughness property [48-56]. The incorporation of cardanol resulted in an enhancement of the compatibility of the immiscible blend of polylactide (PLA) and poly(acrylonitrile-butadiene-styrene) (ABS) by reactive blending [57].

There is still more room to improve the properties of poly(lactic acid) especially stiffness-toughness. Acrylonitrile-butadiene-styrene (ABS) as impact modifier for toughening PLA was interesting this study. ABS is a copolymer exhibiting an effective capability of toughness and dimensional stability due to the fact that ABS particle behaves like a rubber which acts as an impact strength modifier [1]. Industrially, ABS is produced by graft copolymerization of acrylonitrile and styrene onto polybutadiene backbone. The nitrile groups from neighboring chains attract each other by polar force and bind the chains together, rendering ABS strong while the polybutadiene elastomeric component provides resilience [3, 4, 58]. In industrial application, ABS rubber is compounded with styrene-acrylonitrile copolymer (SAN), hence providing impact resistance and toughness. These properties could further be enhanced by the addition of nanosized particles including silica nanoparticles, naming nanoblends materials [5, 59].

# CHAPTER III

# METHODOLOGY

## PART I: Synthesis of ABS rubber containing $SiO_2$ nanoparticle and properties investigation of ABS containing $SiO_2$ nanoparticle

### 3.1 Materials

All materials and chemicals used in this research are shown in Table 3.1.

Table 3.1 Materials and sources.

| Material | Grade | Source |
|---|---|---|
| Polybutadiene latex (PB, SPS 54% solid content) | - | IRPC Public Company Limited, Rayong, Thailand |
| Polybutadiene latex (PB, MPS 54% solid content) | - | IRPC Public Company Limited, Rayong, Thailand |
| Polybutadiene latex (PB, LPS 54% solid content) | - | IRPC Public Company Limited, Rayong, Thailand |
| Styrene-acrylonitrile (SAN) resin | - | IRPC Public Company Limited, Rayong, Thailand |
| Commercial silica dispersion | AERODISP W7512S (12 wt%) | Evonik |
| Hexadecyltrimethoxysilane | Dynasylan 9116 | Evonik |
| Sodium silicate, 50% | - | Evonik |
| NonylphenolethoxylateEO15 | Analytical grade | StarTechChemical Co., Ltd |
| Styrene monomer | - | IRPC Public Company Limited, Rayong, Thailand |
| Acrylonitrile monomer | - | IRPC Public Company Limited, Rayong, Thailand |

| Material | Grade | Source |
|---|---|---|
| Lactose | Analytical grade | Davisco Food International Inc. |
| Tert-Dodecyl mercaptan (TDM) | Analytical grade | Arkema Inc. |
| Magnesium sulfate | Analytical grade | K+S Kali GmbH |
| Antioxidant | Analytical grade | Aquaspersion (M) Sdn. |
| Ferrous Sulfate | Analytical grade | Hayashi Pure Chemical Industries |
| Tert-Butylhydroperoxide (TBHP) | Analytical grade | Arkema Inc. |
| Tert-Sodium pyrophosphate 97% | Analytical grade | Aditya Birla Chemical (Thailand) Ltd. |
| Potassium hydroxide 48% | Analytical grade | AGC Chemical (Thailand) Co., Ltd. |
| Oleic acid | Analytical grade | Palm Oleo Sdn. Bhd. |



### 3.2 Apparatus and experiments

Followings are the list of major instruments used in this research

1. Reactor 20LHP autoLab HEL, UK

2. LTE26-40 Co-rotating intermeshing twin-screw Lab Tech Engineering twin screw extruder, Thailand, having a screw diameter, D of 26 mm with an L/D ratio = 40, with a rotational speed of 40 rpm.

3. Thermogravimetric analyzer TGA/DSC1 Mettller Toledo, USA

4. Transmission electron microscope TECNAI 20 Phillips, Netherlands

5. Scanning Electron Microscope JSM-5800 LV JEOL, Japan

6. Fourier Transform Infrared spectrometer Bruker Tensor 27, Germany

7. Particle size analyzer 90Plus Brookhaven, USA

8. X-ray diffractometer (D8 Advance Bruker, Germany)

9. Injection molding machine NEX80 Nissei, USA

10. Universal testing machine Instron 4302, USA

11. Pendulum impact tester Tenius Olsen IT504, USA

12. Universal testing machine Instron 5966, USA

13. Hotplate

14. Overhead stirrer

15. Hot air oven

16. Homogenizer

17. 100 mesh sieve

**3.3 Preliminary investigation of effect of ABS rubber sizes on mechanical properties of ABS**

Morphology of ABS rubber particle is spherical and its diameter can be tailor-made according to synthesis conditions. ABS rubber particle size greatly affects mechanical properties of ABS product. Therefore, in this section, various ABS rubbers with three different sizes were prepared and evaluated for mechanical properties. The ABS rubber which exhibited the optimum mechanical properties was chosen for the synthesis of ABS rubber containing hydrophobic silica nanoparticle.

Polybutadiene latex (PB, SPS rubber particle size 180-200nm, MPS 300-320nm and LPS 450-500nm) and styrene-acrylonitrile (SAN) resin were provided by IRPC Public Company Limited. Synthesis of ABS rubber was carried out as follows:

PB latex (900 ml) was charged into a reactor. The temperature was raised to 65 ºC. The persulfate solution (initiator) was fed into PB latex. Simultaneously, styrene

(500 ml), acrylonitrile (188 ml) and dodecyl mercaptan (6 ml) were well-mixed and then continuously fed into PB latex for a period of 3.5 h. After completion, the reaction was further continued at the temperature of 70 ºC for another 3 h. Finally, the reaction vessel was cooled down to the temperature of 50 ºC by water circulation jacket. Flocculants were introduced into flocculation tank. Temperature was gradually elevated from ambient to 85-92 ºC and then grafted latex was continuously introduced into the flocculation tank. ABS powder in suspension form was obtained and followed by filtration and drying in an oven at 80 ºC for 24 h.

Preparation of ABS compound

ABS powder and SAN were physically mixed in a hi-speed mixer. Then, well pre-mixed materials were loaded into a twin-screw extruder via a hopper. Twin screw extruder parameters were set as follows: L/D ratio = 40; a rotational speed of 150 rpm; barrel temperature zone1, zone2, zone3, zone4, zone5, zone6, zone7, zone8, zone9, and die zone = 190 ºC , 190 ºC , 200 ºC, 200 ºC, 200 ºC, 200 ºC, 200 ºC, 200 ºC, 210 ºC, and 210 ºC, respectively. The long-strand extrudate was chopped into granules.

Characterizations and Testings

For properties testing, the izod impact strength, tensile strength and flexural strength were evaluated following to ASTM D4101. Testing specimens according to the standard test method of ASTM D256 were prepared for Izod impact strength testing. The dumbbell specimens were prepared for the tensile testing in accordance with ASTM D638. Test specimens of 3.2 mm x 12.7 mm x 128 mm for the measurement of flexural strength were prepared according to the standard test method of ASTM D790.

**3.4 Synthesis of hydrophobic silica nanoparticle (HDTMS-silica) and In-situ preparation of styrene/HDTMS-silica dispersion**

AERODISP W7512S (15 g based on dry weight) was dispersed in hexadecyltrimethoxysilane/polypropylene glycol/methanol emulsion using a high speed homogenizer. Hexadecyltrimethoxysilane to AERODISP weight ratios of 3 : 1, 2 : 1, and 1 : 1 were studied. Then, HCl solution was added dropwise until pH value reached pH 2-3. After vigorously stirring for 3 h, the mixture was left standing to allow the complete silanization reaction for 1 h. The resultant Silane-g-silica (HDTMAS-silica) was washed off, dried and then ground into powder prior to sieving through the 140 mesh sieve screen.

Figure 3.1 HDTMS-silica nanoparticles preparation

In-situ styrene/HDTMS-silica dispersions having HDTMS-silica contents of 0.5 wt%, 1.0 wt%, 2.0 wt%, 3.0 wt%, 4.0 wt% and 5.0 wt% were prepared using a high speed homogenizer.

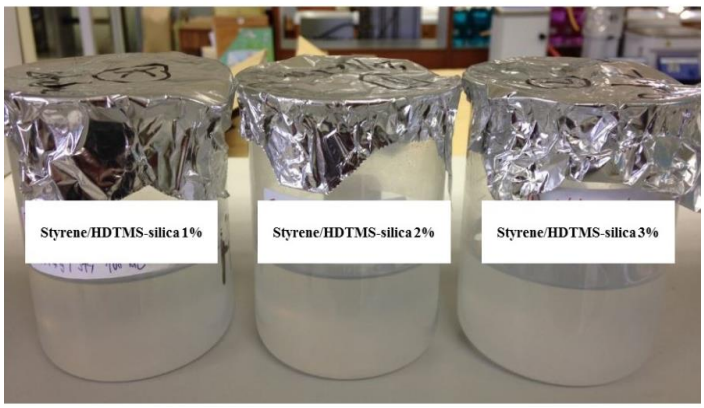


Figure 3.2 Styrene/HDTMS-silica dispersions preparation

### 3.5 In-situ synthesis of ABS/HDTMS-silica nanocomposite

PB latex (900 ml) was charged into a reactor. The temperature was raised to 65 ºC. The persulfate solution (initiator) was fed into PB latex. Simultaneously, styrene/HDTMS-silica dispersion (500 ml), acrylonitrile (188 ml) and dodecyl mercaptan (6 ml) were well-mixed and then continuously fed into PB latex for a period of 3.5 h. After completion, the reaction was further continued at the temperature of 70 ºC for another 3 h. Finally, the reaction vessel was cooled down to the temperature of 50 ºC by water circulation jacket.

Figure 3.3 Synthesis of ABS/HDTMS-silica nanocomposites

Flocculants were introduced into flocculation tank. Temperature was gradually elevated from ambient to 85-92 ºC and then grafted latex was continuously introduced into the flocculation tank. ABS powder in suspension form was obtained and followed by filtration and drying in an oven at 80 ºC for 24 h.

Figure 3.4 Flocculation and drying of ABS/HDTMS-silica nanocomposites

**3.6 Preparation of ABS/ HDTMS-silica nanocomposite compound**

ABS/HDTMS-silica powder and SAN were physically mixed in a hi-speed mixer. Then, well pre-mixed materials were loaded into a twin-screw extruder via a hopper. Twin screw extruder parameters were set as follows: L/D ratio = 40; a rotational speed of 150 rpm; barrel temperature zone1, zone2, zone3, zone4, zone5, zone6, zone7, zone8, zone9, and die zone = 190 ºC , 190 ºC , 200 ºC, 200 ºC, 200 ºC, 200 ºC, 200 ºC, 200 ºC, 210 ºC, and 210 ºC, respectively. The long-strand extrudate was chopped into granules.

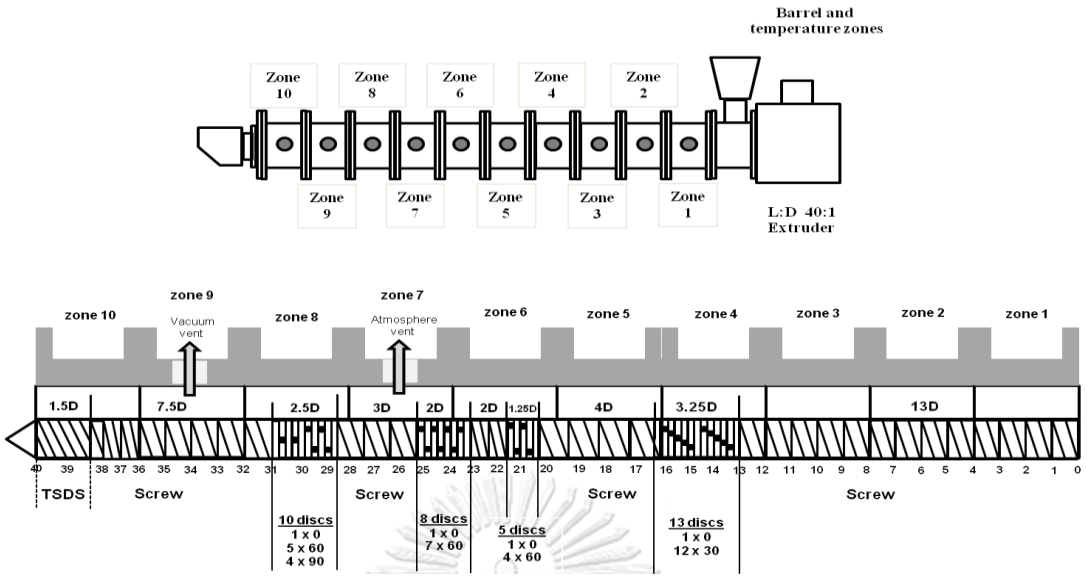


Figure 3.5 Configurations, barrel and temperature zones of the twin-screw extruder

The compounding recipes of ABS/HDTMS-silica nanocomposite are given in Table 3.2

Table 3.2 Recipes of ABS/HDTMS-silica nanocomposites compound

| Content | Compositions | | | HDTMS-Silica (wt%) |
|---|---|---|---|---|
| | ABS powder | ABS-Si powder | SAN | |
| ABS STD | 33.0 | 0.0 | 67.0 | 0 |
| ABS/HDTMS unmodified 1.0 wt% | 0.0 | 33.0 | 67.0 | 1 (unmod) |
| ABS/HDTMS-Silica2 0.5 wt% | 0.0 | 33.0 | 67.0 | 0.5 |
| ABS/HDTMS-Silica2 1.0 wt% | 0.0 | 33.0 | 67.0 | 1 |
| ABS/HDTMS-Silica2 2.0 wt% | 0.0 | 33.0 | 67.0 | 2 |
| ABS/HDTMS-Silica2 3.0 wt% | 0.0 | 33.0 | 67.0 | 3 |
| ABS/HDTMS-Silica2 4.0 wt% | 0.0 | 33.0 | 67.0 | 4 |
| ABS/HDTMS-Silica2 5.0 wt% | 0.0 | 33.0 | 67.0 | 5 |


Figure 3.6 Twin Screw Extruder (LTE26-40 Labtech Scientific)

## 3.7 Characterizations and Testings

*3.7.1HDTMS-silica nanoparticles*

3.7.1.1 Particle Size distribution

The particle size distribution of HDTMS-silica nanoparticles was measured by a dynamic light scattering instrument (90Plus, Brookhaven USA). HDTMS-silica nanoparticles was dispersed in water and dropped into a quartz cuvette before measurement whereas toluene was used as a medium for HDTMS-silica.




Figure 3.7 Particle size analyzer (90Plus, Brookhaven USA)

3.7.1.2 Thermal analysis

The thermal stability of HDTMS-silica1, HDTMS-silica2 and HDTMS-silica3 were characterized by a thermogravimetric analyzer (TGA/DSC1, Mettller Toledo USA). About 5.0 mg of sample was heated from 50 to 800 ºC at a heating rate of 20 ºC/min under nitrogen atmosphere with a gas flow rate of 25 ml/min.

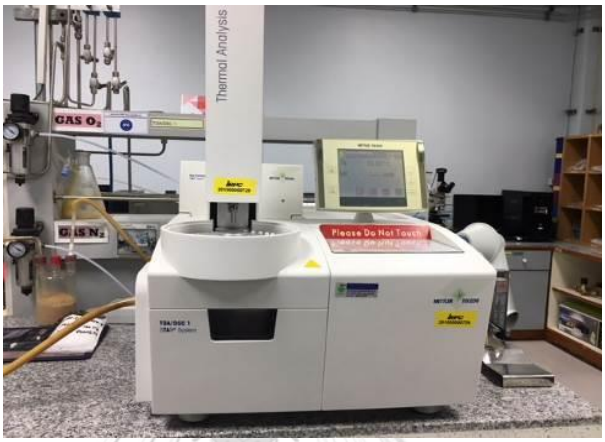


Figure 3.8 Thermogravimetric analyzer (TGA/DSC1, Mettller Toledo USA)

3.7.1.3 Morphological observation

The transmission electron micrographs of Aerodisp (silica) and HDTMS-silicas nanoparticles were records using a Transmission electron microscope (TECNAI 20 Phillips, Netherlands). The nanoparticles samples were diluted with ethanol, dried on carbon-coated copper grids for TEM analysis and the filament voltage was set at 100 kV.




Figure 3.9 Transmission electron microscope (TECNAI 20 Phillips, Netherlands)

3.7.1.4 Functional Groups

The Aerodisp (silica) and HDTMS-silicas powder were compression-molded into a thin film disc with a thickness of less than 50 μm for Fourier Transform Infrared (FTIR) characterization. Then FTIR spectra of the Aerodisp (silica) and HDTMS-silicas were recorded using a Fourier Transform Infrared spectrometer (Bruker Tensor 27, Germany) with 4 cm-1 resolution for 32 scans. For comparison, Aerodisp (silica) and HDTMS-silicas were also characterized by the IR technique.

Figure 3.10 FT-IR spectrometer (Bruker Tensor 27, Germany)

*3.7.2 ABS/HDTMS-silica nanocomposites*

3.7.2.1 Morphological observation



The ABS/HDTMS-silica nanocomposites samples for morphology studies were directly taken from the broken pieces of the nanocomposites samples after the impact test by using scanning electron microscope (JSM-5800 LV JEOL, Japan). The sample surfaces were etched with toluene to better reveal the microstructure. Etching was performed at room temperature for 2 h, after which the surfaces were rinsed, dried at 70 ºC for 6 h. The sample was immersed in 2% $OsO_4$ aqueous solution for staining the unsaturated components at room temperature for 12 h. After removal from the staining solution, the samples were carefully washed to remove the unreacted $OsO_4$. Then the samples were coated with gold to prevent charging before they were examined under SEM observation. And the element mapping by scanning electron

microscopy-energy dispersive X-ray spectrometry (SEM-EDS) was analyzed to provide Si mapping and their distribution in ABS matrix.


Figure 3.11 Scanning electron microscope (JSM-5800 LV JEOL, Japan)

3.7.2.2 Crystal Morphology

An X-ray diffractometer (D8 advance Bruker, Germany) was employed to investigate the crystallinity of the ABS/HDTMS-silica nanocomposites using a Cu K**α** target at 40 kV and the diffraction angle raging from 5-40°.

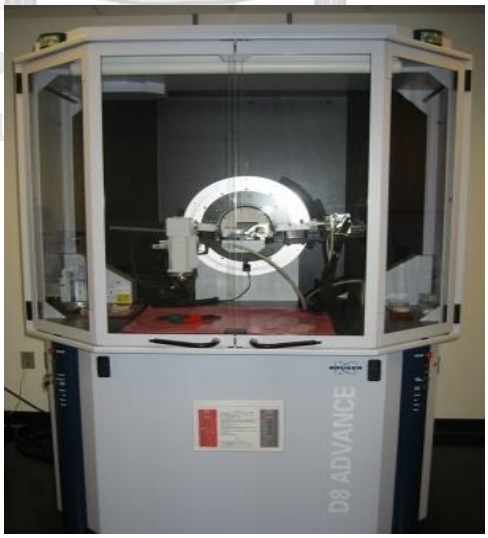


Figure 3.12 X-ray diffractometer (D8 Advance Bruker, Germany)

3.7.2.3 Thermal stability

The thermal stability of the ABS/HDTMS-silica nanocomposites was investigated by TGA. About 10 mg of the composite pellet was heated from 50 to 800 ºC at a heating rate 20 ºC/min under N2 atmosphere with the gas flow rate of 25 ml/min.

3.7.2.4 Mechanical properties

The test specimens of ABS/HDTMS-silica nanocomposites for impact test, tensile test and flexural test were also prepared via an injection molding machine (NEX80 Nissei, USA). The temperature profile from feed zone to nozzle was set as 30/200/200/200/200/220 ºC, respectively.


Figure 3.13 Injection molding machine (NEX80 Nissei, USA)



3.7.2.4.1 Izod impact strength testing

Testing specimens of 64 mm x 12.7 mm x 3.2 mm for the measurement of Izod impact strength were prepared by following ASTM D4101. They were tested according to ASTM D256 by using a pendulum impact tester (Tenius Olsen IT504, USA). A pendulum swung on its track and struck a notched, cantilevered plastic sample. The energy lost (required to break the sample) as the pendulum continued on its path was measured from the distance of its follow through.


Figure 3.14 Pendulum impact tester (Tenius Olsen IT504, USA)

3.7.2.4.2 Tensile properties measurement

The dumbbell specimens for the tensile property measurement were prepared according to ASTM D4101. They were tested in accordance with ASTM D638 by using the universal testing machine (Instron 4302, USA). The sample was pulled, by the tensile testing machine, from both ends. The force required to pull the specimen apart, and the extents that the sample was stretched before its breakage were measured.

Figure 3.15 Universal testing machine (Instron 4302, USA)

3.7.2.4.3 Flexural strength testing

The flexural test measures the force required to bend a beam under a 3- point loading condition. Test specimens of 3.2 mm x 12.7 mm x 128 mm for the measurement of flexural strength were prepared following ASTM D4101. They were tested according to the standard test method of ASTM D790 by using the Universal testing machine (Instron 5966, USA). The specimen was placed on the two supports and a load was applied at the center. The load at yield measured at a 5% deformation/strain of the outer surface is the flexural strength. The test beam is under compressive stress at the concave surface and tensile stress at the convex surface.

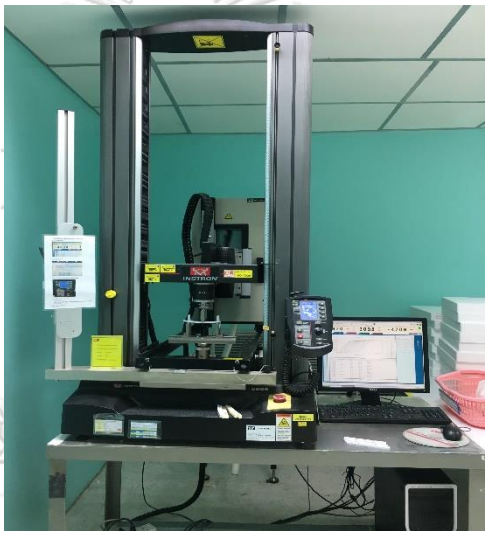

Figure 3.16 Universal testing machine (Instron 5966, USA)



**3.8 Synthesis of $SiO_2$ nanoparticles by precipitation technique**

*3.8.1 Synthesis of hydrophobic $SiO_2$ nanoparticle (HDTMS-$SiO_2$) and In-situ preparation of styrene/HDTMS-$SiO_2$ dispersion*

1000 ml solution containing 100 g of 50 wt% sodium silicate was dispersed in hexadecyltrimethoxysilane/polypropylene glycol/methanol emulsion using a high speed homogenizer. Hexadecyltrimethoxysilane to sodium silicate weight ratios of 2 : 1 was studied. Then, HCl solution was added dropwise until pH value reached pH 2-3. The solution was left standing for 2 days to allow the formation of $SiO_2$ nanoparticles.. The resultant Silane-*g*-silica (HDTMAS-$SiO_2$) was washed off, dried and then ground into

powder prior to sieving through the 140 mesh sieve screen. The schematic of HDTMS-$SiO_2$ preparation is shown in Scheme

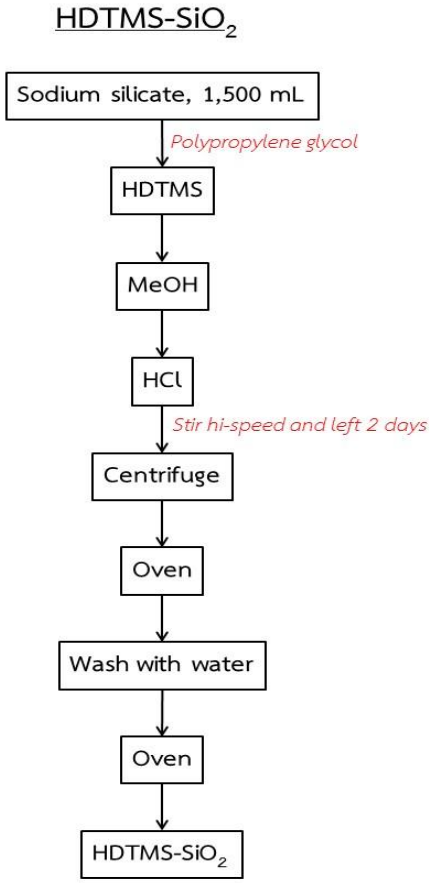


Scheme 3.1 Representative of HDTMS-$SiO_2$ preparation



In-situ styrene/HDTMS-$SiO_2$ dispersions having HDTMS-$SiO_2$ contents of 0.5 wt%, 1.0 wt%, 2.0 wt%, 3.0 wt%, 4.0 wt% and 5.0 wt% were prepared using a high speed homogenizer.

*3.8.2 In-situ synthesis of ABS/HDTMS-$SiO_2$ nanocomposite*

PB latex (900 ml) was charged into a reactor. The temperature was raised to 65 ºC. The persulfate solution (initiator) was fed into PB latex. Simultaneously, styrene/HDTMS-$SiO_2$ dispersion (500 ml), acrylonitrile (188 ml) and dodecyl mercaptan (6 ml) were well-mixed and then continuously fed into PB latex for a period of 3.5 h. After completion, the reaction was further continued at the temperature of 70 ºC for

another 3 h. Finally, the reaction vessel was cooled down to the temperature of 50 ºC by water circulation jacket.

Flocculants were introduced into flocculation tank. Temperature was gradually elevated from ambient to 85-92 ºC and then grafted latex was continuously introduced into the flocculation tank. ABS powder in suspension form was obtained and followed by filtration and drying in an oven at 80 ºC for 24 h.

*3.8.3 Preparation of ABS/ HDTMS-$SiO_2$ nanocomposite compound*

ABS/HDTMS-$SiO_2$ powder and SAN were physically mixed in a hi-speed mixer. Then, well pre-mixed materials were loaded into a twin-screw extruder via a hopper. Twin screw extruder parameters were set as follows: L/D ratio = 40; a rotational speed of 150 rpm; barrel temperature zone1, zone2, zone3, zone4, zone5, zone6, zone7, zone8, zone9, and die zone = 190 ºC , 190 ºC , 200 ºC, 200 ºC, 200 ºC, 200 ºC, 200 ºC, 200 ºC, 210 ºC, and 210 ºC, respectively. The long-strand extrudate was chopped into granules. The compounding recipes of ABS/HDTMS-silica nanocomposite are given in Table 3.3.

Table 3.3 Recipes of ABS/HDTMS-$SiO_2$ nanocomposites compound

| Content | Compositions | | | HDTMS-$SiO_2$ (wt%) |
|---|---|---|---|---|
| | ABS powder | ABS-$SiO_2$ powder | SAN | |
| ABS STD | 33.0 | 0.0 | 67.0 | 0 |
| ABS/HDTMS-$SiO_2$ 0.5 wt% | 0.0 | 33.0 | 67.0 | 0.5 |
| ABS/HDTMS-$SiO_2$ 1.0 wt% | 0.0 | 33.0 | 67.0 | 1 |
| ABS/HDTMS-$SiO_2$ 2.0 wt% | 0.0 | 33.0 | 67.0 | 2 |
| ABS/HDTMS-$SiO_2$ 3.0 wt% | 0.0 | 33.0 | 67.0 | 3 |
| ABS/HDTMS-$SiO_2$ 4.0 wt% | 0.0 | 33.0 | 67.0 | 4 |
| ABS/HDTMS-$SiO_2$ 5.0 wt% | 0.0 | 33.0 | 67.0 | 5 |

*3.8.4 Characterization and testing*

3.8.1.1 Morphological observation

The transmission electron micrographs of $SiO_2$ nanoparticles were records using a Transmission electron microscope (TECNAI 20 Phillips, Netherlands). The nanoparticles samples were diluted with ethanol, dried on carbon-coated copper grids for TEM analysis and the filament voltage was set at 100 kV.

3.8.1.2 Izod impact strength testing

Testing specimens of 64 mm x 12.7 mm x 3.2 mm for the measurement of Izod impact strength were prepared by following ASTM D4101. They were tested according to ASTM D256 by using a pendulum impact tester (Tenius Olsen IT504, USA). A pendulum swung on its track and struck a notched, cantilevered plastic sample. The energy lost (required to break the sample) as the pendulum continued on its path was measured from the distance of its follow through.

3.8.1.3 Tensile strength testing

The dumbbell specimens for the tensile property measurement were prepared according to ASTM D4101. They were tested in accordance with ASTM D638 by using the universal testing machine (Instron 4302, USA). The sample was pulled, by the tensile testing machine, from both ends. The force required to pull the specimen apart, and the extents that the sample was stretched before its breakage were measured.



3.8.1.4 Flexural strength testing

The flexural test measures the force required to bend a beam under a 3- point loading condition. Test specimens of 3.2 mm x 12.7 mm x 128 mm for the measurement of flexural strength were prepared following ASTM D4101. They were tested according to the standard test method of ASTM D790 by using the Universal testing machine (Instron 5966, USA). The specimen was placed on the two supports and a load was applied at the center. The load at yield measured at a 5% deformation/strain of the outer surface is the flexural strength. The test beam is under compressive stress at the concave surface and tensile stress at the convex surface.

**PART II: Preparation of PLA/ABS-*g*-MAA PLA/ABS$^{Si}$-*g*-MAA blends and properties investigation**

**3.1 Materials**

All materials and chemicals used in this research are shown in Table 3.4.

Table 3.4 Materials and sources

| Material | Grade | Source |
|---|---|---|
| Polylactic acid (PLA) pellets | 3052D | Naturework® |
| Methacrylic acid | Analytical grade | Tokyo Chemical Industry Co., Ltd. |
| Acrylonitrile Butadiene Styrene rubber | - | IRPC Public Company Limited, Rayong, Thailand |
| Potassium persulfate | Analytical grade | Sigma-Aldrich, Belgium |

**3.2 Apparatus and experiments**

Followings are the list of major instruments used in this research.

1. Reactor 20LHP autoLab HEL, UK
2. Thermogravimetric analyzer TGA/DSC1 Mettller Toledo, USA
3. Scanning Electron Microscope JSM-5800 LV JEOL, Japan
4. Differential scanning calorimeter (DSC1), Mettler Toledo, USA
5. Injection molding machine NEX80 Nissei, USA
6. Universal testing machine Instron 4302, USA
7. Pendulum impact tester Tenius Olsen IT504, USA
8. Universal testing machine Instron 5966, USA
9. Internal mixer Brabender BmbH & Co.KG, Germany
10. Heat distortion tester YASUDA SEIKI HD-148 PC, Japan

11. Hotplate

12. Overhead stirrer

13. Hot air oven

**3.3 Synthesis of ABS-*g*-MAA rubber**

ABS rubber (2,000 g) was poured into a close vessel reactor containing of water (10,000 mL). The temperature was raised to 65 °C. Then, potassium persulfate (15 g) and MAA (200 g, 10 wt% of ABS) / (400 g, 20 wt% of ABS for a separate batch) were continuously fed for a period of 3.5 h. After completion, the reaction was further continued at the temperature of 70 °C for another 3 h. Finally, the reaction vessel was cooled down to the temperature of 50 °C by water circulation jacket. PMAA-*g*-ABS suspension was obtained and followed by filtration and drying in an oven at 80 °C for 24 h. The carboxylic acid functional group was observed using FTIR analysis with transmission mode. IR spectrum was recorded in a range of 4000 $cm^{-1}$ – 600 $cm^{-1}$. Carboxylic acid group of PMAA-*g*-ABS was found at 1710 $cm^{-1}$ in case of 20 wt% MAA. Hence, ABS-*g*-MAA prepared using 20 wt% MAA was employed for preparation of PLA/PLA-*g*-ABS blends.

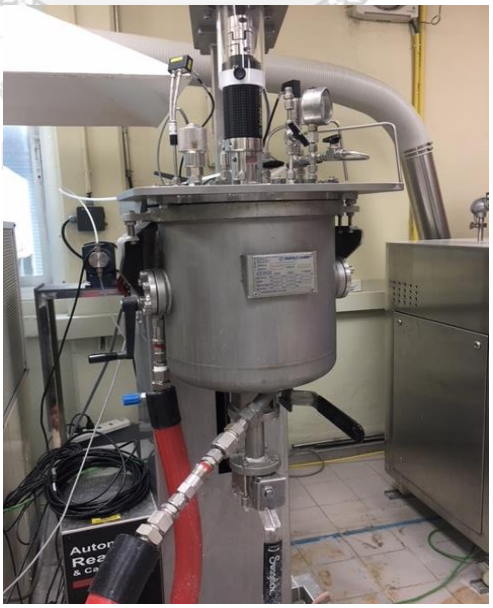

Figure 3.17 Reactor 20LHP autoLab HEL, UK

### 3.4 Preparation of PLA/ABS-*g*-MAA and PLA/ABS$^{Si}$-*g*-MAA blends by reactive blending

PLA and ABS-*g*-MAA at weight ratios shown in Table 3.5 were melt mixed using an internal mixer at 180 °C for 5 min. The esterification between carboxylic acid group of ABS-*g*-MAA and hydroxy end group of PLA occurred at the interphase PLA and ABS-*g*-MAA, resulting in PLA/ABS-*g*-MAA blends. Then, compounds were ground and injected using an injection molding machine set barrel temperature zones at 30/170/200/200/200/220 for preparing test specimens, respectively. Resultant injection molded samples were evaluated for mechanical properties according to ASTM D638 for tensile strength and ASTM D256 for impact strength, respectively. The fracture specimens were observed by scanning electron microscopy at an acceleration voltage of 22.0 kV.

Table 3.5 Blending recipes of PLA/ABS-*g*-MAA ratios

| Materials | PLA/ABS 10 wt% | PLA/ABS-*g*-MAA 10 wt% | PLA/ABS-*g*-MAA 20 wt% | PLA/ABS-*g*-MAA 30 wt% |
|---|---|---|---|---|
| Neat PLA | 90 | 90 | 80 | 70 |
| Neat ABS | 10 | - | - | - |
| ABS-*g*-MAA | - | 10 | 20 | 30 |




Figure 3.18 Internal mixer machine (Brabender BmbH & Co.KG, Germany)

Table 3.6 Blending recipes of PLA/ABS$^{Si}$-*g*-MAA ratios

| Materials | PLA/ABS$^{Si}$ 10 wt% | PLA/ABS$^{Si}$-*g*-MAA 10 wt% | PLA/ABS$^{Si}$-*g*-MAA 20 wt% | PLA/ABS$^{Si}$-*g*-MAA 30 wt% |
|---|---|---|---|---|
| Neat PLA | 90 | 90 | 80 | 70 |
| Neat ABS | 10 | - | - | - |
| ABS$^{Si}$-*g*-MAA | - | 10 | 20 | 30 |

**3.6 Characterizations and Testings**

*3.6.1 Mechanical properties*

3.6.1.1 Izod impact strength testing

Testing specimens of 64 mm x 12.7 mm x 3.2 mm for the measurement of Izod impact strength were prepared by following ASTM D4101. They were tested according to ASTM D256 by using a pendulum impact tester (Tenius Olsen IT504, USA). A pendulum swung on its track and struck a notched, cantilevered plastic sample. The energy lost (required to break the sample) as the pendulum continued on its path was measured from the distance of its follow through.

3.6.1.2 Tensile properties measurement



The dumbbell specimens for the tensile property measurement were prepared according to ASTM D4101. They were tested in accordance with ASTM D638 by using the universal testing machine (Instron 4302, USA). The sample was pulled, by the tensile testing machine, from both ends. The force required to pull the specimen apart, and the extents that the sample was stretched before its breakage were measured.

3.6.1.3 Thermal analysis

The thermal stability of PLA/ABS-*g*-MAA blends were characterized by a thermogravimetric analyzer (TGA/DSC1, Mettller Toledo USA). About 5.0 mg of sample was heated from 50 to 800 ºC at a heating rate of 20 ºC/min under nitrogen atmosphere with a gas flow rate of 25 ml/min.

3.6.1.4 Heat distortion temperature

Testing specimens for the measurement of heat distortion temperature were prepared by following ASTM ASTM D4101. They were tested according to ASTM D648 by using a heat distortion tester (YASUDA SEIKI HD-148 PC, Japan). The Testing specimens is placed horizontally in the heated bath under vertical pressure and increased the heating rate 2 ℃ / min. and measured the temperature when the testing specimens is bent from 0.254 mm.


Figure 3.19 Heat distortion tester (YASUDA SEIKI HD-148 PC, Japan)



3.6.1.5 Morphological observation

The PLA/ABS-*g*-MAA blends samples for morphology studies were directly taken from the broken pieces of the nanocomposites samples after the impact test by using scanning electron microscope (JSM-5800 LV JEOL, Japan). The sample was immersed in 2% $OsO_4$ aqueous solution for staining the unsaturated components at room temperature for 12 h. After removal from the staining solution, the samples were carefully washed to remove the unreacted $OsO_4$. Then the samples were coated with gold to prevent charging before they were examined under SEM observation.

# CHAPTER IV
# RESULTS AND DISCUSSION

## PART I: Synthesis of ABS rubber containing $SiO_2$ nanoparticle and properties investigation of ABS containing $SiO_2$ nanoparticle

### 4.1 Preliminary investigation of effect of ABS rubber sizes on mechanical properties of ABS

Typically, morphology of ABS rubber particle is spherical and its diameter can be tailor-made according to synthesis conditions. ABS rubber particle size greatly affects mechanical properties of ABS product. Therefore, in this section, various ABS rubbers with three different sizes (SPS size 180-200 nm, MPS size 300-320 nm and LPS size 450-500 nm) were prepared and evaluated for mechanical properties. The ABS rubber which exhibited the optimum mechanical properties was chosen for the synthesis of ABS rubber containing hydrophobic silica nanoparticle.

Effect of ABS rubber sizes on impact strength was evaluated. Impact strength values of ABS containing SPS, MPS and LPS are shown in Figure 4.1. It is found that ABS samples containing SPS rubber particle, MPS rubber, and LPS rubber have impact strength values of 8.30 kg-cm/cm$^2$, 23.10 kg-cm/cm$^2$, and 19.00 kg-cm/cm$^2$, respectively. As seen, MPS raises the impact resistance by 178% when compared to SPS. Then, the value significantly decreases by 21% in case of ABS containing LPS. It is understandable that too small ABS rubber underperforms in terms of energy absorption as well as energy dissipation, resulting in a significant drop of impact strength value. On the other hand, too large ABS rubber also reduces the impact strength property. Therefore, for the following experiments, MPS synthesis recipe was chosen throughout.

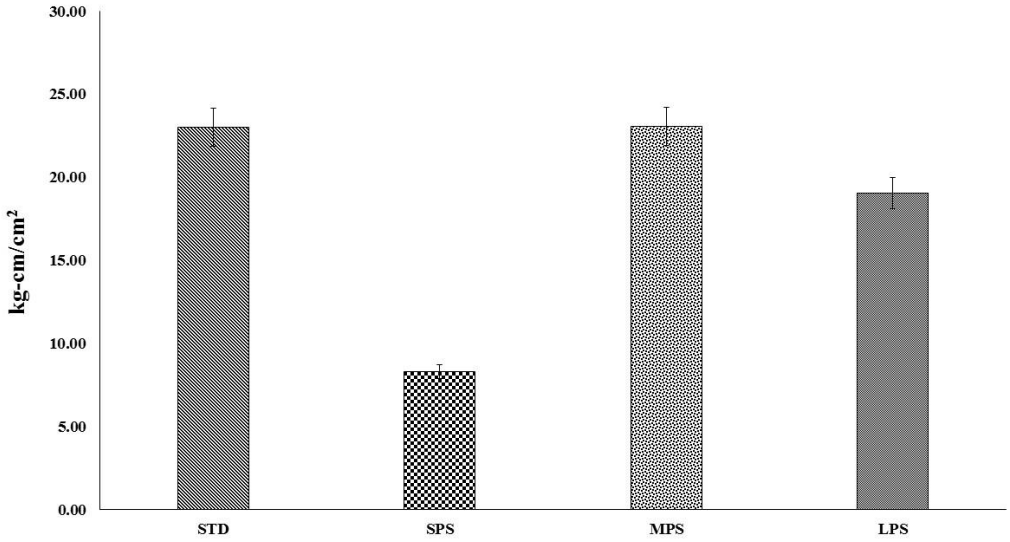


Figure 4.1 Representative impact strength of ABS containing three different rubber particle sizes (LPS, MPS and SPS)

In addition to impact resistance, tensile properties are evaluated and shown in Figure 4.2. In comparison, the tensile strength values of ABS containing SPS, MPS, and LPS marginally increases from 438 kg.cm$^2$, 454 kg.cm$^2$, and 449 kg.cm$^2$ for LPS, MPS, and SPS, respectively. It can be assumed that different rubber sizes play an insignificant role in improving the tensile strength property.

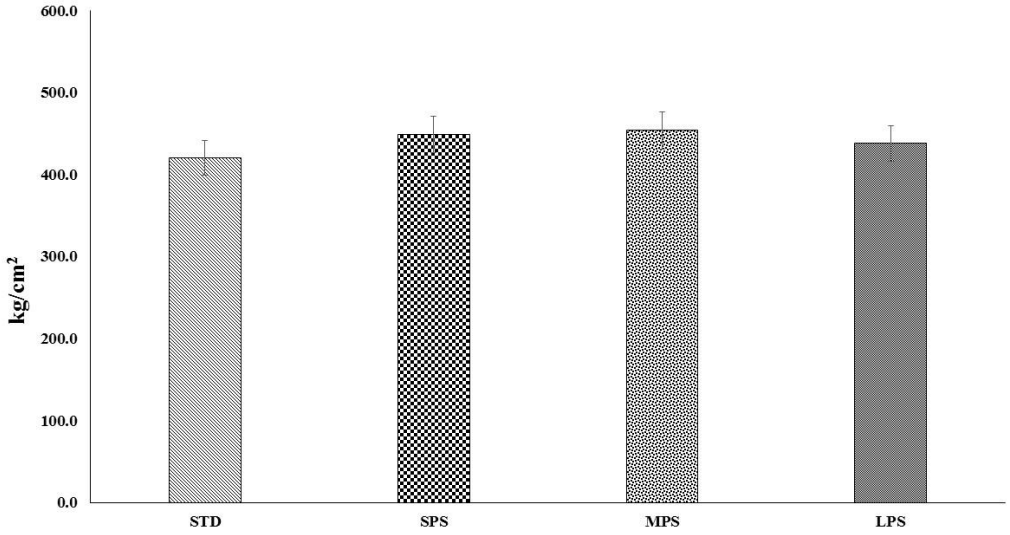


Figure 4.2 Representative tensile strength of ABS containing three different rubbers (LPS, MPS and SPS)

Flexural strengths are shown in Figure 4.3. When compared to standard ABS, the flexural strength value of nanocomposites gradually increases by 12.07%, 13.28%, and 13.84% for LPS, MPS and SPS ABS rubber respectively.

This means that MPS ABS rubber exhibited the optimum mechanical properties and the MPS ABS rubber size was chosen for the synthesis of ABS rubber containing hydrophobic silica nanoparticle.

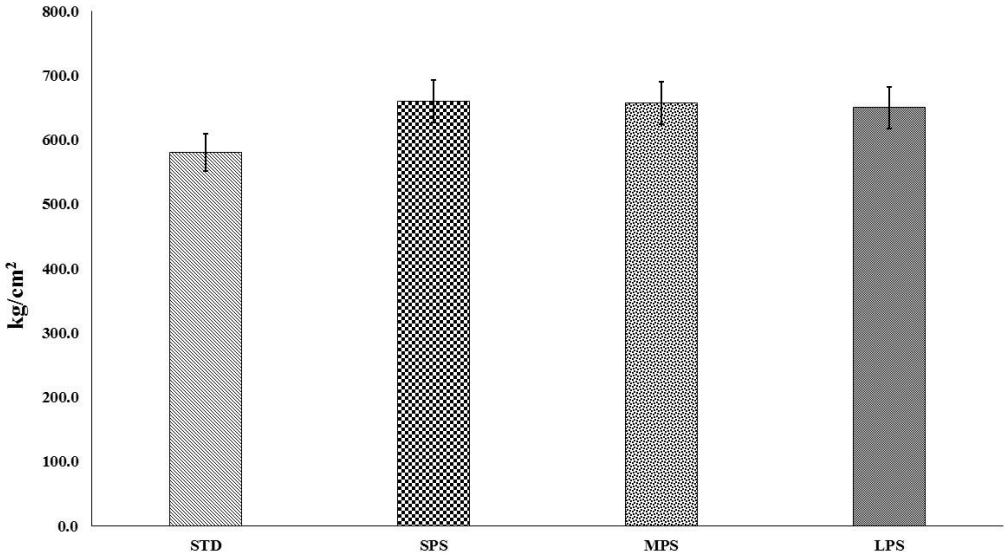


Figure 4.3 Representative flexural strength of ABS containing three different rubbers (LPS, MPS and SPS)

## 4.2 Characterizations of HDTMS-silica nanoparticles

*4.2.1 Dispersion test of HDTMS-Silicas in toluene medium*

The presence of hydroxyl groups on the surface of silica nanoparticles increases the agglomeration which can inversely influence on the dispersion of the nanoparticle in polymer matrix. Besides, the strength of interactions between the polymer and inorganic fillers (such as silica) phases is more determining factor affecting the properties of the obtained materials, which can often cause phase separation . Surface modification is one of the method to enhance the compatibility between the hydrophobic polymer and hydrophilic nanosilica. However, a good dispersion may be achieved by using reactive chemical modifier such as silane coupling agents.

Furthermore, the organofunctional groups of coupling agent could replace with hydroxyl groups on the surface of nanoparticles and react with polymer chains [27].

Since the direct addition of hydrophilic silica into ABS leads to the agglomeration problem, resulting in adverse effect on mechanical properties including impact strength. Therefore, it is crucial that hydrophobicity surface modification of silica nanoparticles is required in order to achieve the uniform dispersion of silica nanoparticles in ABS matrix, resulting in an improvement in energy absorption capacity. In this experiment, hydrophilic silica (AERODISP) was hydrophobically modified by HDTMS, resulting in hydrophobic silica (HDTMS-silica) derived from the surface silanization. Thus prepared HDTMS-silica is hydrophobic, hence exhibiting stable dispersion in toluene as shown in Figure 4.4.

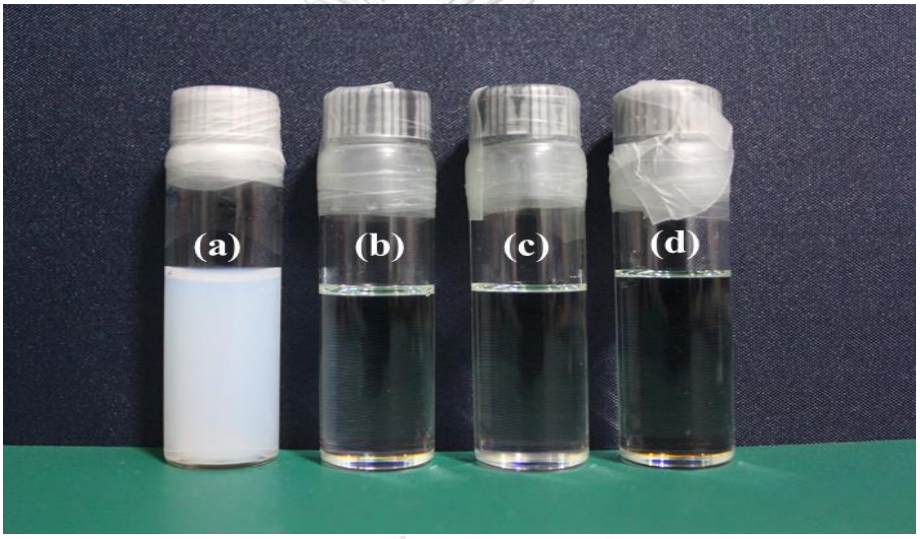


Figure 4.4 A 12 wt% Silica dispersion (in water) and 12 wt% HDTMS-silica dispersion (in toluene) b HDTMS-silica1, c HDTMS-silica2, and d HDTMS-silica3

Ideally, an individual particle should be hydrophobically modified in order to prevent a formation of a silica cluster which occurred during the drying step, yielding a micron-sized hard agglomerate. Practically, such a hard cluster formation could be minimized by adjusting HDTMS to $SiO_2$ weight ratio. In this work, three of HDTMS-silicas (HDTMS-silica1, HDTMS-silica2, and HDTMS-silica3) were prepared by varying HDTMS to $SiO_2$ weight ratios of 1 : 1, 2 : 1, 3 : 1, respectively. As observed, HDTMS-silicas exhibit good dispersibility in toluene in all cases as shown in Figure 4.4.

*4.2.2 The percent grafting of HDTMS onto the Silica surface*

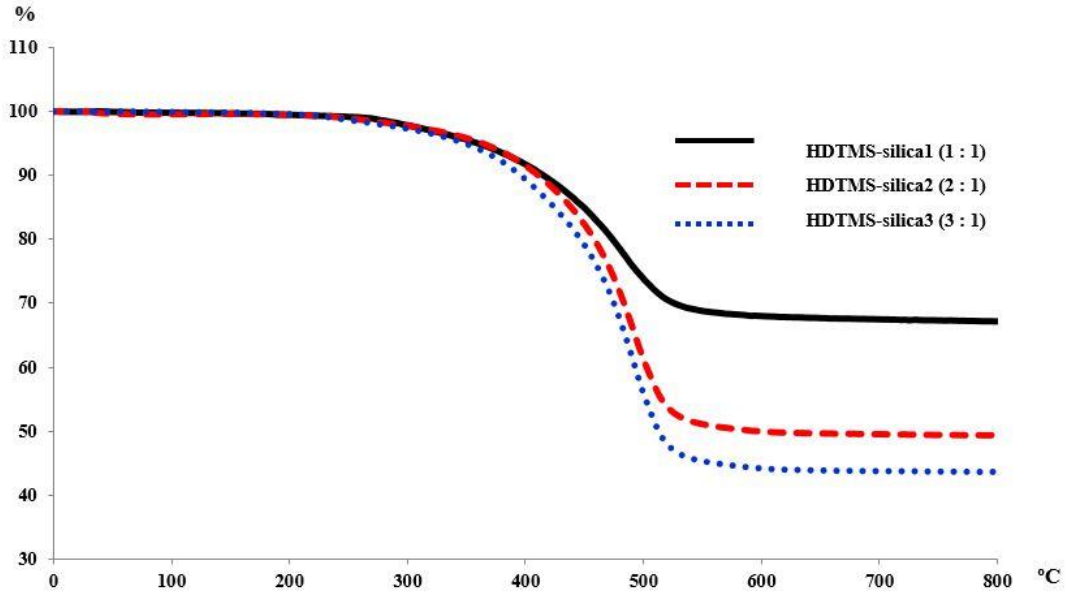


Figure 4.5 TGA thermograms of HDTMS-silica1, HDTMS-silica2 and HDTMS-silica3

The amount of grafting HDTMS was determined by TGA (Figure 4.5). It is found that the percent grafting increases with an increase in HDTMS : $SiO_2$ ratios as follows: 32.95%, 50.55%, 56.37% for 1 : 1, 2 : 1, 3 : 1, respectively

*4.2.3 Functional groups of Aerodisp and HDTMS-Silicas*



Then, HDTMS-silicas were further characterized by FTIR analysis using transmission mode in Figure 4.6. As seen, silica spectrum shows a dominant $SiO_2$ silanol band in a region of 3000-3500 $cm^{-1}$. This absorption band almost disappears from the IR spectra of 1 : 1, and 2 : 1 HDTMS-silicas. At 3 : 1 ratio, this absorption band no longer exists, indicating that full hydrophobicity modification is reached.

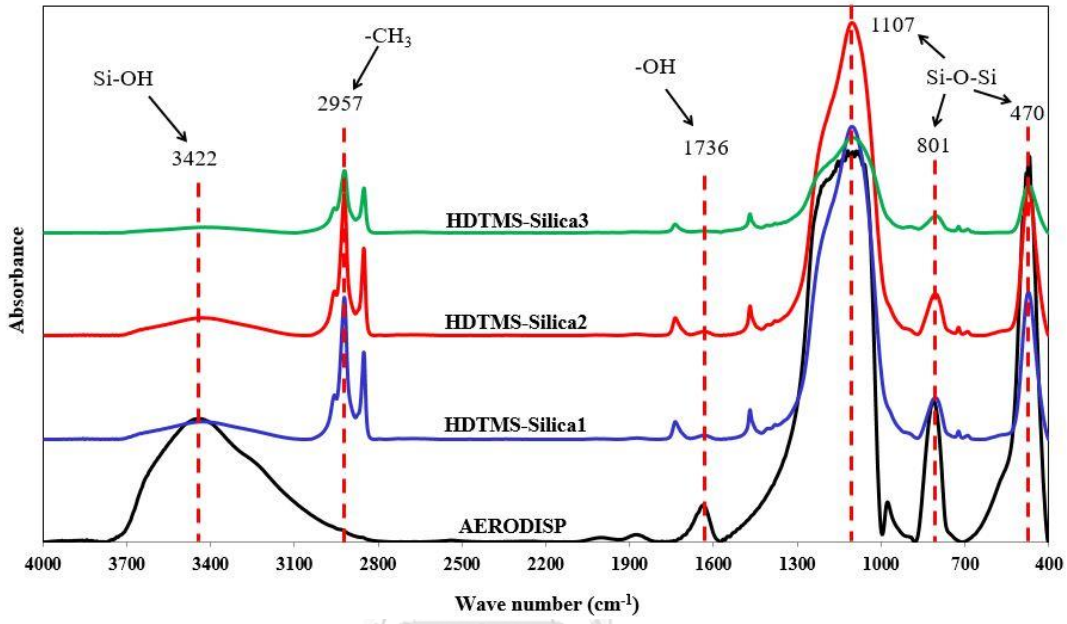


Figure 4.6 FTIR spectra of Aerodisp (Silica) and HDTMS-Silicas

In addition to, the absorption band at 2957 $cm^{-1}$ correspond to the stretching vibration of $–CH_3$ of the HDTMS grafted on the surface of the silica nanoparticles. And the absorption band at 1736 $cm^{-1}$ correspond to the bending vibration of –OH. Moreover, the absorption bands at 470, 801 and 1107 $cm^{-1}$ correspond to the bending vibration, symmetric stretching vibration and asymmetric stretching vibration of Si-O-Si [60, 61]. The functional groups with the wave number of each sample are summarized in Table 4.1

Table 4.1 Functional groups and wave number of Aerodisp and HDTMS-Silicas

| Sample | Wave no. ($cm^{-1}$) | Functional Group |
|---|---|---|
| Aerodisp | 3500-3000 | O-H stretching |
| | 1736 | O-H bending |
| | 1107 | Si-O-Si asymmetric stretching |
| | 801 | Si-O-Si symmetric stretching |
| | 470 | Si-O-Si bending |
| HDTMS-Silicas | 3500-3000 | O-H stretching |
| | 2957 | $-CH_3$ stretching |
| | 1107 | Si-O-Si asymmetric stretching |
| | 801 | Si-O-Si symmetric stretching |
| | 470 | Si-O-Si bending |

*4.2.4 Particle Size Distribution of Silica and HDTMS-Silicas*

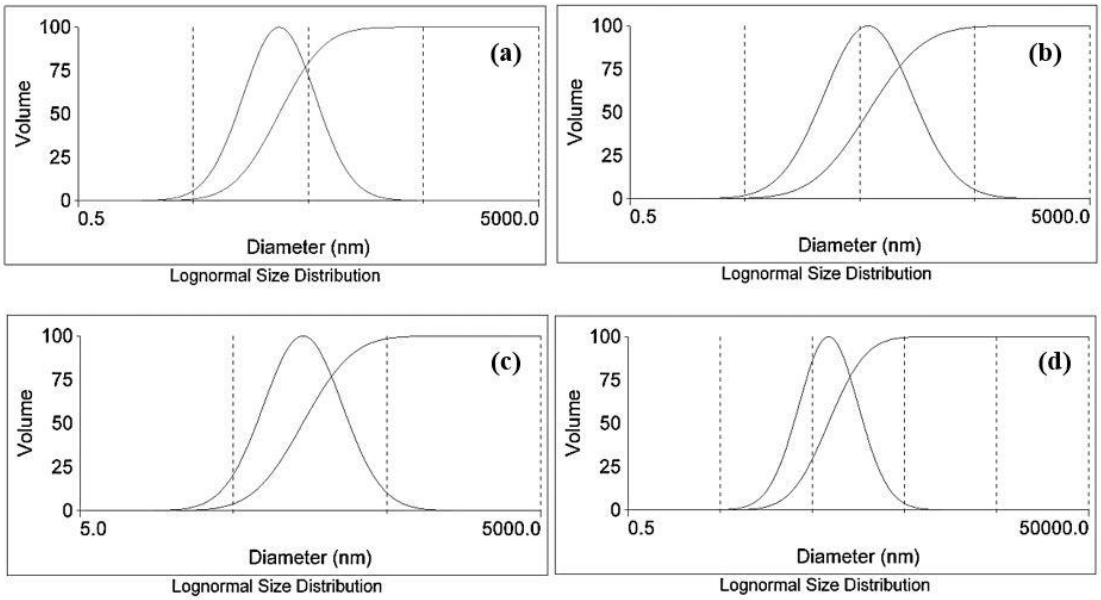


Figure 4.7 Particle size distribution of (a) Silica, (b) HDTMS-Silica1, (c) HDTMS-Silica2 and (d) HDTMS-Silica3

It was anticipated that swelling behavior of HDTMS-silicas was altered, arising from surface hydrophobicity. As seen in Figure 4.4, HDTMS-silicas are well-swollen and well-dispersed in toluene medium. Then, particle size and particle size distribution (PSD) were measured by nano ZetaPLAS particle sizer as shown in Figure 4.7. As found, average particle sizes of silica, HDTMS-silica1, HDTMS-silica2, and HDTMS-silica3 are 36.3, 87.1, 99.6 and 169.0 nm, respectively.

The particle size increases with an increase in HDTMS ratio due to enhanced swellability of HDTMS-silica in toluene medium.

*4.2.5 Morphology of Silica and HDTMS-Silicas*

A stable dispersion of grafted nanomaterials occurs due to the steric repulsion among polymer chains, which arises from the osmotic pressure, and the affinity of surface polymer chains for itself rather than the solvent. The silane functionalized nanoparticles also show better dispersibility in organic solvent or polymer matrix [62]. In fact, the actual size of $SiO_2$ remains unchanged as shown by TEM images (Figure 4.8).

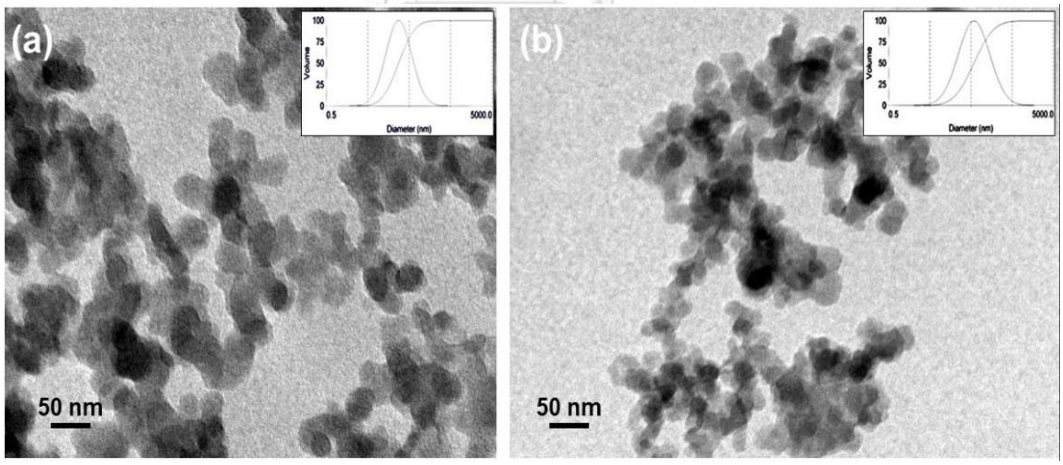


Figure 4.8 Representative TEM images and particle size distribution (a) AERODISP and (b) HDTMS-silica2

4.2.6 The schematic of the condensation reaction between HDTMS and silica

A schematic 1.1 explanation of the condensation reaction between HDTMS silanol group and silica Aerodisp silanol functional group occurred on the surface of silica particle, displayed it hydrophobic. The hydrochloric was required to catalyze the condensation reaction of silanol functional group (Si-OH) to form siloxane bond (Si-O-Si).

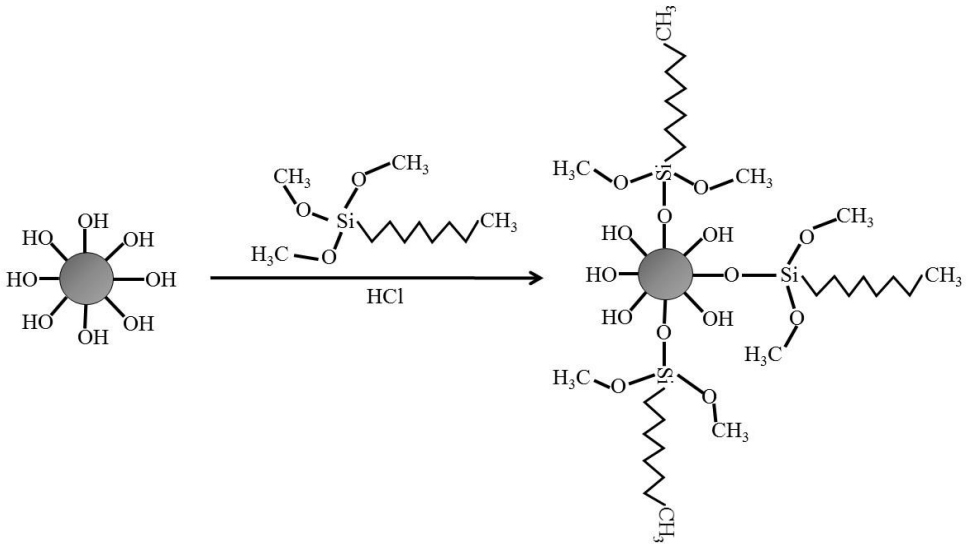


Scheme 4.1 The condensation between HDTMS silanol group and Silica Aearodisp silanol group on the silica surface



**4.3 Characterizations of ABS/HDTMS-silica nanocomposites**

Homogeneous dispersion and distribution of filler particles (such as silica) in polymer matrix is very importance for improvement the mechanical properties of polymer nanocomposites. And the problem in preparation of polymer nanocomposites is poor dispersion and distribution of nanoparticles in polymer matrix. Moreover, the agglomeration is dependent on dispersion of particles in polymer matrix.

On the other hand, the distribution indicates how uniformly the primary nanoparticles are distributed through the volume (Figure 4.9) [63].

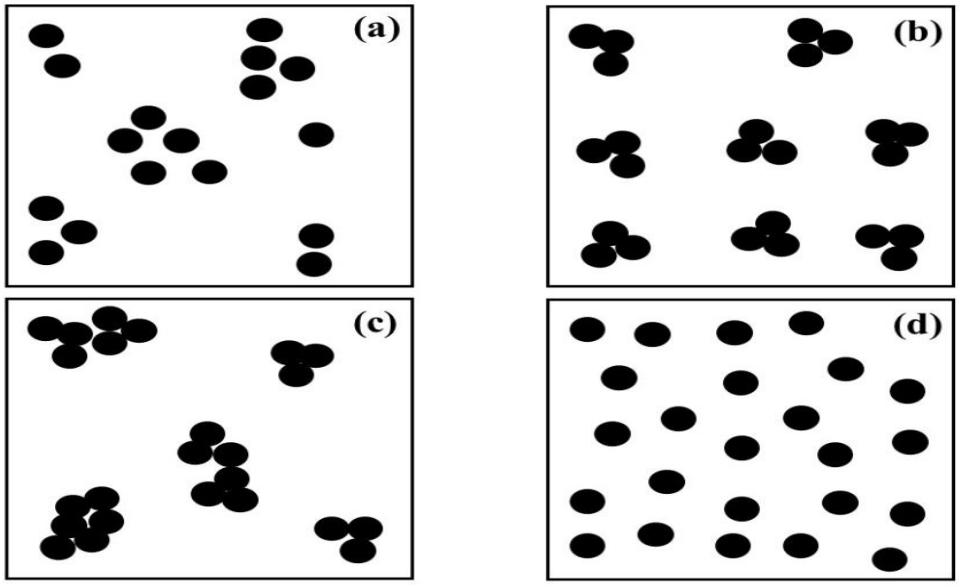


Figure 4.9 Schematic representation of the degree of dispersion and agglomeration of particles in a polymer matrix; (a) dispersion, no agglomeration, (b) poor dispersion, agglomeration, (c) agglomeration, (d) good dispersion, no agglomeration

*4.3.1 Morphology of ABS/HDTMS-silica nanocomposites*



SEM images of ABS/HDTMS-silica nanocomposites are illustrated in Figure 4.10. ABS/HDTMS-silica nanocomposites exhibit spherical shape which is similar in morphology to ABS standard. A variety of particle sizes are found, ranging from 50 nm and 300 nm.

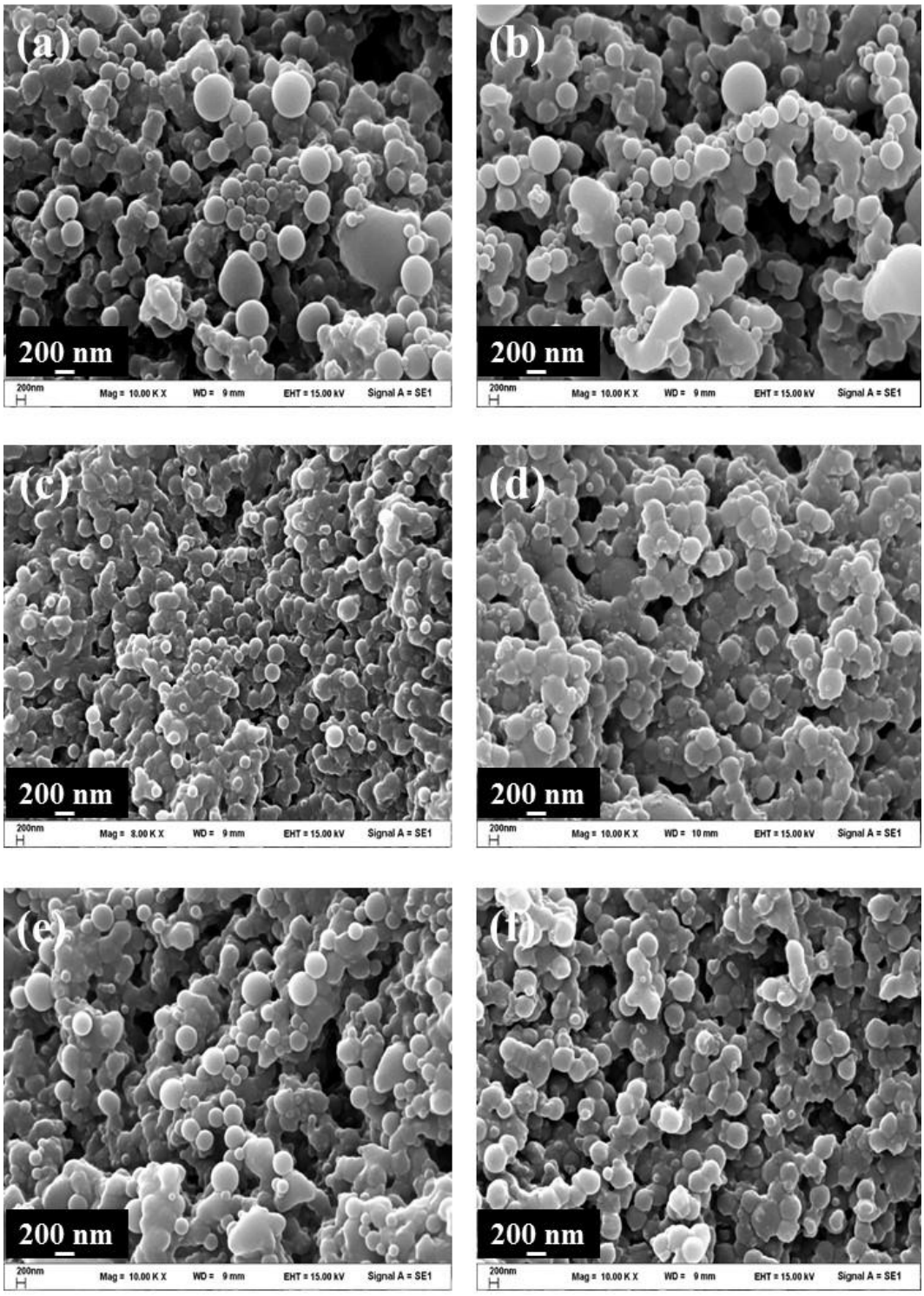


Figure 4.10 Representative SEM images of (a) Neat ABS and ABS/HDTMS-silica nanocomposites having HDTMS-silica contents of (b) 1 wt%, (c) 2 wt%, (d) 3 wt%, (e) 4 wt% and (f) 5 wt%

In addition, elemental mapping by scanning electron microscopy-energy dispersive x-ray spectrometry (SEM-EDS) was analyzed to provide Si mapping and their distribution in ABS matrix. The resultant Si EDX mapping of ABS samples containing 1 wt% HDTMS-silica are presented in Figure 4.11. As seen, AERODISP is not well distributed in ABS matrix due to agglomeration problem, judged by the relatively lower amount of bright spots when compared HDTMS-silicas. In case of HDTMS-silicas, the amount of bright spots exhibiting more uniform distribution is significantly higher, indicating that HDTMS-silicas are compatible with ABS matrix. Particularly, Si EDX mapping of HDTMS-silica2 provides information that HDTMS-$SiO_2$ particles exhibit the most dense and uniform. In case of HDTMS-silica3, the Si EDX mapping shows that the amount of bright spots decreases significantly when compared to HDTMS-silica1 and HDTMS-silica2. In this case, HDTMS : silica ratio is far beyond optimum ratio, leading to a decrease in $SiO_2$ content. Therefore, it was anticipated that HDTMS-silica3 was likely to underperform its impact resistance enhancement when compared to HDTMS-silica2 (see discussion in section 4.3.4.1).

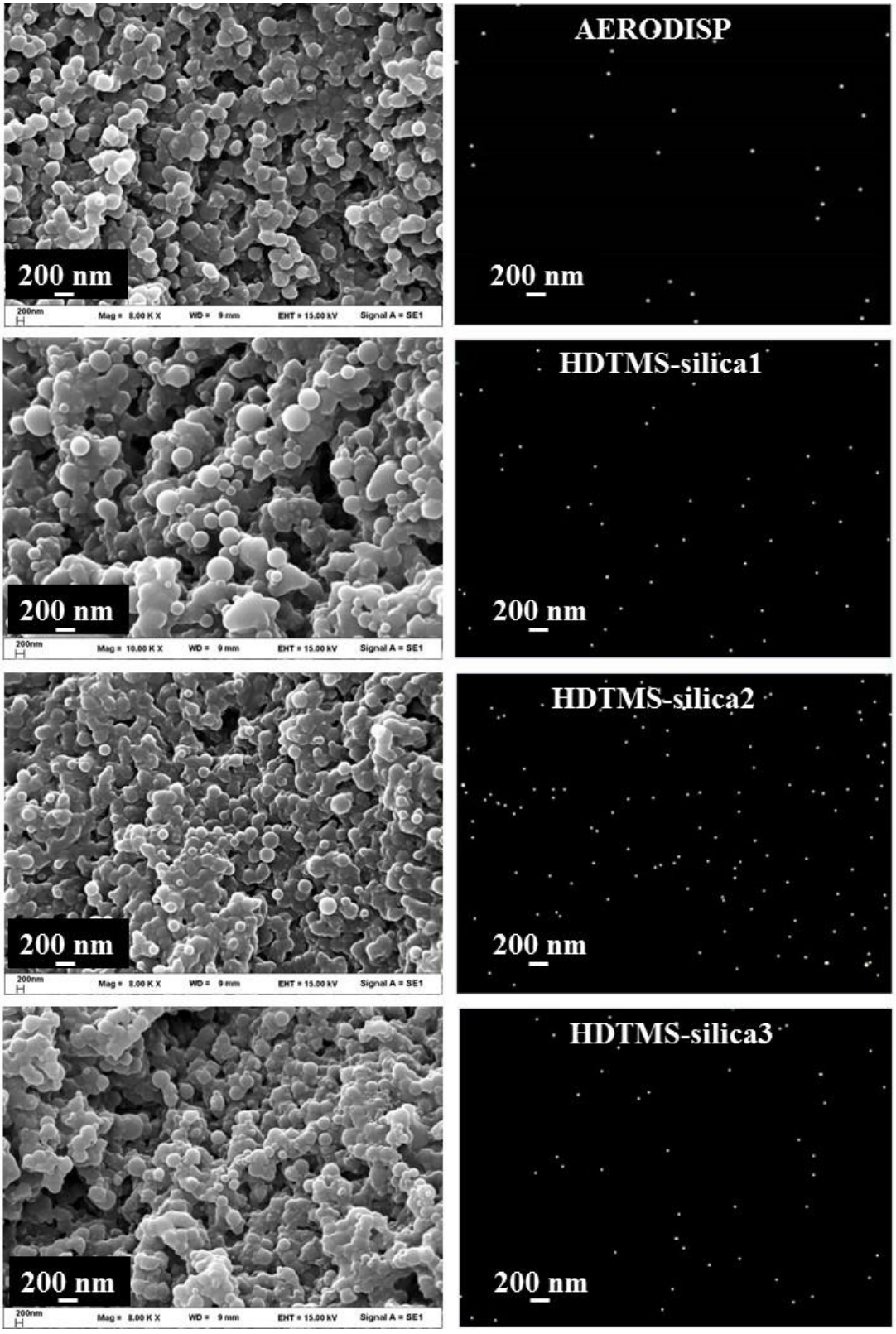


Figure 4.11 Si EDX mapping images of ABS nanocomposites containing 1 wt% filler loading

*4.3.2 Crystal Morphology of ABS/HDTMS-Silica nanocomposites*

In addition, the existence of silica particles embedded in ABS rubber, XRD analysis was employed.

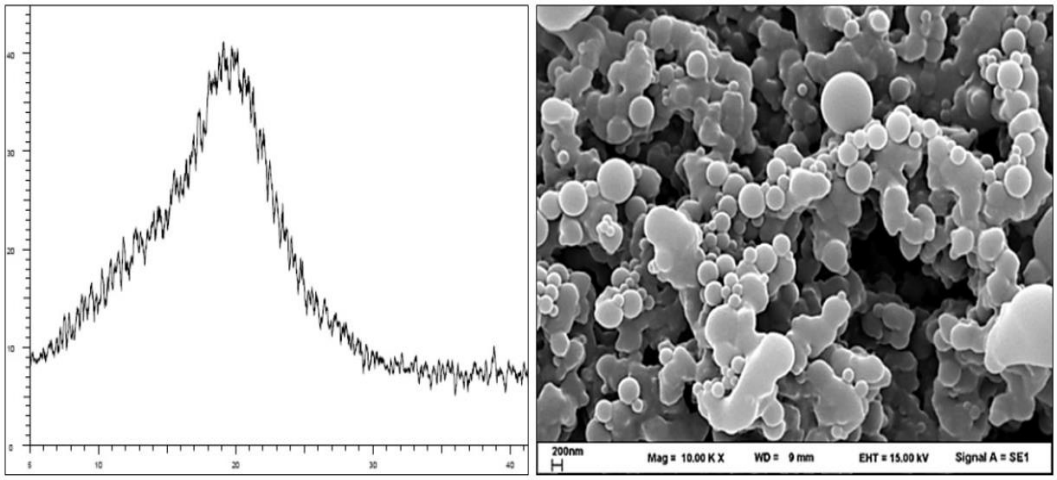


Figure 4.12 XRD pattern of HDTMS-Silica nanoparticles inside ABS rubber.

XRD results (Figure 4.12) show that silica peak at 2θ = 22° is present, indicating that HDTMS-silica nanoparticles were successfully imbedded inside ABS rubber. The strong and broad XRD pattern from 18° to 31° (2θ) of nano silica shows that the prepared nano $SiO_2$ is amorphous [61, 64].

*4.3.3 Thermal stability of ABS/HDTMS-Silica nanocomposites*

The incorporation of nano-inorganic particles into the polymer matrix can enhance thermal stability by acting as a superior thermal insulator and as a mass transport barrier to the volatile products generated during decomposition [62].

It was anticipated that thermal properties of nanocomposites were altered when compared to standard ABS. In this experiment, thermal property of nanocomposites were evaluated using TGA analysis. TG thermograms are presented in Figure 4.13. ABS nanocomposites begins to degrade at 410 °C ($T_{onset}$) which is significantly higher than that of standard ABS, indicating the higher thermal stability of nanocomposites due to the presence of HDTMS-silica nanoparticles. The results confirmed that HDTMS-silica nanoparticles can enhance the thermal stability of ABS

evidenced by the fact that the degradation temperature of ABS composites shifted up by 20 °C when compared to standard ABS.

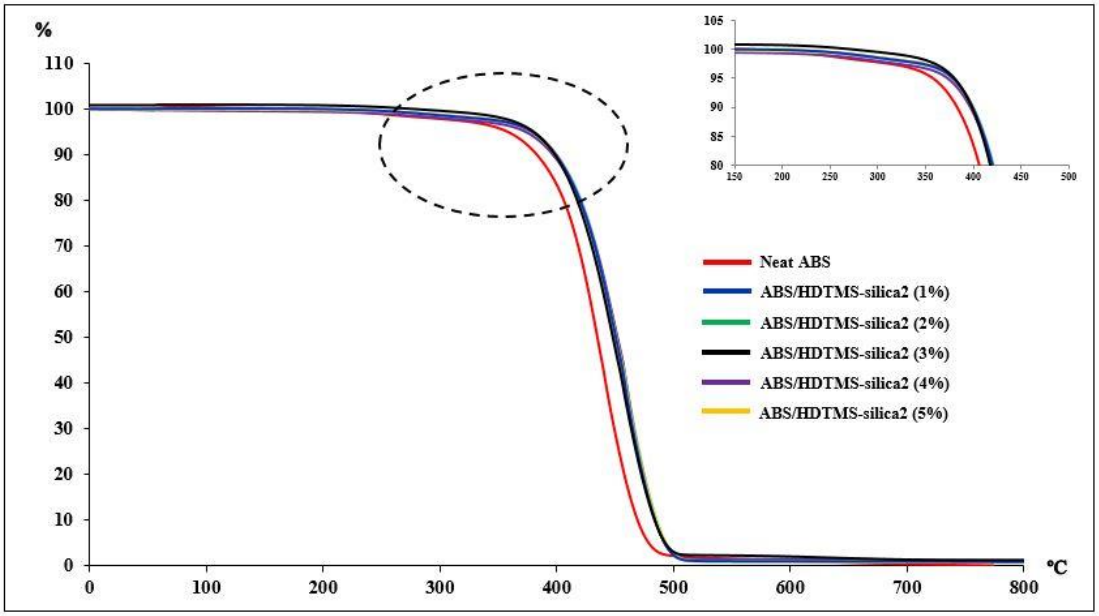


Figure 4.13 TGA thermograms of (-) Neat ABS and ABS/HDTMS-silica Nanocomposites

*4.3.4 Mechanical properties*

The main reason to incorporate the inorganic nanoparticles into polymer matrices is to produce a product with improved mechanical properties (including tensile strength, impact strength, flexural strength, hardness, Young's modulus or stiffness) via reinforcement mechanisms [62].

4.3.4.1 Effect of HDTMS-silica1, HDTMS-silica2, and HDTMS-silica3 on impact strength

It was reported that nanosized rigid particles such as $SiO_2$, $TiO_2$, $CaSiO_3$, $Al_2O_3$, carbon nanotubes and nanoclays were capable of enhancing plastic toughness via energy absorption and dissipation mechanisms. Previous reports showed that incorporation of $SiO_2$ nanoparticles into ABS resulted in an improvement in mechanical properties of hybrid materials including impact strength [4-6, 8, 16, 18-22, 24, 26].

4.3.4.1.1 Impact Strength

In this study, three types of HDTMS-silica nanoparticles (HDTMS-silica1, HDTMS-silica2, and HDTMS-silica3) were incorporated into ABS rubber, resulting in ABS/HDTMS-silica nanocomposite compounds. ABS compounds containing $SiO_2$ nanoparticles were injection molded and then evaluated for impact resistance.

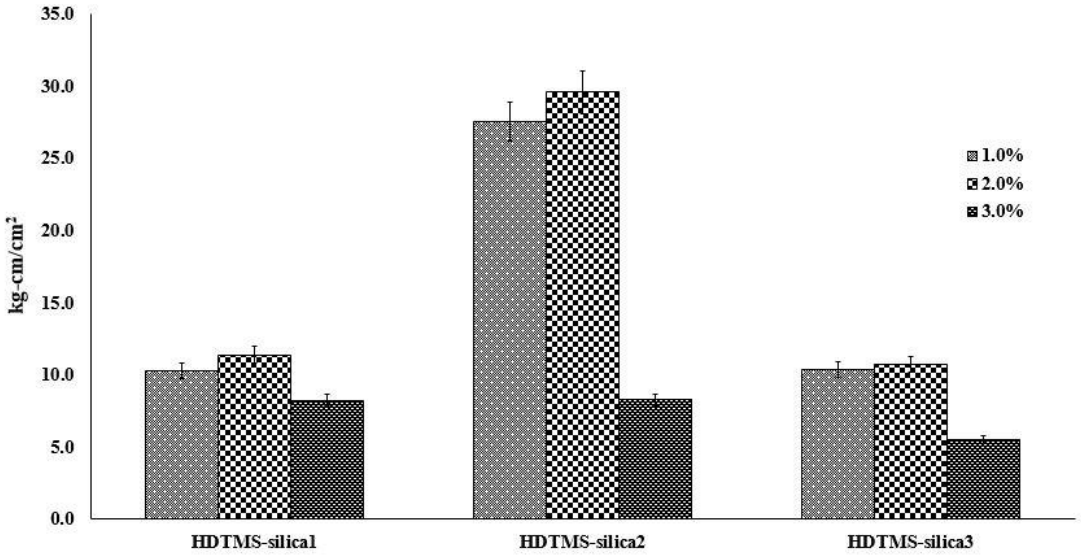


Figure 4.14 Impact strengths of ABS-HDTMS-silica1, HDTMS-silica2, and HDTMS-silica3 at various HDTMS-silica loadings



The results are shown in Figure 4.14. As shown, HDTMS-silica1 significantly underperforms in terms of impact resistance performance when compared to standard ABS. It is understandable that poorer performance of HDTMS-silica1 is associated to those HDTMS-silica1 nanoparticles having imperfect surface modification. As a consequence, the corresponding impact resistance decreases significantly.

For HDTMS-silica2, its impact resistance significantly outperforms standard ABS, deriving from the optimum distribution of $SiO_2$ nanoparticles in ABS as shown in Figure 4.18. However, the percent loading was found to play a role in determining the composite properties (see discussion in section 4.2.2). In case of HDTMS-silica3, the

impact strength notably decrease despite the presence of hydrophobic nanoparticle. It can be explainable that, in this case, the excessive HDTMS ratio suppresses $SiO_2$ energy absorption performance by reducing $SiO_2$ loading content in ABS. The impact strength of ABS/HDTMS-Silica nanocomposites via the HDTMS-Silicas loading are showed in Table 4.2.

Table 4.2 The impact strength of ABS/HDTMS-Silica nanocomposites via the HDTMS-Silicas loading

| %Loading | HDTMS-silica1 | HDTMS-silica2 | HDTMS-silica3 |
|---|---|---|---|
| 1.0% | 10.3±0.1 | 27.6±0.2 | 8.2±0.1 |
| 2.0% | 27.6±0.1 | 29.9±0.2 | 8.3±0.1 |
| 3.0% | 10.4±0.1 | 15.8±0.1 | 5.5±0.1 |

Number of mechanical testing is 5

4.3.4.1.2 Fracture Surface Morphology

Fracture surface images of ABS compounds containing 1 wt% HDTMS-$SiO_2$ were analyzed as shown in Figure 4.15. In all cases, rough fracture surface which is indicative of toughness characteristic of ABS is found in a similar pattern. However, mechanical properties were found varied which was associated to the distribution as well as content of HDTMS-silicas containing in ABS rubber particles.

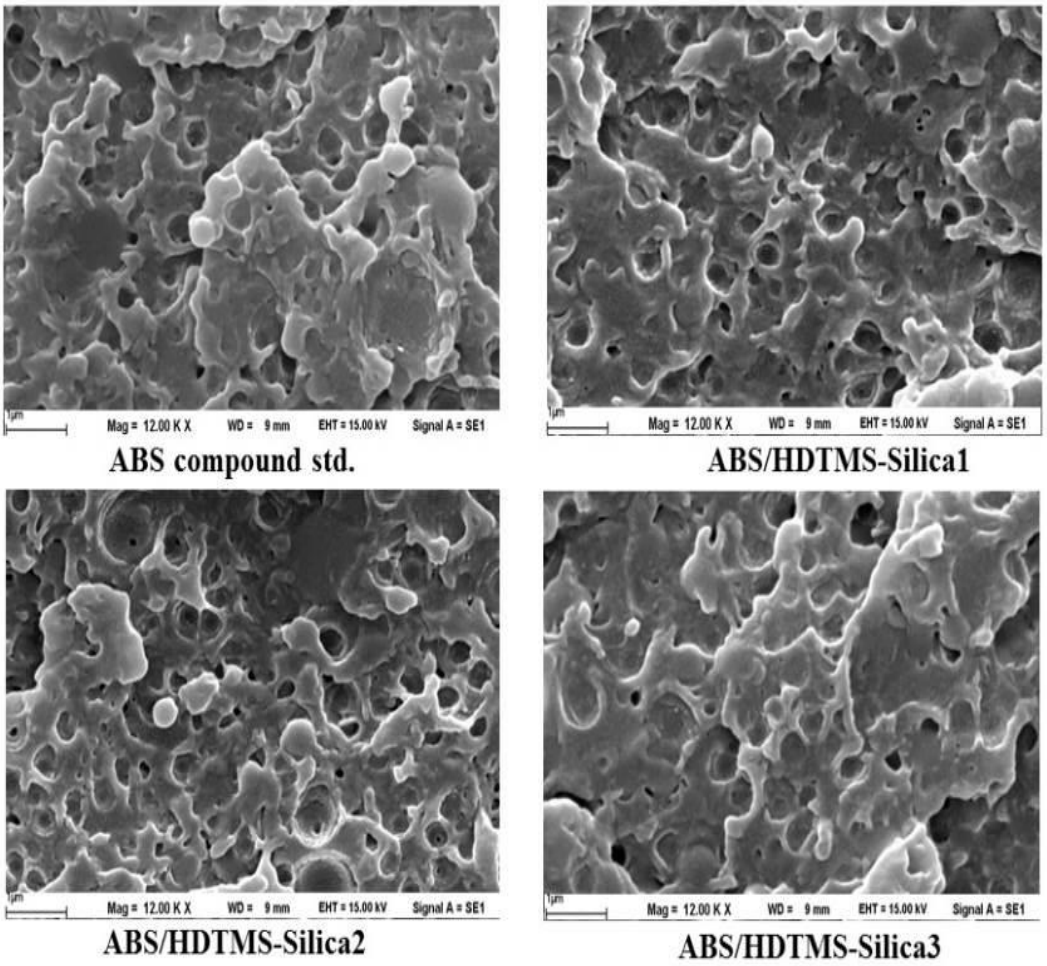


Figure 4.15 Fracture surface morphology of ABS nanocomposite compounds containing 1 wt% HDTMS-silicas



4.3.4.2 Effect of HDTMS-silica2 loading on impact strength of ABS Composites

From Figure 4.16, it is found that the addition of 0.5, 1.0 and 2.0 wt% HDTMS-silica2 nanoparticles raises the impact resistance by 3.89%, 19.48%, and 29.44% respectively. Then, the values gradually decrease by 32.03%, 64.10%, and 70.13% at filler loadings of 3%, 4%, and 5%, respectively due to an agglomeration of filler particles. The improved impact resistance is indicative of the compatibility between filler and matrix. This means that hydrophobic nanoparticles play a key role in improving the properties of ABS composites. In this case, the surface modification of

silica nanoparticles by organosilane led to hydrophobic HDTMS-silica nanoparticles which then enhance compatibility as well as interfacial adhesion. As consequence, impact resistance is improved due to the enhancement of toughness. In contrast, the virgin silica particles fail to improve the toughness of ABS compound and the impact resistance dramatically drops approximately by 20.78% when compared to ABS standard. This result is indicative of the poorer interfacial adhesion due to the incompatibility between hydrophilic silica particles and hydrophobic SAN matrix. The impact strength of ABS/HDTMS-Silica nanocomposites are showed in Table 4.3.

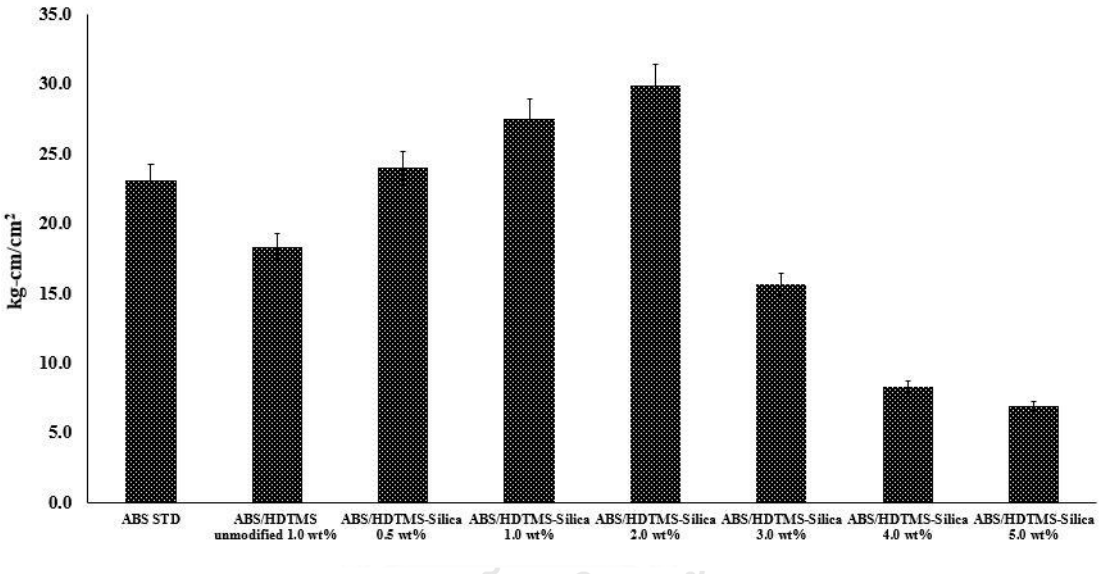


Figure 4.16 Representative impact strengths of neat ABS and ABS/HDTMS-silica2 at various HDTMS-silica2 loadings

Table 4.3 The Impact strength of ABS STD and ABS/HDTMS-Silica2 nanocomposites

| Sample | Impact strength (kg-cm/cm$^2$) |
|---|---|
| ABS STD | 23.1±0.1 |
| ABS/HDTMS unmodified 1.0 wt% | 18.3±0.3 |
| ABS/HDTMS-Silica2 0.5 wt% | 24.0±0.3 |
| ABS/HDTMS-Silica2 1.0 wt% | 27.6±0.2 |
| ABS/HDTMS-Silica2 2.0 wt% | 29.6±0.3 |
| ABS/HDTMS-Silica2 3.0 wt% | 15.7±0.2 |
| ABS/HDTMS-Silica2 4.0 wt% | 8.3±0.1 |
| ABS/HDTMS-Silica2 5.0 wt% | 6.9±0.1 |

Number of mechanical testing is 5

4.3.4.3 Effect of HDTMS-silica2 loading on tensile strength of ABS Composites

In addition to impact resistance, tensile properties are evaluated and shown in Figure 4.17. In comparison with standard ABS, the tensile strength value of nanocomposites gradually increases by 0.24%, 4.04%, and 6.42% for HDTMS-silica loadings of 0.5, 1.0 and 2.0 wt% respectively. Then, the values are gradually reduced by 4.71%, 15.89%, 23.79% at filler loadings of 3%, 4%, and 5%, respectively. The results are found in a similar trend to those of impact strength values. The tensile strength of ABS/HDTMS-Silica nanocomposites are showed in Table 4.4.

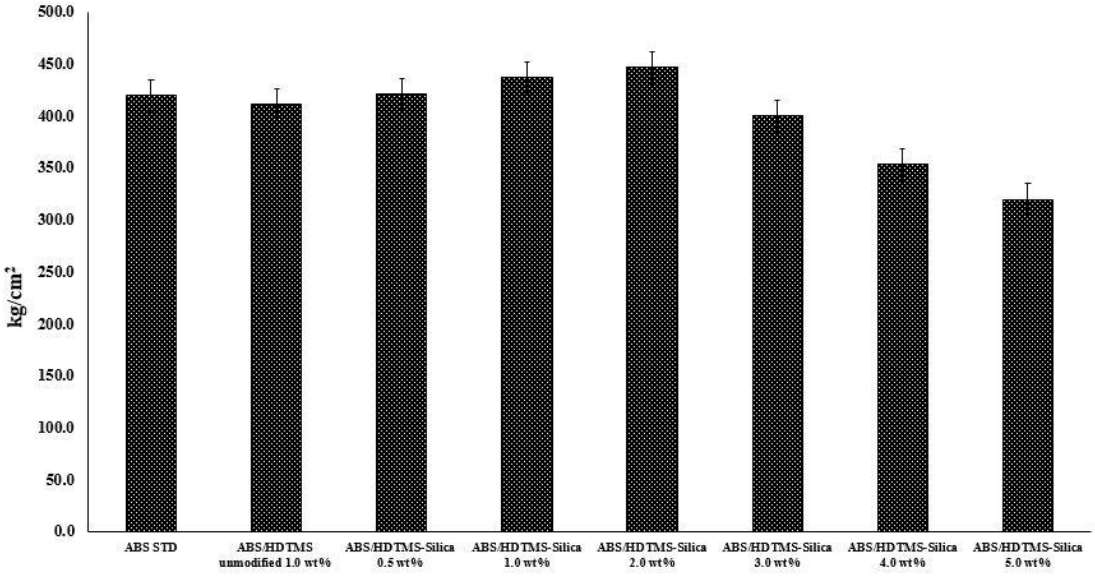


Figure 4.17 Representative tensile strengths of neat ABS and ABS/HDTMS-silica2 at various HDTMS-silica2 loadings

Table 4.4 The tensile strength of ABS STD and ABS/HDTMS-Silica2 nanocomposites

| Sample | Tensile strength (kg/cm$^2$) |
|---|---|
| ABS STD | 420.3±0.8 |
| ABS/HDTMS unmodified 1.0 wt% | 411.3±0.4 |
| ABS/HDTMS-Silica2 0.5 wt% | 421.3±0.8 |
| ABS/HDTMS-Silica2 1.0 wt% | 437.3±0.4 |
| ABS/HDTMS-Silica2 2.0 wt% | 447.3±0.4 |
| ABS/HDTMS-Silica2 3.0 wt% | 400.5±0.5 |
| ABS/HDTMS-Silica2 4.0 wt% | 353.5±0.5 |
| ABS/HDTMS-Silica2 5.0 wt% | 320.3±0.8 |

Number of mechanical testing is 5.

4.3.4.4 Effect of HDTMS-silica2 loading on flexural strength of ABS Composites

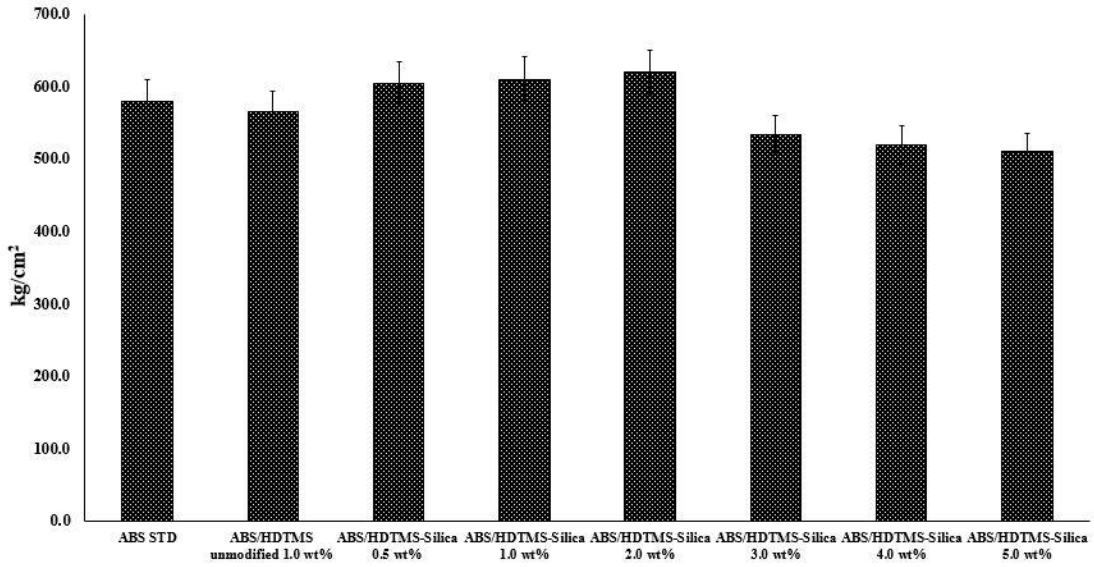


Figure 4.18 Representative flexural strengths of neat ABS and ABS/HDTMS-silica2 at various HDTMS-silica2 loadings

Flexural strengths are shown in Figure 4.18. When compared to standard ABS, the flexural strength value of nanocomposites gradually increases by 4.10%, 5.25%, and 6.94% for HDTMS-silica loadings of 0.5, 1.0 and 2.0 wt% respectively. Then, the values are gradually reduced by 7.95%, 10.34%, 12.06% at filler loadings of 3%, 4%, and 5%, respectively. The results are found in a similar trend to those of impact strength values as well as flexural strength values. These finding properties provide solid evidence that hydrophobicity modification of hydrophilic silica nanoparticle is a crucial strategy in order to achieve a noticeable improvement in mechanical properties of ABS. The flexural strength of ABS/HDTMS-Silica nanocomposites are showed in Table 4.5.

Table 4.5 The flexural strength of ABS STD and ABS/HDTMS-Silica2 nanocomposites

| Sample | Flexural strength (kg/cm$^2$) |
|---|---|
| ABS STD | 580.5±0.5 |
| ABS/HDTMS unmodified 1.0 wt% | 565.5±0.5 |
| ABS/HDTMS-Silica2 0.5 wt% | 604.3±0.8 |
| ABS/HDTMS-Silica2 1.0 wt% | 611.0±0.7 |
| ABS/HDTMS-Silica2 2.0 wt% | 620.8±0.4 |
| ABS/HDTMS-Silica2 3.0 wt% | 534.3±0.4 |
| ABS/HDTMS-Silica2 4.0 wt% | 520.5±0.5 |
| ABS/HDTMS-Silica2 5.0 wt% | 510.5±0.5 |

Number of mechanical testing is 5.

## 4.4 Characterizations of HDTMS-$SiO_2$ nanoparticles prepared by precipitation technique

### *4.4.1 Morphology of HDTMS-$SiO_2$ nanoparticles*

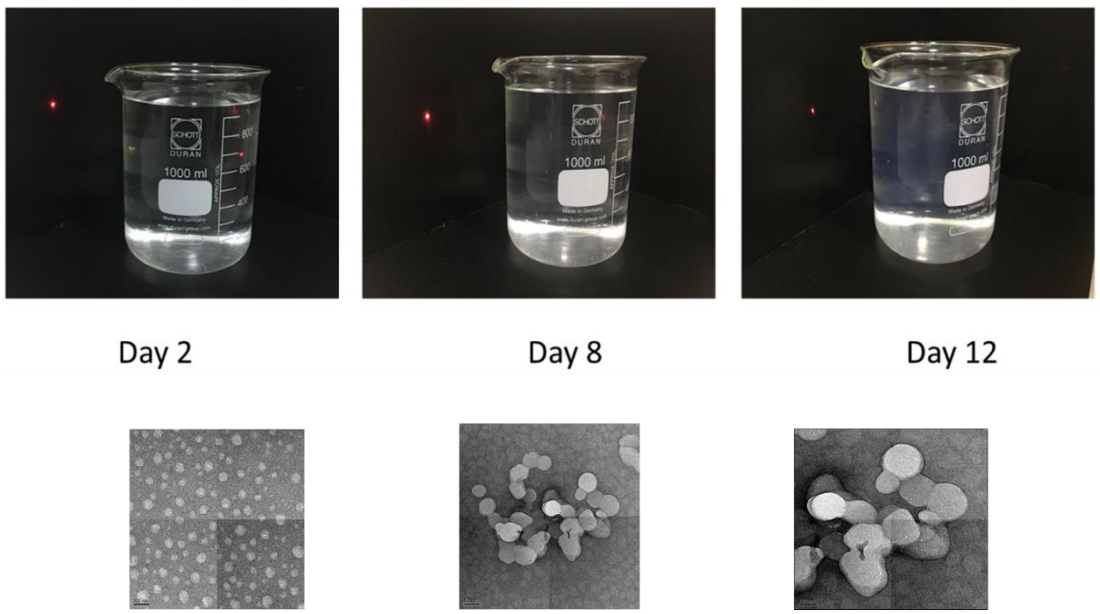


Figure 4.19 TEM images of $SiO_2$ nanoparticles

From Figure 4.19 shows representative TEM image of HDTMS-$SiO_2$ nanoparticles prepared by precipitation of sodium silicate. The image reveals both primary particle and agglomerate. A primary particle diameter and an agglomerate diameter are found 150 - 250 nm and 400 - 600 nm, respectively. The optimum conditions to achieve nanosized ranges of particle sizes with minimum agglomeration are as follows: silicate concentration below 55 g/L, pH values between 1-2, room temperature and reaction time of 12 days. Longer reaction time than 12 days led to the formation of silica gel.

*4.4.2 Izod impact strength of ABS/HDTMS-$SiO_2$ nanocomposite*

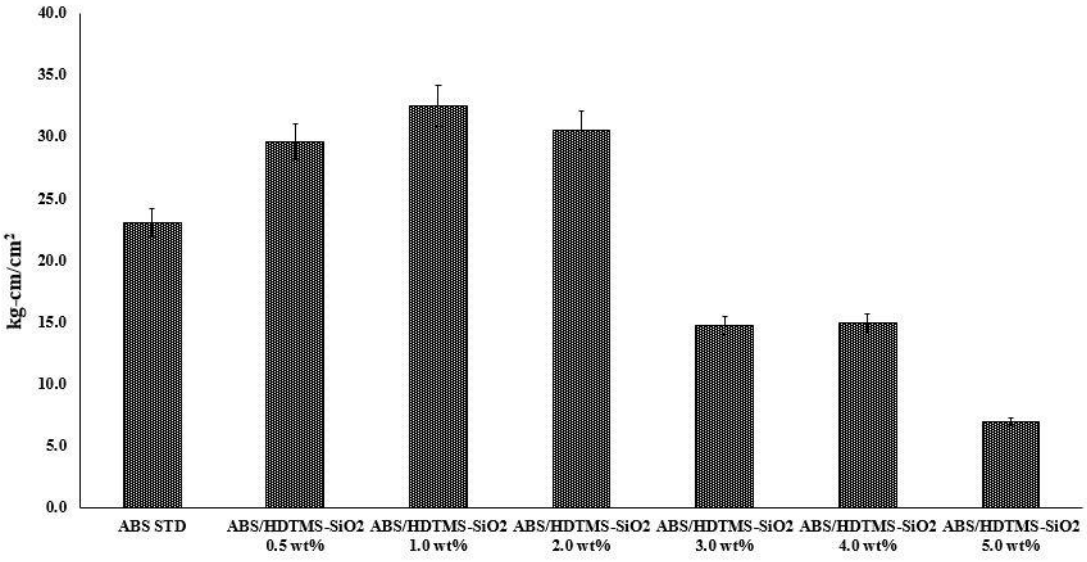


Figure 4.20 Representative impact strengths of neat ABS and ABS/HDTMS-$SiO_2$ at various HDTMS-$SiO_2$ loadings

From Figure 4.20, it is found that the addition of 0.5, 1.0 and 2.0 wt% HDTMS-$SiO_2$ nanoparticles raises the impact resistance by 28.14%, 40.69%, and 32.46% respectively. Then, the values gradually decrease by 36.36%, 35.10%, and 69.70% at filler loadings of 3%, 4%, and 5%, respectively due to an agglomeration of filler particles. Therefore, the surface modification of $SiO_2$ nanoparticles by organosilane led to hydrophobic HDTMS-$SiO_2$ nanoparticles which then enhance compatibility as well as interfacial adhesion between filler and matrix. The impact strength of ABS/HDTMS-$SiO_2$ nanocomposites are showed in Table 4.6.

Table 4.6 The impact strength of ABS STD and ABS/HDTMS-$SiO_2$ nanocomposites

| Sample | Impact strength (kg-cm/$cm^2$) |
|---|---|
| ABS STD | 23.1±0.1 |
| ABS/HDTMS-$SiO_2$ 0.5 wt% | 29.6±0.3 |
| ABS/HDTMS-$SiO_2$ 1.0 wt% | 32.5±0.4 |
| ABS/HDTMS-$SiO_2$ 2.0 wt% | 30.6±0.3 |
| ABS/HDTMS-$SiO_2$ 3.0 wt% | 14.7±0.3 |
| ABS/HDTMS-$SiO_2$ 4.0 wt% | 15.0±0.4 |
| ABS/HDTMS-$SiO_2$ 5.0 wt% | 7.0±0.3 |

Number of mechanical testing is 5.

*4.4.3 Tensile strength of ABS/HDTMS-$SiO_2$ nanocomposite*

In addition to impact resistance, tensile properties are evaluated and shown in Figure 4.21. In comparison with standard ABS, the tensile strength value of nanocomposites when compared to standard ABS gradually increases by 13.65%, 8.94%, and 3.65% for HDTMS-$SiO_2$ loadings of 0.5, 1.0 and 2.0 wt% respectively. Then, the values are gradually reduced by 1.58%, 2.30%, 3.44% at filler loadings of 3%, 4%, and 5%, respectively. The results are found in a similar trend of impact strength values. The tensile strength of ABS/HDTMS-$SiO_2$ nanocomposites are showed in Table 4.7.

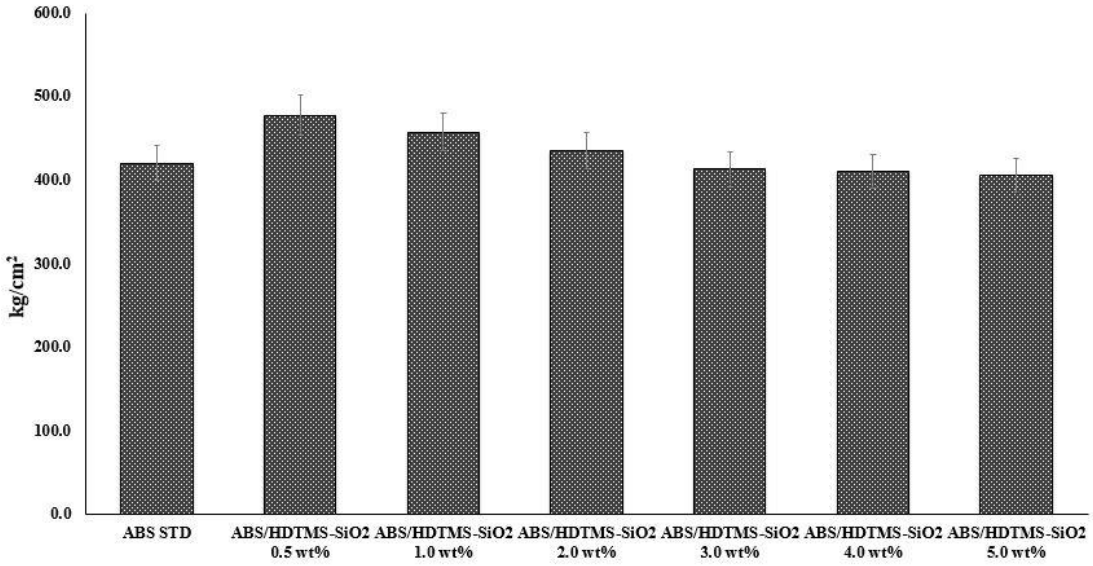


Figure 4.21 Representative tensile strengths of neat ABS and ABS/HDTMS-$SiO_2$ at various HDTMS-$SiO_2$ loadings

Table 4.7 The tensile strength of ABS STD and ABS/HDTMS-$SiO_2$ nanocomposites

| Sample | Tensile strength (kg/cm$^2$) |
|---|---|
| ABS STD | 420.3±0.8 |
| ABS/HDTMS-$SiO_2$ 0.5 wt% | 477.6±0.8 |
| ABS/HDTMS-$SiO_2$ 1.0 wt% | 457.8±0.8 |
| ABS/HDTMS-$SiO_2$ 2.0 wt% | 435.6±0.5 |
| ABS/HDTMS-$SiO_2$ 3.0 wt% | 413.6±0.5 |
| ABS/HDTMS-$SiO_2$ 4.0 wt% | 410.6±0.5 |
| ABS/HDTMS-$SiO_2$ 5.0 wt% | 405.8±0.8 |

Number of mechanical testing is 5.

*4.4.4 Flexural strength of ABS/HDTMS-$SiO_2$ nanocomposite*

Flexural strengths are shown in Figure 4.22. When compared to standard ABS, the flexural strength value of nanocomposites gradually increases by 8.63%, 8.22 %, and 8.11% for HDTMS-$SiO_2$ loadings of 0.5, 1.0 and 2.0 wt% respectively. Then, the values are gradually reduced by 1.71%, 3.46%, 5.01% at filler loadings of 3%, 4%, and 5%, respectively. The results are found in a similar trend to those of impact strength values as well as flexural strength values. The flexural strength of ABS/HDTMS-$SiO_2$ nanocomposites are showed in Table 4.8.

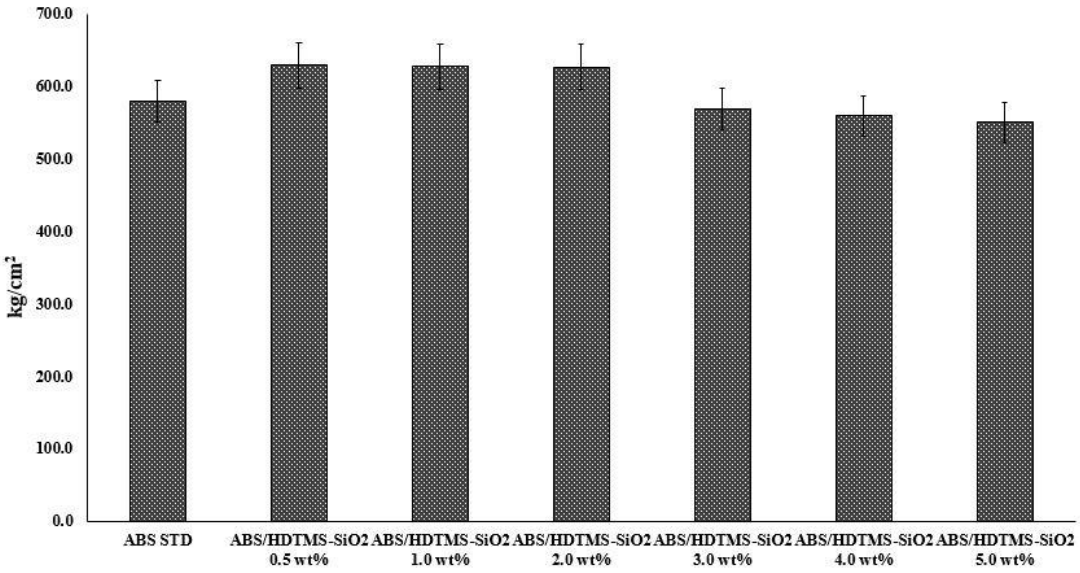


Figure 4.22 Representative flexural strengths of neat ABS and ABS/HDTMS-$SiO_2$ at various HDTMS-$SiO_2$ loadings

Table 4.8 The flexural strength of ABS STD and ABS/HDTMS-$SiO_2$ nanocomposites

| Sample | Flexural strength ($kg/cm^2$) |
|---|---|
| ABS STD | 580.5±0.5 |
| ABS/HDTMS-$SiO_2$ 0.5 wt% | 630.6±0.5 |
| ABS/HDTMS-$SiO_2$ 1.0 wt% | 628.2±0.8 |
| ABS/HDTMS-$SiO_2$ 2.0 wt% | 627.6±0.8 |
| ABS/HDTMS-$SiO_2$ 3.0 wt% | 570.6±0.8 |
| ABS/HDTMS-$SiO_2$ 4.0 wt% | 560.4±0.5 |
| ABS/HDTMS-$SiO_2$ 5.0 wt% | 551.4±0.8 |

Number of mechanical testing is 5.

**PART II: Preparation of PLA/ABS-*g*-MAA and PLA/ABS$^{Si}$-g-MAA blends and properties investigation**

It was reported that polymers having low *Tg* including natural rubber, poly(**ε**-caprolactone) [39, 40], poly(ethylene oxide) [41, 42], poly(butylene succinate) [44, 45], poly(butylene adipate-co-terephthalate)(PBAT) [48], polyurethane [49, 50], poly(vinyl acetate-co-vinyl alcohol) (PVA) [51] or polyisoprene [52] were able to toughen poly(lactic acid). However, these polymers tend to have a negative effect on tensile strength property. Reaction at the interphase flavors interfacial adhesion between two phases, resulting in an increase in both toughness and tensile strength. ABS rubber, an impact modifier, is capable of enhancing impact resistance of PLA through energy absorption and energy dissipation. However, PLA and ABS has different surface energy, resulting in incompatible mixing. The reaction mechanism was proposed as shown in Scheme 4.2.

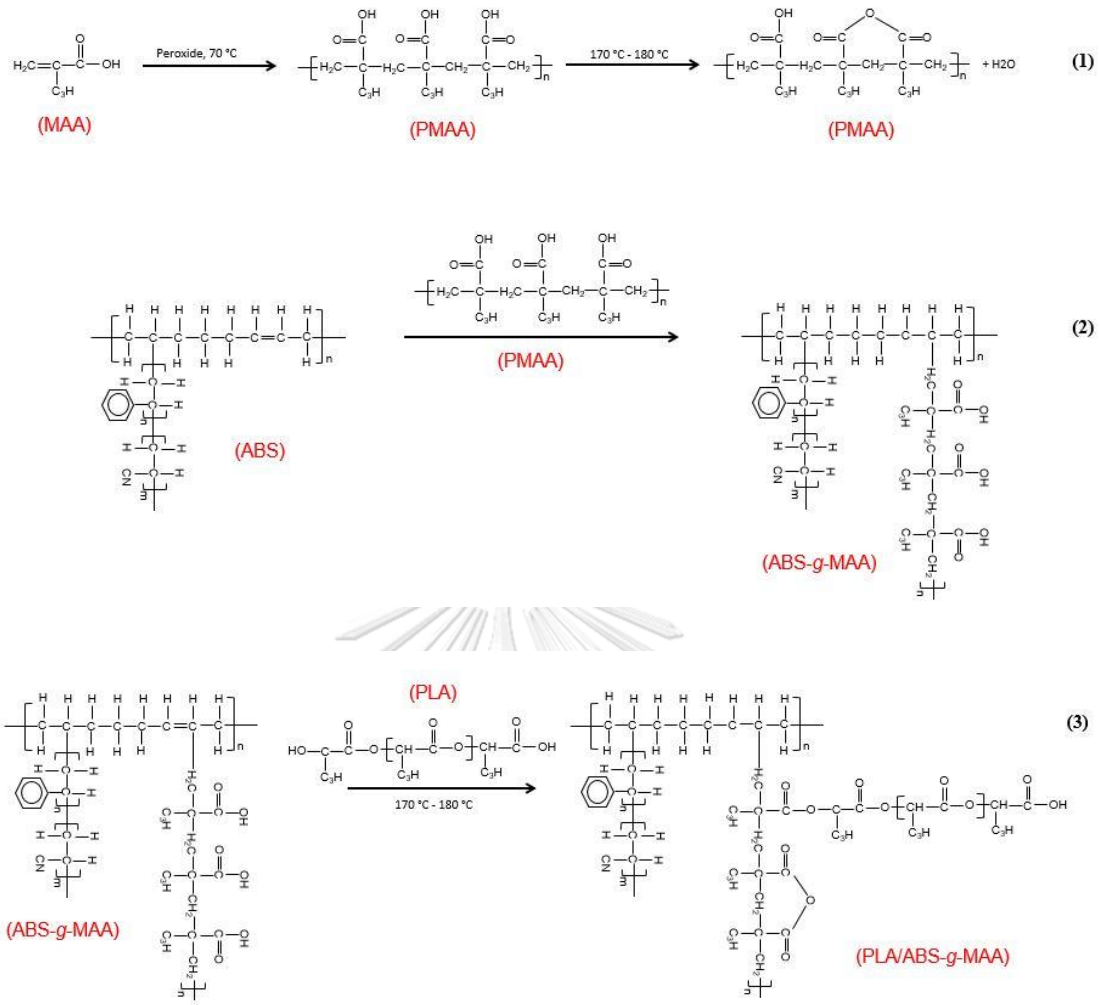


Scheme 4.2 Grafting reaction between ABS rubber and MAA to produce ABS-*g*-MAA



In this work, grafting of PLA onto ABS particle surface was carried out in order to obtain ABS-*g*-MAA.

## 4.1 Mechanical Properties of PLA/ABS-*g*-MAA and PLA/ABS$^{Si}$-*g*-MAA blends

### *4.1.1 Impact strength of PLA/ABS-g-MAA and PLA/ABS$^{Si}$-g-MAA blends*

PLA/ABS-*g*-MAA and PLA/ABS$^{Si}$-*g*-MAA blends were prepared and evaluated for mechanical properties. Impact strength of PLA/ABS-*g*-MAA blends was shown in Figure 4.23. As shown, control sample exhibits slight decrease in impact strength deriving from incompatible characteristic of different polymers. For PLA/ABS-*g*-MAA blends,

impact resistance values significantly outperform neat PLA by 60%, 87%, and 150% for PLA/ABS-*g*-MAA 10 wt%, PLA/ABS-*g*-MAA 20 wt%, and PLA/ABS-*g*-MAA 30 wt%, respectively. The impact strength of PLA, PLA/ABS and PLA/ABS-*g*-MAA are showed in Table 4.9.

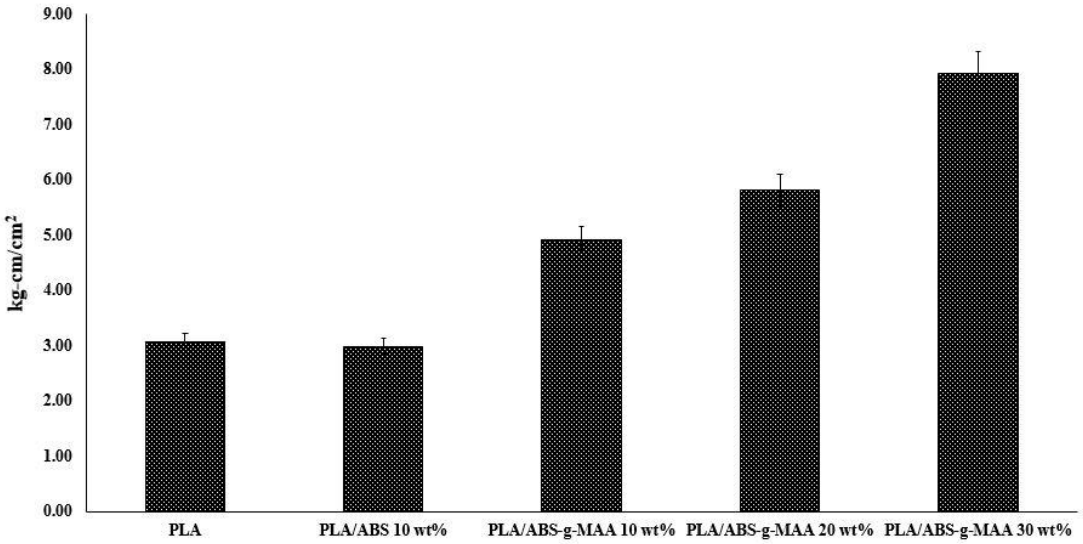


Figure 4.23 Representative of the impact strength of PLA, PLA/ABS and PLA/ABS-*g*-MAA

Table 4.9 The impact strength of PLA, PLA/ABS and PLA/ABS-*g*-MAA

| Sample | Impact strength (kg-cm/cm$^2$) |
|---|---|
| PLA | 3.08±0.1 |
| PLA/ABS 10 wt% | 2.99±0.1 |
| PLA/ABS-*g*-MAA 10 wt% | 4.92±0.5 |
| PLA/ABS-*g*-MAA 20 wt% | 5.81±0.1 |
| PLA/ABS-*g*-MAA 30 wt% | 7.92±0.3 |

Number of mechanical testing is 5.

For PLA/ABS$^{Si}$-*g*-MAA blends, impact strength was shown in Figure 4.24. Impact resistance values significantly outperform neat PLA by 56%, 69% and 101% for PLA/ABS$^{Si}$-*g*-MAA 10 wt%, PLA/ABS$^{Si}$-*g*-MAA 20 wt% and PLA/ABS$^{Si}$-*g*-MAA 30 wt%, respectively. A significant increase in impact strength is contributable to ABS rubber

which exhibited good interfacial adhesion. The impact strength is dependent on the percent loading of ABS-*g*-MAA and ABS$^{Si}$-*g*-MAA; the more the PLA/ABS-*g*-MAA and PLA/ABS$^{Si}$-*g*-MAA the higher the impact strength value. The impact strength of PLA, PLA/ABS$^{Si}$ and PLA/ABS$^{Si}$-*g*-MAA are showed in Table 4.10.

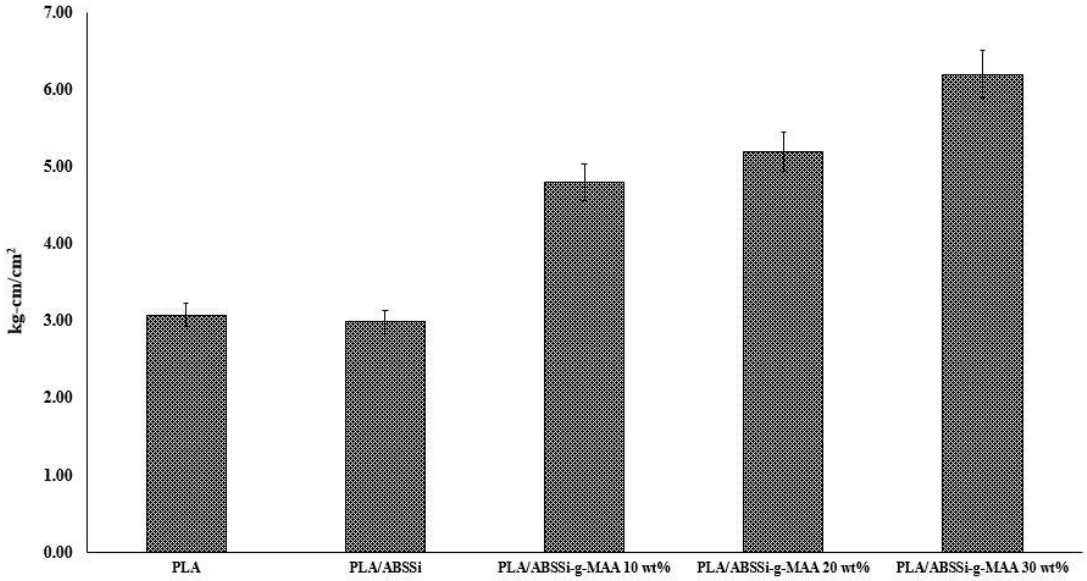


Figure 4.24 Representative of the impact strength of PLA, PLA/ABS$^{Si}$ and PLA/ABS$^{Si}$-*g*-MAA

Table 4.10 The impact strength of PLA, PLA/ABS$^{Si}$ and PLA/ABS$^{Si}$-*g*-MAA

| Sample | Impact strength (kg-cm/cm$^2$) |
|---|---|
| PLA | 3.08±0.1 |
| PLA/ABS$^{Si}$ 10 wt% | 2.99±0.1 |
| PLA/ABS$^{Si}$-*g*-MAA 10 wt% | 4.80±0.5 |
| PLA/ABS$^{Si}$-*g*-MAA 20 wt% | 5.20±0.1 |
| PLA/ABS$^{Si}$-*g*-MAA 30 wt% | 6.20±0.3 |

Number of mechanical testing is 5.

*4.1.2 Tensile strength of PLA/ABS-g-MAA and PLA/ABS$^{Si}$-g-MAA blends blends*

In a similar manner, tensile strength increases when loaded with PLA/ABS-*g*-MAA and PLA/ABS$^{Si}$-*g*-MAA albeit at lesser effect (Figure 4.25 and Figure 4.26). These results implies that PLA/ABS-*g*-MAA and PLA/ABS$^{Si}$-*g*-MAA acts as an effective impact modifier when compared to reinforcing role. The tensile strength of PLA, PLA/ABS and PLA/ABS-*g*-MAA are showed in Table 4.11 and PLA, PLA/ABS$^{Si}$ and PLA/ABS$^{Si}$-*g*-MAA are showed in Table 4.12.

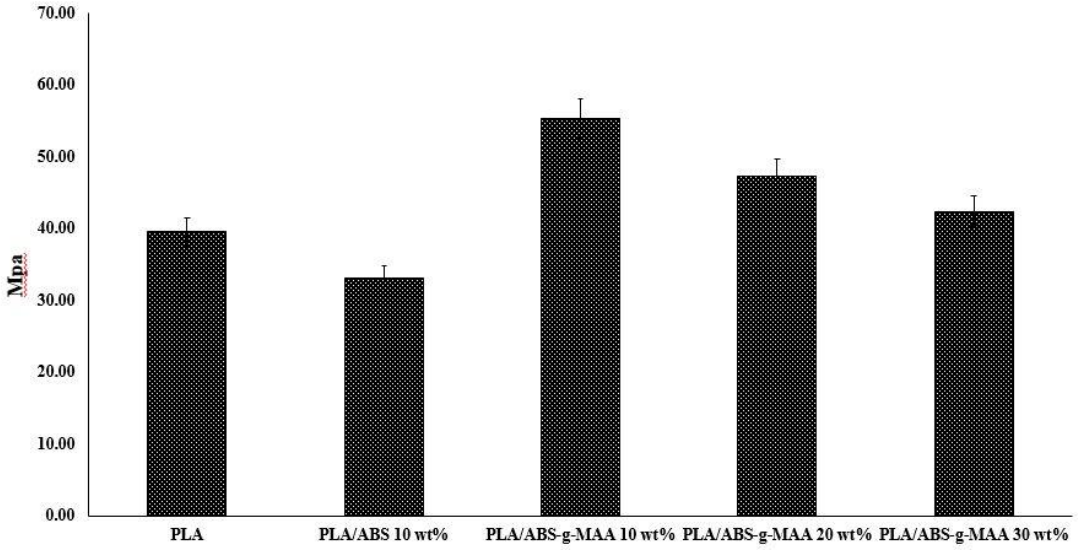


Figure 4.25 Representative of the tensile strength of PLA, PLA/ABS and PLA/ABS-*g*-MAA



Table 4.11 The tensile strength of PLA, PLA/ABS and PLA/ABS-*g*-MAA

| Sample | Tensile strength (MPa) |
|---|---|
| PLA | 39.56±0.1 |
| PLA/ABS 10 wt% | 33.18±0.1 |
| PLA/ABS-*g*-MAA 10 wt% | 55.34±0.1 |
| PLA/ABS-*g*-MAA 20 wt% | 47.36±0.5 |
| PLA/ABS-*g*-MAA 30 wt% | 42.42±0.5 |

Number of mechanical testing is 5.

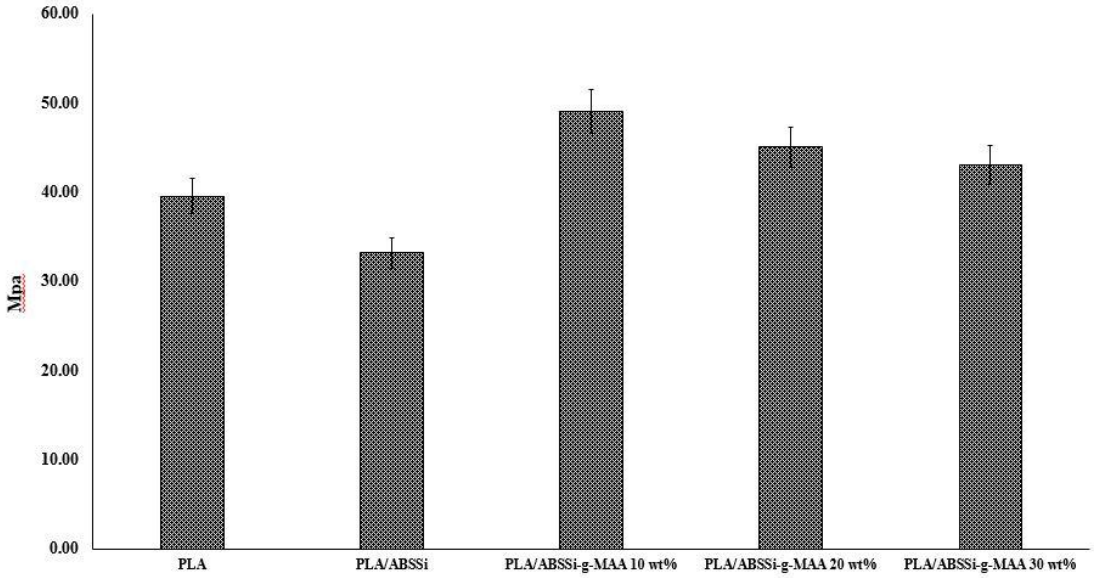


Figure 4.26 Representative of the tensile strength of PLA, PLA/ABS$^{Si}$ and PLA/ABS$^{Si}$-*g*-MAA

Table 4.12 *The tensile strength of PLA,* PLA/ABS$^{Si}$ and PLA/ABS$^{Si}$-*g*-MAA

| Sample | Tensile strength (MPa) |
|---|---|
| PLA | 39.56±0.1 |
| PLA/ABS$^{Si}$ 10 wt% | 33.18±0.1 |
| PLA/ABS$^{Si}$-*g*-MAA 10 wt% | 49.10±0.1 |
| PLA/ABS$^{Si}$-*g*-MAA 20 wt% | 45.10±0.5 |
| PLA/ABS$^{Si}$-*g*-MAA 30 wt% | 43.10±0.5 |

Number of mechanical testing is 5.

*4.1.3 Elongation at break of PLA/ABS-g-MAA and PLA/ABS$^{Si}$-g-MAA blends*

Considering the percent elongation (Figure 4.27), a massive increase in percent elongation is recorded in case of PLA/ABS-*g*-MAA 20 wt% and PLA/ABS-*g*-MAA 30 wt%, implying that these blends are extremely flexible and tough when compared to neat PLA, control, and PLA/ABS-*g*-MAA 10 wt%. The elongation at break of PLA, PLA/ABS and PLA/ABS-*g*-MAA are showed in Table 4.13.

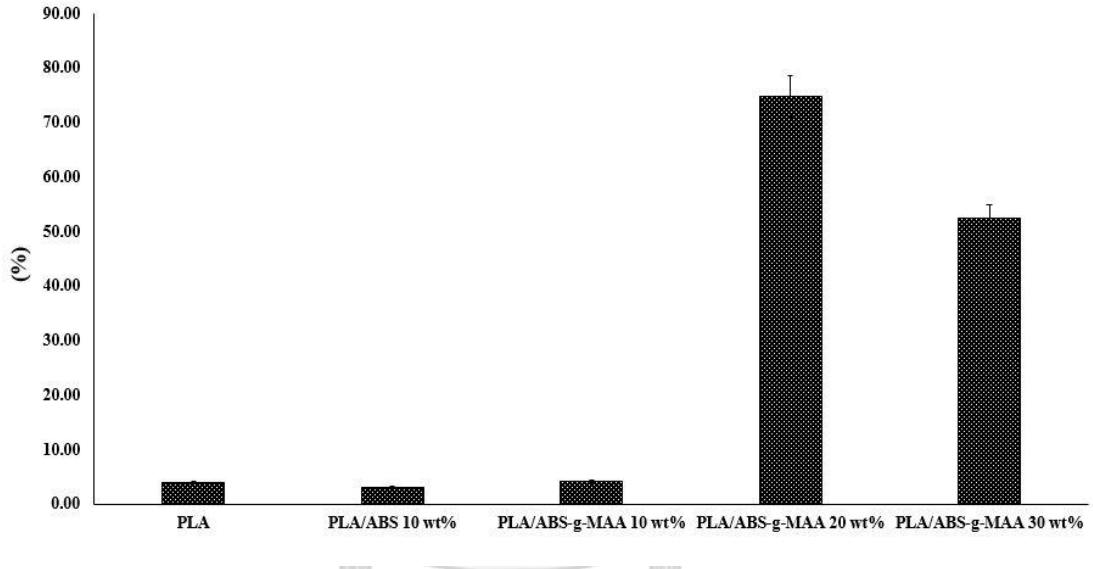


Figure 4.27 Representative of the elongation at brake of PLA, PLA/ABS and PLA/ABS-*g*-MAA



Table 4.13 The elongation at break of PLA, PLA/ABS and PLA/ABS-*g*-MAA

| Sample | Elongation at break (%) |
|---|---|
| PLA | 4.06±0.1 |
| PLA/ABS 10 wt% | 3.16±0.1 |
| PLA/ABS-*g*-MAA 10 wt% | 4.20±0.1 |
| PLA/ABS-*g*-MAA 20 wt% | 74.80±0.4 |
| PLA/ABS-*g*-MAA 30 wt% | 52.40±0.5 |

Number of mechanical testing is 5.

Photographs of specimens after tensile testing are illustrated as shown in Figure 4.28. This indicates that the percent loading of PLA/ABS-*g*-MAA plays an important role in control the flexibility of the blends.

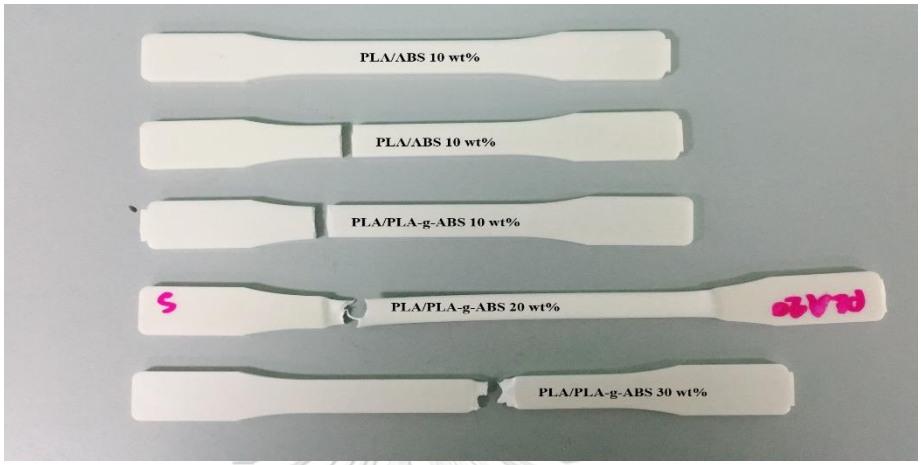


Figure 4.28 Photograps of specimens after tensile testing

For PLA/ABS$^{Si}$-*g*-MAA, the percent elongation was shown in Figure 4.29. The percent elongation increases when loaded with PLA/ABS$^{Si}$-*g*-MAA 10 wt%, PLA/ABS$^{Si}$-*g*-MAA 20 wt%, and PLA/ABS$^{Si}$-*g*-MAA 30 wt%, implying that these blends are extremely flexible and tough when compared to neat PLA and control. The elongation at break of PLA, PLA/ABS$^{Si}$ and PLA/ABS$^{Si}$-*g*-MAA are showed in Table 4.14.

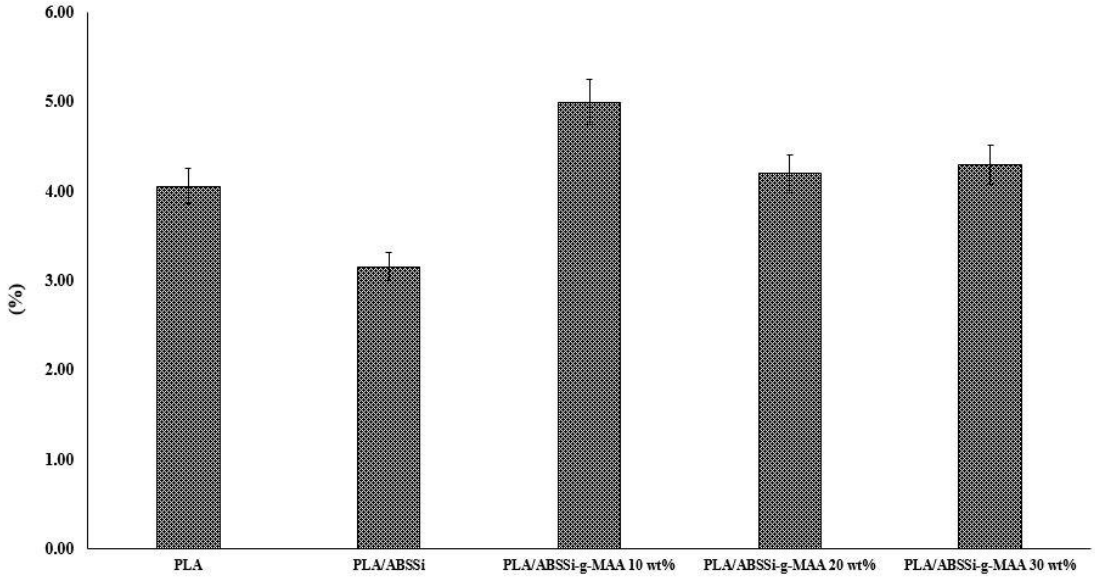


Figure 4.29 Representative of the elongation at brake of PLA, PLA/ABS$^{Si}$ and PLA-ABS$^{Si}$-*g*-MAA

Table 4.14 The elongation at break of PLA, PLA/ABS$^{Si}$ and PLA- ABS$^{Si}$-*g*-MAA

| Sample | Elongation at break (%) |
|---|---|
| PLA | 4.06±0.1 |
| PLA/ABS$^{Si}$ 10 wt% | 3.16±0.1 |
| PLA/ABS$^{Si}$-*g*-MAA 10 wt% | 5.00±0.1 |
| PLA/ABS$^{Si}$-*g*-MAA 20 wt% | 4.20±0.4 |
| PLA/ABS$^{Si}$-*g*-MAA 30 wt% | 4.30±0.5 |

Number of mechanical testing is 5.

## 4.2 Thermal Properties

### *4.2.1 Thermal analysis of ABS and ABS-g-MAA*

*Tg* values of ABS and ABS-*g*-MAA are found at -81 ℃ and -76 ℃, respectively (Figure 4.30). An increase in *Tg* value of grafted ABS results from the partial conversion of ethylene bonds (C=C) to C-C bonds at the grafting site. It can be said that grafting of MAA onto ABS rubber surface was successful according to change in *Tg* value and IR evidence. Further reaction of PLA hydroxyl group with functionalized MAA carboxylic acid group on ABS surface was carried out using an internal mixer, resulting in ABS-*g*-MAA which exhibited good compatibility with PLA as confirmed by mechanical properties evaluation. Disadvantageously, thermal stability of PLA is relatively lower than that of polypropylene counterpart.

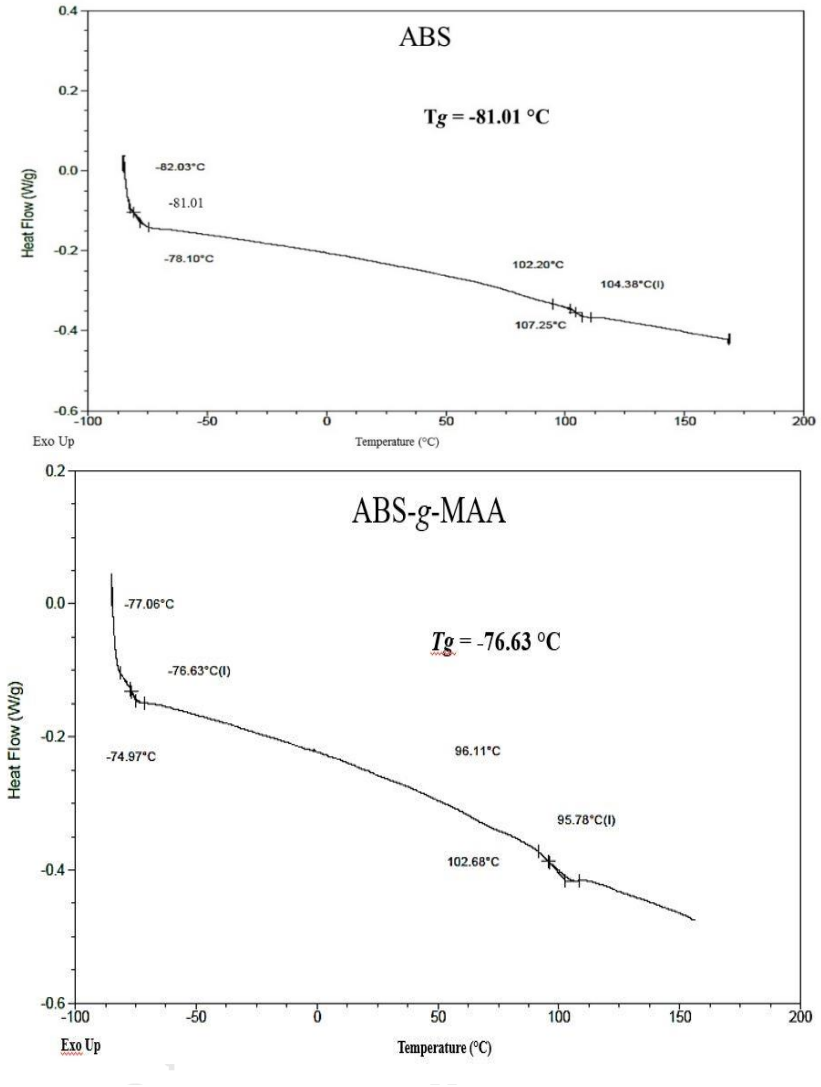


Figure 4.30 Representative DSC curve of ABS and ABS-*g*-MAA

*4.2.2 Heat distortion measurement of PLA, PLA/ABS and PLA/ABS-g-MAA* and PLA/ABS$^{Si}$-g-MAA *blends*

In this experiment, heat distortion temperature (HDT) was measured according to ASTM D648. The test specimen was loaded in three-point bending in the edgewise direction. The temperature was raised at 2 °C/min until the specimen deflected 0.32 mm. HDT values are illustrated in Figure 4.31 and Figure 4.32. It is found that HDT value of PLA/ABS-*g*-MAA and *PLA/ABS$^{Si}$-g-MAA blends* are higher than PLA by 2 °C,

implying that PLA/ABS-*g*-MAA and PLA/ABS$^{Si}$-*g*-MAA blends are thermally stable that neat PLA. It could be claimed that at the presence of ABS-*g*-MAA and ABS$^{Si}$-*g*-MAA distributing particles, the PLA chain mobility is restricted which flavors an improvement in thermal stability of PLA. The heat distortion temperture of PLA, PLA/ABS, PLA/ABS-*g*-MAA and *PLA/ABS$^{Si}$-g-MAA* are showed in Table 4.15 and Table 4.16.

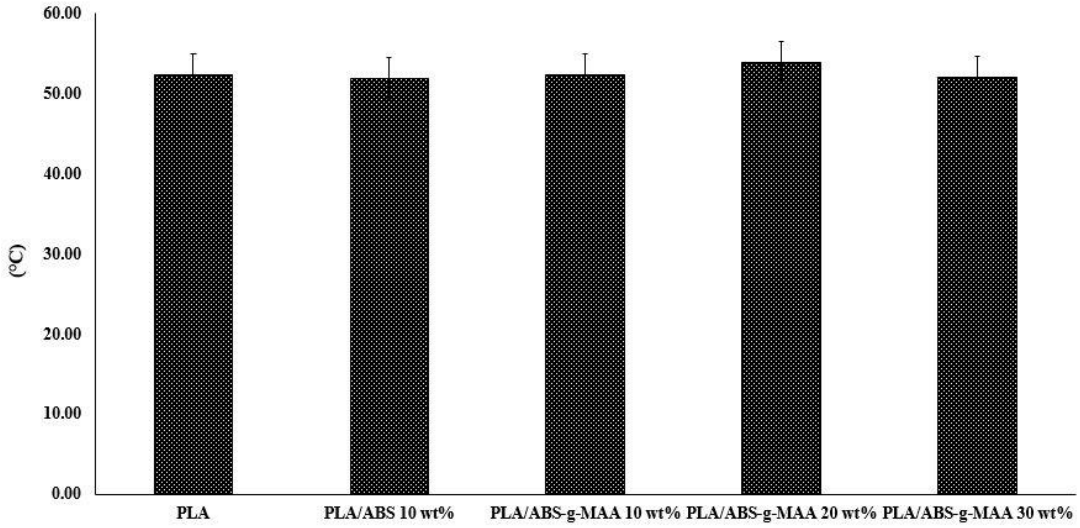


Figure 4.31 Representative of the heat distortion temperature of PLA, PLA/ABS and PLA/ ABS-*g*-MAA



Table 4.15 The heat distortion temperature of PLA, PLA/ABS and PLA/ABS-*g*-MAA

| Sample | Heat distortion temperature (°C) |
|---|---|
| PLA | 52.32±0.1 |
| PLA/ABS 10 wt% | 51.94±0.3 |
| PLA/ABS-*g*-MAA 10 wt% | 52.34±0.2 |
| PLA/ABS-*g*-MAA 20 wt% | 53.90±0.1 |
| PLA/ABS-*g*-MAA 30 wt% | 52.10±0.2 |

Number of mechanical testing is 5.

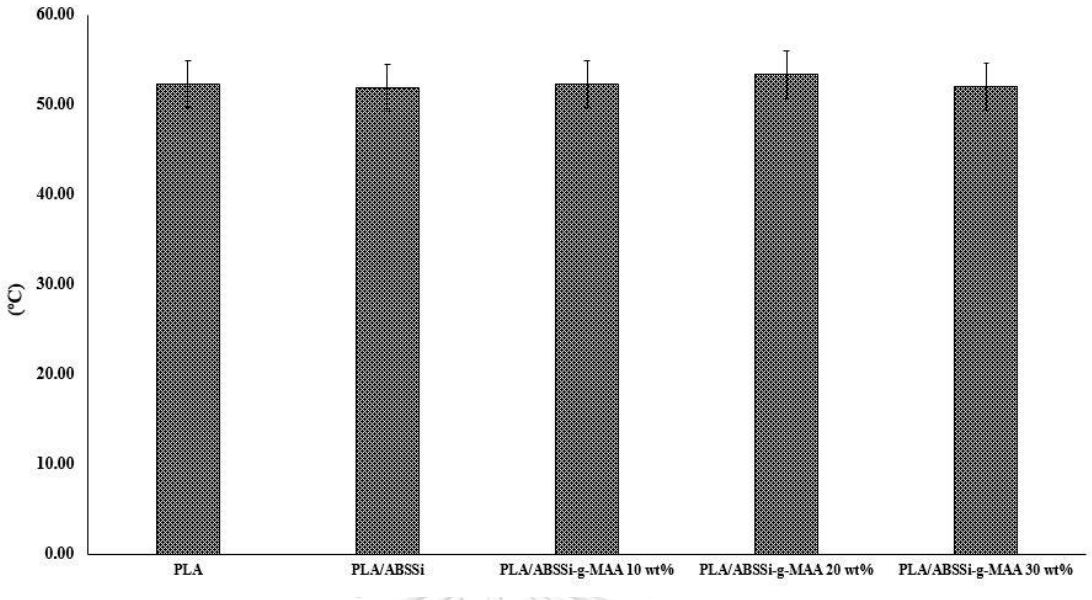


Figure 4.32 Representative of the heat distortion temperature of PLA, PLA/ABS$^{Si}$ and PLA/ ABS$^{Si}$-*g*-MAA

Table 4.16 The heat distortion temperature of PLA, PLA/ABS$^{Si}$ and PLA/ ABS$^{Si}$-*g*-MAA

| Sample | Heat distortion temperature (°C) |
|---|---|
| PLA | 52.32±0.1 |
| PLA/ABS$^{Si}$ 10 wt% | 51.94±0.3 |
| PLA/ABS$^{Si}$-*g*-MAA 10 wt% | 52.34±0.2 |
| PLA/ABS$^{Si}$-*g*-MAA 20 wt% | 53.40±0.1 |
| PLA/ABS$^{Si}$-*g*-MAA 30 wt% | 52.00±0.2 |



**4.3 Morphology of PLA/ABS-*g*-MAA blends**

Fracture surface morphology of blends was observed by scanning electron microscopy as shown in Figure 4.29. Typically, PLA and ABS rubber are incompatible in nature, resulting in obvious agglomeration as observed in the SEM (Figure 4.22a). In addition, fracture surface of PLA is smooth, reflecting its brittleness characteristic. SEM images of PLA/ABS-*g*-MAA show that rubber particles which are much smaller than

those of control blends are present as disperse phase in PLA matrix. As seen, tiny ABS particles are evenly distributed in PLA matrix, indicating the compatibility characteristic deriving from the similar surface energy between PLA and ABS-*g*-MAA. In case of PLA/ABS-*g*-MAA 10 wt%, the number ofmABS-*g*-MAA particles is relatively lower than that of PLA/ABS-*g*-MAA 20 wt% and PLA/ABS-*g*-MAA 30 wt%. Therefore, it can be assumed that improved properties of PLA/ABS-*g*-MAA blends are related to the amount of disperse particles; the smaller the disperse particle the higher the amount of disperse particles. As a result, compatibility between ABS-*g*-MAA and PLA is improved due to the enhancement of interfacial adhesion. In this study, PLA/ABS-*g*-MAA blends with ABS-*g*-MAA content up to 30 % was achievable. For PLA/ABS 10 wt% blend, ABS agglomerate with a variety of particle size distribution is seen which is derived from the problem of poor compatibility, resulting in decrease in mechanical properties.

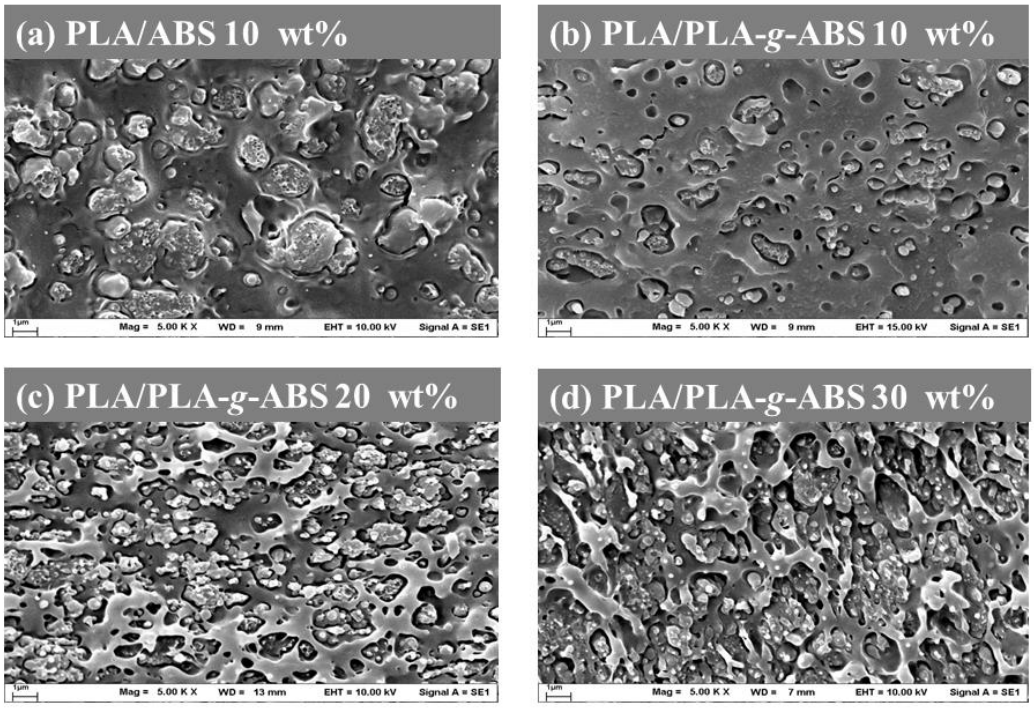


Figure 4.33 Representative SEM images of (a) PLA/ABS and (b) PLA/ABS-*g*-MAA 10 wt%, (c) PLA/ABS-*g*-MAA 20%, (d) PLA/ABS-*g*-MAA 30%

# CHAPTER V
# CONCLUSIONS

## PART I: Synthesis of ABS rubber containing $SiO_2$ nanoparticle and properties investigation of ABS containing $SiO_2$ nanoparticle

Hydrophobic silica particles (HDTMS-silica) having various HDTMS ratios was synthesized by silanization reaction of silica nanoparticle with hexadecyltrimethoxysilane (HDTMS : silica wt ratios of 1 : 1, 2 : 1, and 3 : 1) in an emulsion system. Then, in-situ synthesis of ABS rubber containing HDTMS-silicas (HDTMS-silica1, HDTMS-silica2, and HDTMS-silica3) was carrie out.

It was found that all of HDTMS : silica wt ratios produced HDTMS-silicas exhibiting good dispersibility in toluene. In fact, 3 : 1 HDTMS : silica showed the complete hydrophobicity modification, judged by the absence of silanol absorption band.

Mechanical properties of ABS nanocomposites were notably enhanced by the addition of HDTMS-silica loading. An insight investigation led to findings that the optimum mechanical properties were achieved at 2 wt% loading of 2 : 1 HDTMS : silica. Below 2 : 1 ratio, the HDTMS ratio was not enough to obtain the full hydrophobicity surface modification. On the other hand, above 2: 1 ratio, the excessive HDTMS ratio led to a decrease in $SiO_2$ content, causing a gradual decrease in its energy absorption as well as reinforcing performance. In case of 2 : 1 HDTMS : silica, optimum mechanical properties were achievable at 2 wt% loading, resulting from the maximized filler particle dispersibility. Further increase in filler loading resulted in a reverse effect due to agglomeration problem.

In addition, the impact strength of ABS nanocomposites were enhanced by adding of HDTMS-$SiO_2$ from precipitation technique play a major role the same trend as HDTMS-silica. Moreover, the optimum impact strength was achieved at 1% loading.

**PART II: Preparation of PLA/ABS-*g*-MAA and PLA/ABS$^{Si}$-*g*-MAA blends**

ABS-*g*-MAA and ABS$^{Si}$-*g*-MAA were successfully prepared and then melt-mixed with PLA to obtain PLA/ABS-*g*-MAA and PLA/ABS$^{Si}$-*g*-MAA blends using an internal mixer. The loading of ABS-*g*-MAA and ABS$^{Si}$-*g*-MAA up to 30 wt% was obtainable.

It was found that impact resistance values significantly outperformed neat PLA by 60%, 87%, and 150% for PLA/ABS-*g*-MAA 10 wt%, PLA/ABS-*g*-MAA 20 wt%, and PLA/ABS-*g*-MAA 30 wt%, respectively. For PLA/ABSSi-g-MAA blends, impact resistance values significantly outperform neat PLA by 56%, 69% and 101% for PLA/ABS$^{Si}$-*g*-MAA 10 wt%, PLA/ABS$^{Si}$-*g*-MAA 20 wt% and PLA/ABS$^{Si}$-*g*-MAA 30 wt%, respectively. A significant increase in impact strength is contributable to ABS rubber which exhibited good interfacial adhesion.

The impact strength is dependent on the percent loading of ABS-*g*-MAA and ABS$^{Si}$-*g*-MAA; the more the PLA/ABS-*g*-MAA and PLA/ABS$^{Si}$-*g*-MAA the higher the impact strength value. In a similar manner, tensile strength increases when loaded with PLA/ABS-*g*-MAA and PLA/ABS$^{Si}$-*g*-MAA albeit at lesser effect.

These results implies that PLA/ABS-*g*-MAA and PLA/ABS$^{Si}$-*g*-MAAacts as an effective impact modifier when compared to a reinforcing role. Considering the percent elongation, a massive increase in percent elongation was recorded in case of PLA/ABS-*g*-MAA 20 wt%, PLA/ABS-*g*-MAA 30 wt%, PLA/ABS$^{Si}$-*g*-MAA 10 wt%, PLA/ABS$^{Si}$-*g*-MAA 20 wt% and PLA/ABS$^{Si}$-*g*-MAA 30 wt%, implying that these blends were extremely flexible and tough when compared to neat PLA, control, PLA/ABS 10 wt% and PLA/ABS$^{Si}$ 10 wt%. This indicated that the percent loading of PLA/ABS-*g*-MAA and PLA/ABS$^{Si}$-*g*-MAA played an important role in control the flexibility of the blends.

# REFERENCES


1. Brydson, J.A., *Plastic materials*, ed. 7. 1999, Oxford : Butterworth-Heinemann.
2. Liu, X.Q., et al., *Effect of nano-silica on the phase inversion behavior of immiscible PA6/ABS blends.* Polymer Testing, 2013. **32**: p. 141-149.
3. Wei, P., et al., *Synthesis of a novel organic-inorganic hybrid mesoporous silica and its flame retardancy application in PC/ABS.* Polymer Degradation and Stability, 2013. **98**: p. 1022-1029.
4. Kim, I.J., et al., *Synthesis and characterization of ABS/silica hybrid nanocomposites.* Current Applied Physics, 2006. **6S1**: p. e43-e47.
5. Allahverdi, A., et al., *The effect of nanosilica on machanical, thermal and morphological properties of epoxy coating.* Progress in Organic Coatings, 2012. **75**: p. 543-548.
6. Roy, K., et al., *Effect of sol-gel modified nano calcium carbonate (CaCO3) on the cure, mechanical and thermal properties of acrylonitrile butadiene rubber (NBR) nanocomposites.* Journal of Sol-Gel Science Technology, 2015. **73**: p. 306-313.
7. Pawinzadeh, M., et al., *Surface characterization of polyethylene terephthalate/silica nanocomposites.* Applied Suface Science, 2010. **256**: p. 2792-2802.
8. Rostamiyan, Y., Mashhadzadeh, A.H. and SalmanKhani, A. *Optimization of mechanical properties of epoxy-based hybrid nanocomposite: Effect of using nano silica and high-impact polystyrene by mixture design approach.* Materials and Desigh, 2014. **56**: p. 1068-1077.
9. Xiao, H. and Cezar, N. *Organo-modified cationic silica nanoparticles/anionic polymer as flocculants.* Journal of Colloid and Interface Science, 2003. **267**: p. 343-351.
10. Tianbin, W. and Yangchuan, K. *Preparation of silica-PS composite particles and their application in PET.* European Polymer Journal, 2006. **42**: p. 274-285.

11. Zhang, L., et al., *Preparation of monodisperse polystyrene/silica core-shell nano-composite abrasive with controllable size and its chemical polishing performance on copper.* Applied Suface Science, 2011. **258**: p. 1217-1224.
12. Elias, L., et al., *Morphology and rheology of immiscible polymer blends filled with silica nanoparticles.* Polymer, 2007. **48**: p. 6029-6040.
13. Agudelo, N.A., Perez, L.D. and Lopez, B.L. *Anovel method for the synthesis of polystyrene-graft-silica particles using random copolymers based on styrene and triethoxyvinylsilane.* Applied Suface Science, 2011. **257**: p. 8581-8586.
14. Suhendi, A., et al., *Agglomeration-free core-shell polystyrene/silica particles preparation using an electrospray method and additive-free cationic polystyrene core.* Matterials Letters, 2013. **91**: p. 161-164.
15. Tarrio-Saavedra, J., et al., *Effect of silica content on thermal stability of fumed silica/epoxy composites.* Polymer Degradation and Stability, 2008. **93**: p. 2133-2137.
16. Zhang, Q., et al., *Silane-grafted silica-covered kaolinite as filler of styrene butadiene rubber.* Applied Clay Science, 2012. **65-66**: p. 134-138.
17. Chuayjuljit, S. and Boonmahithisud, A. *Natural rubber nanocomposites using polystyrene-encapsulated nanosilica prepared by differential nicroemulsion polymerization.* Applied Suface Science, 2010. **256**: p. 7211-7216.
18. Liu, Q., Zhang, Y. and Xu, H. *Properties of vulcanized rubber nanocomposites filled with nanokaolin and precipitated silica.* Applied Clay Science, 2008. **42**: p. 232-237.
19. Samarzija-Jovanovic, S., et al., *Nanocomposites based on silica-reinforced ethylene-propylene-diene-mnomer/acrylonitrile-butatidne rubber blends.* Compsites: Part B, 2011. **42**: p. 1244-1250.
20. Sun, S., et al., *Effects of surface modification of fumed silica on interfacial structures and mechanical properties of poly(vinyl chloride) composites.* European Polymer Journal, 2006. **42**: p. 1643-1652.
21. Lavorgna, M., et al., *Silanization and silica enrichment of multiwalled carbon nanotubes: Synergistic effects on the thermal-mechanical properties of epoxy nanocomposites.* European Polymer Journal, 2013. **49**: p. 428-438.

22. Zhang, J., et al., *Surface modification of ultrafine precipitated silica with 3-methacryloxypropyltrimethoxysilane in carbonization process.* Colloids and Surfaces A: Physicochemical and Engineering Aspects, 2013. **418**: p. 174-179.
23. He, W., et al., *Surface Modification of Colloidal Silica Nanoparticles: Controlling the size and Grafting Process.* Bulletin of the Korean Chemical Society 2013. **34**: p. 2747-2752.
24. Shin, Y., et al., *Surface properties of silica nanoparticles modified with polymers for polymer nanocomposite applications.* Journal of Industrial and Engineering Chemistry, 2008. **14**: p. 515-519.
25. Lijima, M., Tsukada, M. and Kamiya, H. *Effect of surface interaction of silica nanoparticles modified by silane coupling agents on viscosity of methylethylketone suspension.* Journal of Colloid and Interface Science, 2007. **305**: p. 315-323.
26. Jumahat, A., et al., *Tensile properties of nanosilica/epoxy nanocomposites.* Procedia Engineering, 2012. **41**: p. 1634-1640.
27. Zou, H., S. Wu, and Shen, J. *Polymer/silica nanocomposites: Preparation, characterization, properties, and applications.* Chemistry Review, 2008. **108**: p. 3893-3957.
28. Caris, C.H.M., et al., *Polymerization of MMA at the surface of inorganic particles.* British Polymer Journal, 1989. **21**: p. 133-140.
29. Huang, C., Partch, R.E. and Matijevic, E. *Coating of uniform inorganic particles with polymers: II. Polyaniline on copper oxide.* Journal Colloid Interface Science, 1995. **170**: p. 275-283.
30. Li, X. and Sun, Z. *Synthesis of magnetic polymer micospheres and application for immobilization of proteinase of balillus.* Journal Apply Polymer Science, 1995. **58**: p. 1991-1997.
31. Oyama, H.T., et al., *Coating of uniform inorganic particles with polymers.* Journal Colloid Interface Science, 1993. **160**: p. 298-303.
32. Yazdimamaghani, M., Pishvaei, M. and Kaffashi, B. *Synthesis of latex based antibacterial acrylate polymer/nanosilver via in situ miniemulsion polymerization.* Macromolecule Research, 2011. **19**: p. 243-249.

33. Huang, X. and Brittain, W.J. *Synthesis and characterization of PMMA nanocomposites by suspension and emulsion polymerization.* Macromolecules, 2001. **34**: p. 3255-3260.

34. Bakhshaee, M., et al., *Encapsulation of carbon black in suspension polymerized copolymers.* Polymer Communication, 1985. **26**: p. 185-192.

35. Camargo, P.H.C., Styanarayana, K.G. and Wypych, F. *Nanocomposites: Sythesis, Structure, Properites and New Application Opportunities.* Materials Research, 2009. **12**: p. 1-39.

36. Hongbo, Z., et al., *Preparation and characterization of PE and PE-g-MAH/montmorillonite manocomposites.* European Polymer Journal, 2004. **40**: p. 2539-2545.

37. Haiyun, M., et al., *Studied of ABS-graft-maleic anhydride/clay nanocomposites: Morphologies, thermal stability and flammability properties.* Polymer Degradation and Stability, 2006. **91**: p. 2951-2959.

38. Sodergard, A. and Stolt, M. *Properties of lactic acid based polymers and their correlation with composition.* Progress in polymer science, 2002. **27**: p. 1123-1163.

39. Middleton, C.J. and Tipton, J.A. *Synthetic biodegradable polymers as orthopedic devices.* Biomaterials, 2000. **21**: p. 2335-2346.

40. Gupta, A.P. and Kumar, V. *New emerging trends in synthetic biodegradable polymers-Polylactide.* European Polymer Journal, 2007. **43**: p. 4053-4074.

41. Yu, L., et al., *Effect of annealing and orientation on microstructures and mechanical properties of polylactic acid.* Polymer Engineering and Science, 2008. **48**: p. 634-641.

42. Veld, P.J.A., et al., *Melt block copolymerization of e-caprolactone and l-lactide.* Journal of polymer science, 1997. **35**: p. 219-226.

43. Grijpma, D.W., et al., *High impact strength as-polymerized PLLA.* Polymer Bulletin, 1992. **29**: p. 571-578.

44. Hijanen-Vainio, M., Karjalainen, T. and Seppala, J. *Biodegradable lactone copolymers. I. Characterization and mechanical behavior of e-caprolactone*

*and lactide compolymers.* Journal of Applide polymer science, 1996. **59**: p. 1281-1288.

45. Min, C., et al., *Biodegradable shape-memory polymer-polylactide-co-poly(glycolide-co-caprolactone) multiblock copolymer.* Polymer Advance Technologies 2005. **16**: p. 608-615.
46. Zhu, Z., et al., *Preparation of biogegradable polylactide-co-poly(ethylene glycol) copolymer by lactide reacted poly(ethylene glycol).* European Polymer Journal, 1999. **35**: p. 1821-1828.
47. Shibata, M., Teramoto, N. and Inoue, Y. *Mechanical properties, morphologies, and crystallization behavior of plasticized poly(L-lactide)/poly(butylene succinate-co-latctate) blends.* Polymer, 2007. **48**: p. 2768-2777.
48. Gaona, L.A., et al., *Hydrolytic degradation of PLLA/PCL microporous membranes prepared by freeze extraction.* Polymer Degradation and Stability, 2012. **97**: p. 1621-1632.
49. Noroozi, N., Schafer, L.L. and Hatzikiriakos, S.G. *Thermorheological properties of poly(e-caprolactone)/polylactide blends.* Polymer Engineering and Science, 2012. **52**: p. 2348-2359.
50. Tsuji, H. and Muramatsu, H. *Blends of aliphatic polyesters. IV. Morphology, swelling behavior, and surface and bulk properties of blends from hydrophobic poly(L-lactide) and hydrophillic poly(vinyl alcohol).* Journal of Applide polymer science, 2001. **81**: p. 2151-2160.
51. Zhang, N., et al., *Preparation and Properties of Biodegradable Poly(lactic acid)/Poly(butylene adipate-co-terephathalate) Blend with Epoxy-Functional Styrene Acrylic copolymer as Reactive Agent.* Journal of Polymers and the environment, 2013. **21**: p. 286-292.
52. Shibata, M., Inoue, Y. and Miyoshi, M. *Mechanical properties, morphology, and crystallization behavior of blends of poly(L-lactide) with poly(butylene succinate-co-L-latctate) and poly(butylene succinate).* Polymer, 2006. **47**: p. 3557-3564.

53. Wu, D., et al., *Interfacial Properties, Viscoelasticity and Thermal behaviors of Poly(butylene succinate)/Polylactide Blend.* Industrial and Engineering Chemistry research, 2012. **51**: p. 2290-2298.

54. Hu, Y., et al., *Aging of poly(lactide)-poly(ethylene glycol) blends. Part2. Poly(lactide) with high stereoregularity.* Polymer, 2003. **44**: p. 5711-5720.

55. Phetwarotai, W., Potiyarat, P. and Aht-Ong, D. *Properties of compatibilized polylactide blend films with gelatinized corn and tapioca starches.* Journal of Applide polymer science, 2010. **116**: p. 2350-2311.

56. Nitinis, N., et al., *Structure and properties of polylactide/natural rubber blends.* Materials Chemistry and Physics, 2011. **129**: p. 823-831.

57. Rigoussen, A., et al., *In-depth investigation on the effect and role of cardanol in the compatibilization of PLA/ABS immiscible blends by reactive extrusion.* European Polymer Journal, 2017. **93**: p. 271-283.

58. Xi-Qiang Liu, et al., *Effect of nano-silica on the phase inversion behavior of immiscible PA6/ABS blends.* Polymer Testing, 2013. **32**: p. 141-149.

59. Chaikeaw, C. and Srikulkit, K. *In situ synthesis of ABS containing hydrophobic silica nanoparticles and their effects on mechanical properties.* Journal of Sol-Gel Science Technology, 2017. **81**: p. 774-781.

60. Ma, X., et al., *Surface modification and characterization of highly dispersed silica nanoparticles by a cationic surfactant.* Colloids and Surfaces A: Physicochemical and Engineering Aspects, 2010. **358**: p. 172-176.

61. Sadek, M.O., Reda, M.S. and Al-Bilali, K.R. *Preparation and Characterization of Silica and Clay-Silica Core-Shell Nanoparticles Using Sol-Gel Method.* Advances in Nanoparticles, 2013. **2**: p. 165-175.

62. Kango, S., et al., *Surface modification of inorganic nanoparticles for development of organic-inorganic nanocomposites.* Progress in polymer science, 2013. **38**: p. 1232-1261.

63. Hedayati, M., et al., *Ball milling preparation and characterization of poly (ether ether ketone) / surface modified silica nanocomposite.* Powder Technology, 2011. **207**: p. 296-303.

64. Rani, M.K., Palanisamy, P.N. and Sivakumar, P. *Synthesis and characterization of amorphous nano-silica from biomass ash.* International Journal of Advanced Technology in Engineering and Science, 2014. **2**: p. 71-76.

# APPENDIX

| | |
|---|---|
| Elapsed Time | 00:10:00 |
| Median Diam. | 28.0 nm |
| Mean Diam. | 36.3 nm |
| Polydispersity | 0.694 |
| GSD | 2.066 |

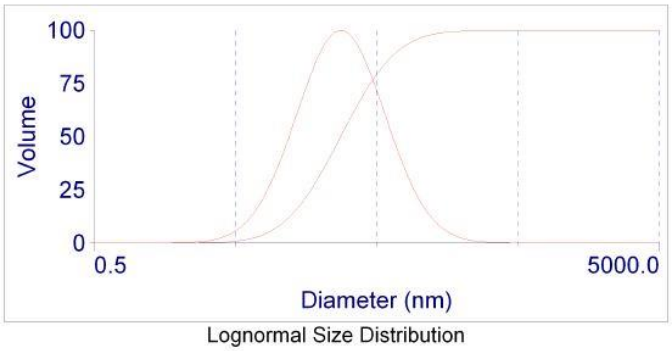

Lognormal Size Distribution

| d(nm) | G(d) | C(d) | d(nm) | G(d) | C(d) | d(nm) | G(d) | C(d) |
|---|---|---|---|---|---|---|---|---|
| 8.6 | 26 | 5 | 23.4 | 97 | 40 | 45.5 | 80 | 75 |
| 11.2 | 44 | 10 | 25.6 | 99 | 45 | 51.3 | 70 | 80 |
| 13.3 | 58 | 15 | 28.0 | 100 | 50 | 59.0 | 58 | 85 |
| 15.3 | 70 | 20 | 30.7 | 99 | 55 | 70.3 | 44 | 90 |
| 17.3 | 80 | 25 | 33.6 | 97 | 60 | 91.3 | 26 | 95 |
| 19.2 | 87 | 30 | 37.0 | 93 | 65 | | | |
| 21.3 | 93 | 35 | 40.8 | 87 | 70 | | | |

Figure A-1 Particle size distribution of Silica

| | |
|---|---|
| Elapsed Time | 00:03:00 |
| Median Diam. | 59.3 nm |
| Mean Diam. | 87.1 nm |
| Polydispersity | 1.177 |
| GSD | 2.416 |

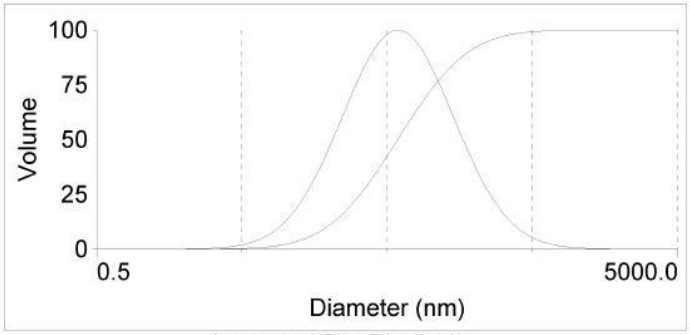

Lognormal Size Distribution

| d(nm) | G(d) | C(d) | d(nm) | G(d) | C(d) | d(nm) | G(d) | C(d) |
|---|---|---|---|---|---|---|---|---|
| 14.0 | 26 | 5 | 47.5 | 97 | 40 | 107.1 | 80 | 75 |
| 19.3 | 44 | 10 | 53.1 | 99 | 45 | 124.1 | 70 | 80 |
| 23.9 | 58 | 15 | 59.3 | 100 | 50 | 147.1 | 58 | 85 |
| 28.4 | 70 | 20 | 66.3 | 99 | 55 | 182.6 | 44 | 90 |
| 32.9 | 80 | 25 | 74.1 | 97 | 60 | 251.0 | 26 | 95 |
| 37.5 | 87 | 30 | 83.2 | 93 | 65 | | | |
| 42.3 | 93 | 35 | 93.9 | 87 | 70 | | | |

Figure A-2 Particle size distribution of HDTMS-Silica1

| | |
|---|---|
| Elapsed Time | 00:03:00 |
| Median Diam. | 75.8 nm |
| Mean Diam. | 99.6 nm |
| Polydispersity | 0.744 |
| GSD | 2.108 |

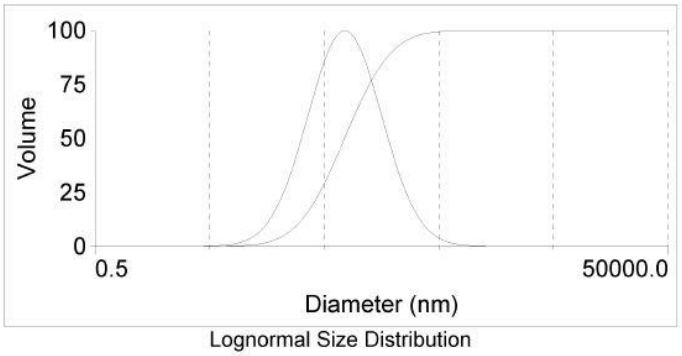

Lognormal Size Distribution

| d(nm) | G(d) | C(d) | d(nm) | G(d) | C(d) | d(nm) | G(d) | C(d) |
|---|---|---|---|---|---|---|---|---|
| 22.5 | 26 | 5 | 62.9 | 97 | 40 | 124.7 | 80 | 75 |
| 29.4 | 44 | 10 | 69.1 | 99 | 45 | 141.2 | 70 | 80 |
| 35.3 | 58 | 15 | 75.8 | 100 | 50 | 162.9 | 58 | 85 |
| 40.7 | 70 | 20 | 83.2 | 99 | 55 | 195.4 | 44 | 90 |
| 46.1 | 80 | 25 | 91.4 | 97 | 60 | 255.4 | 26 | 95 |
| 51.5 | 87 | 30 | 100.8 | 93 | 65 | | | |
| 57.1 | 93 | 35 | 111.6 | 87 | 70 | | | |

Figure A-3 Particle size distribution of HDTMS-Silica2

| | |
|---|---|
| Elapsed Time | 00:03:00 |
| Median Diam. | 142.2 nm |
| Mean Diam. | 169.0 nm |
| Polydispersity | 0.433 |
| GSD | 1.822 |

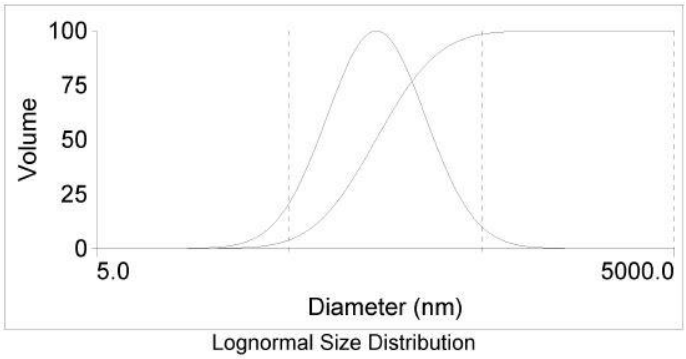

Lognormal Size Distribution

| d(nm) | G(d) | C(d) | d(nm) | G(d) | C(d) | d(nm) | G(d) | C(d) |
|---|---|---|---|---|---|---|---|---|
| 54.1 | 26 | 5 | 122.5 | 97 | 40 | 211.3 | 80 | 75 |
| 66.9 | 44 | 10 | 132.0 | 99 | 45 | 233.3 | 70 | 80 |
| 77.3 | 58 | 15 | 142.2 | 100 | 50 | 261.4 | 58 | 85 |
| 86.7 | 70 | 20 | 153.1 | 99 | 55 | 302.1 | 44 | 90 |
| 95.7 | 80 | 25 | 165.0 | 97 | 60 | 374.0 | 26 | 95 |
| 104.5 | 87 | 30 | 178.3 | 93 | 65 | | | |
| 113.4 | 93 | 35 | 193.5 | 87 | 70 | | | |

Figure A-4 Particle size distribution of HDTMS-Silica3

Table A-1 Impact strength (kg-cm/cm$^2$) of ABS containing three different rubbers (LPS, MPS and SPS)

| Sample | 1 | 2 | 3 | 4 | 5 | Average | SD |
|---|---|---|---|---|---|---|---|
| LPS | 23 | 23.1 | 23 | 23.2 | 23 | 23.1 | 0.08 |
| MPS | 27.1 | 27.7 | 27.1 | 27.7 | 27.7 | 27.6 | 0.26 |
| SPS | 8.2 | 8.5 | 8.2 | 8.3 | 8.3 | 8.3 | 0.11 |

Table A-2 Tensile strength (kg/cm$^2$) of ABS containing three different rubbers (LPS, MPS and SPS)

| Sample | 1 | 2 | 3 | 4 | 5 | Average | SD |
|---|---|---|---|---|---|---|---|
| LPS | 438 | 438 | 437 | 439 | 438 | 438.0 | 0.63 |
| MPS | 455 | 452 | 454 | 455 | 455 | 454.2 | 1.17 |
| SPS | 492 | 493 | 493 | 494 | 494 | 493.2 | 0.75 |

Table A-3 Flexural strength (kg/cm$^2$) of of ABS containing three different rubbers (LPS, MPS and SPS)

| Sample | 1 | 2 | 3 | 4 | 5 | Average | SD |
|---|---|---|---|---|---|---|---|
| LPS | 651 | 648 | 650 | 651 | 651 | 650.2 | 1.17 |
| MPS | 656 | 657 | 657 | 657 | 657 | 656.8 | 0.40 |
| SPS | 660 | 659 | 659 | 660 | 660 | 659.6 | 0.49 |

Table A-4 Impact strengths (kg-cm/cm$^2$) of ABS- HDTMS-silica1, HDTMS-silica2, and HDTMS-silica3 at various HDTMS-silica loadings

| Sample | %loading | 1 | 2 | 3 | 4 | 5 | Average | SD |
|---|---|---|---|---|---|---|---|---|
| HDTMS-silica1 | 1% | 27.5 | 27.6 | 27.5 | 27.5 | 27.7 | 27.6 | 0.1 |
| | 2% | 11.6 | 11.3 | 11.5 | 11.3 | 11.6 | 11.5 | 0.2 |
| | 3% | 8.2 | 8.3 | 8.2 | 8.3 | 8 | 8.2 | 0.1 |
| HDTMS-silica2 | 1% | 27.9 | 27.6 | 27.7 | 27.6 | 27.7 | 27.7 | 0.1 |
| | 2% | 29.8 | 29.6 | 29.9 | 29.9 | 30 | 29.8 | 0.2 |
| | 3% | 8.2 | 8.5 | 8.1 | 8.3 | 8.3 | 8.3 | 0.1 |
| HDTMS-silica3 | 1% | 10.4 | 10.5 | 10.3 | 10.4 | 10.5 | 10.4 | 0.1 |
| | 2% | 16.0 | 15.8 | 15.8 | 15.9 | 15.8 | 15.9 | 0.1 |
| | 3% | 5.4 | 5.4 | 5.6 | 5.5 | 5.5 | 5.5 | 0.1 |

Table A-5 Impact strengths (kg-cm/cm$^2$) of neat ABS and ABS/HDTMS-silica2 at various HDTMS-silica2 loadings

| Sample | 1 | 2 | 3 | 4 | 5 | Average | SD |
|---|---|---|---|---|---|---|---|
| ABS STD | 23.00 | 23.10 | 23.00 | 23.20 | 23.00 | 23.1 | 0.1 |
| ABS/HDTMS unmod1.0 wt% | 18.00 | 18.80 | 18.30 | 18.30 | 18.30 | 18.3 | 0.3 |
| ABS/HDTMS-Silica2 0.5 wt% | 23.50 | 23.90 | 24.00 | 24.20 | 24.20 | 24.0 | 0.3 |
| ABS/HDTMS-Silica2 1.0 wt% | 27.90 | 27.60 | 27.40 | 27.80 | 27.50 | 27.6 | 0.2 |
| ABS/HDTMS-Silica2 2.0 wt% | 29.50 | 29.30 | 29.30 | 30.10 | 29.80 | 29.6 | 0.3 |
| ABS/HDTMS-Silica2 3.0 wt% | 15.50 | 16.00 | 15.50 | 15.70 | 15.70 | 15.7 | 0.2 |
| ABS/HDTMS-Silica2 4.0 wt% | 8.20 | 8.50 | 8.10 | 8.30 | 8.30 | 8.3 | 0.1 |
| ABS/HDTMS-Silica2 5.0 wt% | 6.80 | 7.00 | 6.80 | 7.10 | 6.80 | 6.9 | 0.1 |

Table A-6 Tensile strengths (kg/cm$^2$) of neat ABS and ABS/HDTMS-silica2 at various HDTMS-silica2 loadings

| Sample | 1 | 2 | 3 | 4 | 5 | Average | SD |
|---|---|---|---|---|---|---|---|
| ABS STD | 421.3 | 420.3 | 420.2 | 419.3 | 419.0 | 420.3 | 0.8 |
| ABS/HDTMS unmod 1.0 wt% | 411.0 | 411.2 | 411.0 | 412.0 | 411.2 | 411.3 | 0.4 |
| ABS/HDTMS-Silica2 0.5 wt% | 420.5 | 421.0 | 422.5 | 420.3 | 422.0 | 421.3 | 0.9 |
| ABS/HDTMS-Silica2 1.0 wt% | 437.0 | 437.0 | 438.0 | 437.5 | 437.0 | 437.3 | 0.4 |
| ABS/HDTMS-Silica2 2.0 wt% | 447.0 | 447.0 | 447.0 | 447.5 | 448.0 | 447.3 | 0.4 |
| ABS/HDTMS-Silica2 3.0 wt% | 400.0 | 401.0 | 401.0 | 400.0 | 400.5 | 400.5 | 0.4 |
| ABS/HDTMS-Silica2 4.0 wt% | 353.5 | 353.0 | 353.0 | 354.0 | 354.0 | 353.5 | 0.4 |
| ABS/HDTMS-Silica2 5.0 wt% | 321.0 | 321.0 | 320.5 | 320.0 | 319.0 | 320.3 | 0.7 |

Table A-7 Flexural strengths (kg/cm$^2$) of neat ABS and ABS/HDTMS-silica2 at various HDTMS-silica2 loadings

| Sample | 1 | 2 | 3 | 4 | 5 | Average | SD |
|---|---|---|---|---|---|---|---|
| ABS STD | 579.5 | 581.0 | 580.6 | 581.0 | 580.5 | 580.5 | 0.5 |
| ABS/HDTMS unmod 1.0 wt% | 565.0 | 566.0 | 566.0 | 565.0 | 565.5 | 565.5 | 0.4 |
| ABS/HDTMS-Silica2 0.5 wt% | 604.0 | 605.0 | 603.0 | 605.0 | 604.7 | 604.3 | 0.8 |
| ABS/HDTMS-Silica2 1.0 wt% | 611.0 | 609.8 | 612.0 | 611.3 | 611.0 | 611.0 | 0.7 |
| ABS/HDTMS-Silica2 2.0 wt% | 621.0 | 620.0 | 621.0 | 621.0 | 621.0 | 620.8 | 0.4 |
| ABS/HDTMS-Silica2 3.0 wt% | 535.0 | 534.3 | 534.0 | 534.0 | 534.0 | 534.3 | 0.4 |
| ABS/HDTMS-Silica2 4.0 wt% | 520.6 | 520.0 | 520.0 | 521.0 | 521.0 | 520.5 | 0.4 |
| ABS/HDTMS-Silica2 5.0 wt% | 510.3 | 511.0 | 511.0 | 510.0 | 510.0 | 510.5 | 0.5 |

Table A-8 Impact strengths (kg-cm/cm$^2$) of neat ABS and ABS/HDTMS-$SiO_2$ at various HDTMS-$SiO_2$ loadings

| Sample | 1 | 2 | 3 | 4 | 5 | Average | SD |
|---|---|---|---|---|---|---|---|
| ABS STD | 23.0 | 23.1 | 23.0 | 23.2 | 23.0 | 23.1 | 0.1 |
| ABS/HDTMS-$SiO_2$ 0.5 wt% | 29.9 | 29.6 | 29.6 | 29.0 | 29.9 | 29.6 | 0.3 |
| ABS/HDTMS-$SiO_2$ 1.0 wt% | 32.0 | 32.5 | 33.0 | 32.5 | 32.9 | 32.5 | 0.4 |
| ABS/HDTMS-$SiO_2$ 2.0 wt% | 30.6 | 30.0 | 30.6 | 30.9 | 30.8 | 30.6 | 0.3 |
| ABS/HDTMS-$SiO_2$ 3.0 wt% | 14.9 | 14.9 | 14.0 | 14.7 | 14.9 | 14.7 | 0.3 |
| ABS/HDTMS-$SiO_2$ 4.0 wt% | 14.5 | 15.5 | 14.6 | 15.3 | 15.0 | 15.0 | 0.4 |
| ABS/HDTMS-$SiO_2$ 5.0 wt% | 7.0 | 7.1 | 6.8 | 7.5 | 6.8 | 7.0 | 0.3 |

Table A-9 Tensile strengths (kg/cm$^2$) of neat ABS and ABS/HDTMS-$SiO_2$ at various HDTMS-$SiO_2$ loadings

| Sample | 1 | 2 | 3 | 4 | 5 | Average | SD |
|---|---|---|---|---|---|---|---|
| ABS STD | 421.3 | 420.8 | 420.8 | 419.3 | 419.3 | 420.3 | 0.8 |
| ABS/HDTMS-$SiO_2$ 0.5 wt% | 477.0 | 478.0 | 476.3 | 478.0 | 478.8 | 477.6 | 0.8 |
| ABS/HDTMS-$SiO_2$ 1.0 wt% | 456.9 | 457.0 | 458.5 | 458.6 | 456.8 | 457.8 | 0.8 |
| ABS/HDTMS-$SiO_2$ 2.0 wt% | 435.9 | 435.6 | 436.0 | 435.6 | 435.0 | 435.6 | 0.5 |
| ABS/HDTMS-$SiO_2$ 3.0 wt% | 413.9 | 413.6 | 412.5 | 413.6 | 413.9 | 413.6 | 0.5 |
| ABS/HDTMS-$SiO_2$ 4.0 wt% | 410.9 | 410.3 | 410.0 | 410.9 | 410.9 | 410.6 | 0.5 |
| ABS/HDTMS-$SiO_2$ 5.0 wt% | 405.9 | 405.0 | 405.5 | 405.5 | 406.9 | 405.8 | 0.8 |

Table A-10 Flexural strengths (kg/cm$^2$) of neat ABS and ABS/HDTMS-SiO2 at various HDTMS-SiO2 loadings

| Sample | 1 | 2 | 3 | 4 | 5 | Average | SD |
|---|---|---|---|---|---|---|---|
| ABS STD | 579.5 | 581.0 | 580.6 | 581.0 | 580.5 | 580.5 | 0.5 |
| ABS/HDTMS-$SiO_2$ 0.5 wt% | 630.0 | 631.0 | 630.0 | 631.0 | 631.0 | 630.6 | 0.5 |
| ABS/HDTMS-$SiO_2$ 1.0 wt% | 628.0 | 627.0 | 628.0 | 629.0 | 629.0 | 628.2 | 0.8 |
| ABS/HDTMS-$SiO_2$ 2.0 wt% | 626.5 | 627.9 | 627.4 | 627.9 | 628.5 | 627.6 | 0.8 |
| ABS/HDTMS-$SiO_2$ 3.0 wt% | 570.0 | 570.5 | 570.3 | 572.0 | 570.3 | 570.6 | 0.8 |
| ABS/HDTMS-$SiO_2$ 4.0 wt% | 560.0 | 560.0 | 560.0 | 561.3 | 560.0 | 560.4 | 0.5 |
| ABS/HDTMS-$SiO_2$ 5.0 wt% | 551.0 | 551.4 | 551.8 | 551.0 | 551.9 | 551.4 | 0.8 |

Table A-11 Impact strength (kg-cm/cm$^2$) of PLA, PLA-ABS and PLA-PLA-*g*-ABS

| Sample | 1 | 2 | 3 | 4 | 5 | Average | SD |
|---|---|---|---|---|---|---|---|
| PLA | 3.00 | 3.10 | 3.20 | 3.00 | 3.10 | 3.08 | 0.1 |
| PLA/ABS 10 wt% | 3.11 | 2.91 | 2.93 | 3.00 | 3.01 | 2.99 | 0.1 |
| PLA/PLA-*g*-ABS 10 wt% | 5.20 | 4.00 | 5.10 | 5.30 | 5.00 | 4.92 | 0.5 |
| PLA/PLA-*g*-ABS 20 wt% | 5.61 | 5.85 | 5.87 | 5.86 | 5.87 | 5.81 | 0.1 |
| PLA/PLA-*g*-ABS 30 wt% | 7.80 | 7.70 | 7.90 | 7.70 | 8.50 | 7.92 | 0.3 |

Table A-12 Tensile strength (kg/cm$^2$) of PLA, PLA-ABS and PLA-PLA-*g*-ABS

| Sample | 1 | 2 | 3 | 4 | 5 | Average | SD |
|---|---|---|---|---|---|---|---|
| PLA | 39.50 | 39.80 | 39.40 | 39.60 | 39.50 | 39.56 | 0.1 |
| PLA/ABS 10 wt% | 33.10 | 33.10 | 33.20 | 33.20 | 33.30 | 33.18 | 0.1 |
| PLA/PLA-*g*-ABS 10 wt% | 55.30 | 55.40 | 55.40 | 55.30 | 55.30 | 55.34 | 0.1 |
| PLA/PLA-*g*-ABS 20 wt% | 46.80 | 47.00 | 48.00 | 48.00 | 47.00 | 47.36 | 0.5 |
| PLA/PLA-*g*-ABS 30 wt% | 42.40 | 42.70 | 42.90 | 41.60 | 42.50 | 42.42 | 0.5 |

Table A-13 Elongation at brake (%) of PLA, PLA-ABS and PLA-PLA-*g*-ABS

| Sample | 1 | 2 | 3 | 4 | 5 | Average | SD |
|---|---|---|---|---|---|---|---|
| PLA | 4.00 | 4.00 | 4.20 | 4.00 | 4.10 | 4.06 | 0.1 |
| PLA/ABS 10 wt% | 3.20 | 3.10 | 3.00 | 3.00 | 3.50 | 3.16 | 0.1 |
| PLA/PLA-*g*-ABS 10 wt% | 4.20 | 4.10 | 4.30 | 4.00 | 4.40 | 4.20 | 0.1 |
| PLA/PLA-*g*-ABS 20 wt% | 75.00 | 75.00 | 75.00 | 75.00 | 74.00 | 74.80 | 0.4 |
| PLA/PLA-*g*-ABS 30 wt% | 53.00 | 53.00 | 52.00 | 52.00 | 52.00 | 52.40 | 0.5 |

Table A-14 Heat distortion (°C) of PLA, PLA-ABS and PLA-PLA-g-ABS

| Sample | 1 | 2 | 3 | 4 | 5 | Average | SD |
|---|---|---|---|---|---|---|---|
| PLA | 52.40 | 52.40 | 52.40 | 52.20 | 52.30 | 52.34 | 0.1 |
| PLA/ABS 10 wt% | 51.80 | 51.90 | 51.50 | 52.30 | 52.20 | 51.94 | 0.3 |
| PLA/PLA-*g*-ABS 10 wt% | 52.40 | 52.70 | 52.00 | 52.30 | 52.30 | 52.34 | 0.2 |
| PLA/PLA-*g*-ABS 20 wt% | 54.00 | 53.80 | 53.70 | 54.00 | 54.00 | 53.90 | 0.1 |
| PLA/PLA-*g*-ABS 30 wt% | 52.30 | 51.80 | 52.30 | 51.90 | 52.20 | 52.10 | 0.2 |

Table A- 15 Trial 1; Impact strengths (kg-cm/cm$^2$) of ABS/HDTMS-silica2 at various HDTMS-silica2 loadings

| Sample | 1 | 2 | 3 | 4 | 5 | Average | SD |
|---|---|---|---|---|---|---|---|
| ABS/HDTMS unmod 1.0 wt% | 23.00 | 23.10 | 23.00 | 23.20 | 23.00 | 23.06 | 0.08 |
| ABS/HDTMS-Silica2 0.5 wt% | 18.20 | 18.40 | 18.60 | 18.70 | 18.90 | 18.56 | 0.24 |
| ABS/HDTMS-Silica2 1.0 wt% | 23.70 | 23.90 | 24.50 | 24.20 | 24.00 | 24.06 | 0.27 |
| ABS/HDTMS-Silica2 2.0 wt% | 27.90 | 27.60 | 27.40 | 27.80 | 27.70 | 27.68 | 0.17 |
| ABS/HDTMS-Silica2 3.0 wt% | 29.50 | 29.30 | 30.10 | 30.30 | 29.50 | 29.74 | 0.39 |
| ABS/HDTMS-Silica2 4.0 wt% | 15.30 | 16.00 | 15.00 | 15.50 | 15.30 | 15.42 | 0.33 |
| ABS/HDTMS-Silica2 5.0 wt% | 8.20 | 8.50 | 8.10 | 8.30 | 8.30 | 8.28 | 0.13 |

Table A- 16 Trial 2; Impact strengths (kg-cm/cm$^2$) of ABS/HDTMS-silica2 at various HDTMS-silica2 loadings

| Sample | 1 | 2 | 3 | 4 | 5 | Average | SD |
|---|---|---|---|---|---|---|---|
| ABS/HDTMS unmod 1.0 wt% | 18.00 | 19.00 | 18.00 | 16.00 | 18.90 | 17.98 | 1.08 |
| ABS/HDTMS-Silica2 0.5 wt% | 23.70 | 24.00 | 23.00 | 23.00 | 23.80 | 23.50 | 0.42 |
| ABS/HDTMS-Silica2 1.0 wt% | 27.90 | 26.00 | 27.40 | 25.00 | 27.70 | 26.80 | 1.12 |
| ABS/HDTMS-Silica2 2.0 wt% | 29.50 | 30.00 | 31.00 | 30.30 | 30.00 | 30.16 | 0.49 |
| ABS/HDTMS-Silica2 3.0 wt% | 15.00 | 17.00 | 16.00 | 15.00 | 15.30 | 15.66 | 0.76 |
| ABS/HDTMS-Silica2 4.0 wt% | 7.90 | 8.50 | 8.00 | 8.30 | 8.00 | 8.14 | 0.22 |
| ABS/HDTMS-Silica2 5.0 wt% | 6.00 | 7.50 | 6.80 | 7.00 | 6.80 | 6.82 | 0.48 |

Table A- 17 Trial 3; Impact strengths (kg-cm/cm$^2$) of ABS/HDTMS-silica2 at various HDTMS-silica2 loadings

| Sample | 1 | 2 | 3 | 4 | 5 | Average | SD |
|---|---|---|---|---|---|---|---|
| ABS/HDTMS unmod 1.0 wt% | 18.20 | 18.00 | 18.60 | 18.70 | 17.00 | 18.10 | 0.61 |
| ABS/HDTMS-Silica2 0.5 wt% | 23.00 | 23.90 | 24.00 | 24.20 | 24.00 | 23.82 | 0.42 |
| ABS/HDTMS-Silica2 1.0 wt% | 27.90 | 27.60 | 26.00 | 27.80 | 28.00 | 27.46 | 0.74 |
| ABS/HDTMS-Silica2 2.0 wt% | 30.00 | 30.00 | 30.10 | 30.30 | 29.00 | 29.88 | 0.45 |
| ABS/HDTMS-Silica2 3.0 wt% | 15.30 | 17.00 | 15.00 | 16.00 | 15.30 | 15.72 | 0.72 |
| ABS/HDTMS-Silica2 4.0 wt% | 7.00 | 8.50 | 9.00 | 8.30 | 8.00 | 8.16 | 0.67 |
| ABS/HDTMS-Silica2 5.0 wt% | 6.80 | 6.00 | 6.80 | 8.00 | 6.80 | 6.88 | 0.64 |

Table A- 18 Trial 4; Impact strengths (kg-cm/cm$^2$) of ABS/HDTMS-silica2 at various HDTMS-silica2 loadings

| Sample | 1 | 2 | 3 | 4 | 5 | Average | SD |
|---|---|---|---|---|---|---|---|
| ABS/HDTMS unmod 1.0 wt% | 17.00 | 18.40 | 18.00 | 18.70 | 18.90 | 18.20 | 0.67 |
| ABS/HDTMS-Silica2 0.5 wt% | 23.70 | 23.90 | 24.00 | 24.20 | 25.00 | 24.16 | 0.45 |
| ABS/HDTMS-Silica2 1.0 wt% | 26.00 | 27.60 | 28.00 | 27.80 | 27.70 | 27.42 | 0.72 |
| ABS/HDTMS-Silica2 2.0 wt% | 30.10 | 30.00 | 30.10 | 30.30 | 29.00 | 29.90 | 0.46 |
| ABS/HDTMS-Silica2 3.0 wt% | 16.00 | 16.00 | 15.60 | 15.50 | 15.00 | 15.62 | 0.37 |
| ABS/HDTMS-Silica2 4.0 wt% | 7.90 | 8.50 | 7.80 | 8.30 | 8.00 | 8.10 | 0.26 |
| ABS/HDTMS-Silica2 5.0 wt% | 6.60 | 6.90 | 7.00 | 7.10 | 6.50 | 6.82 | 0.23 |

Table A- 19 Trial 5; Impact strengths (kg-cm/cm$^2$) of ABS/HDTMS-silica2 at various HDTMS-silica2 loadings

| Sample | 1 | 2 | 3 | 4 | 5 | Average | SD |
|---|---|---|---|---|---|---|---|
| ABS/HDTMS unmod 1.0 wt% | 17.00 | 18.40 | 16.00 | 18.70 | 17.00 | 17.42 | 1.00 |
| ABS/HDTMS-Silica2 0.5 wt% | 22.80 | 23.90 | 23.00 | 24.20 | 25.00 | 23.78 | 0.81 |
| ABS/HDTMS-Silica2 1.0 wt% | 26.90 | 27.60 | 28.00 | 27.80 | 28.50 | 27.76 | 0.52 |
| ABS/HDTMS-Silica2 2.0 wt% | 29.00 | 29.30 | 30.00 | 30.30 | 31.00 | 29.92 | 0.71 |
| ABS/HDTMS-Silica2 3.0 wt% | 15.00 | 16.00 | 14.90 | 15.50 | 16.00 | 15.48 | 0.47 |
| ABS/HDTMS-Silica2 4.0 wt% | 8.50 | 8.50 | 9.00 | 8.30 | 8.00 | 8.46 | 0.33 |
| ABS/HDTMS-Silica2 5.0 wt% | 6.60 | 7.50 | 7.00 | 7.10 | 7.10 | 7.06 | 0.29 |

Table A- 20 Trial 6; Impact strengths (kg-cm/cm$^2$) of ABS/HDTMS-silica2 at various HDTMS-silica2 loadings

| Sample | 1 | 2 | 3 | 4 | 5 | Average | SD |
|---|---|---|---|---|---|---|---|
| ABS/HDTMS unmod 1.0 wt% | 18.20 | 18.00 | 17.00 | 17.90 | 18.00 | 17.82 | 0.42 |
| ABS/HDTMS-Silica2 0.5 wt% | 22.00 | 23.00 | 25.00 | 24.20 | 25.30 | 23.90 | 1.24 |
| ABS/HDTMS-Silica2 1.0 wt% | 27.80 | 28.00 | 27.40 | 27.90 | 26.80 | 27.58 | 0.44 |
| ABS/HDTMS-Silica2 2.0 wt% | 31.20 | 31.80 | 29.00 | 29.50 | 30.00 | 30.30 | 1.05 |
| ABS/HDTMS-Silica2 3.0 wt% | 14.90 | 16.00 | 16.20 | 15.50 | 14.90 | 15.50 | 0.54 |
| ABS/HDTMS-Silica2 4.0 wt% | 7.80 | 8.00 | 8.10 | 7.90 | 8.00 | 7.96 | 0.10 |
| ABS/HDTMS-Silica2 5.0 wt% | 7.20 | 6.80 | 6.80 | 7.00 | 6.80 | 6.92 | 0.16 |

Table A- 21 Trial 7; Impact strengths (kg-cm/cm$^2$) of ABS/HDTMS-silica2 at various HDTMS-silica2 loadings

| Sample | 1 | 2 | 3 | 4 | 5 | Average | SD |
|---|---|---|---|---|---|---|---|
| ABS/HDTMS unmod 1.0 wt% | 17.00 | 18.40 | 18.00 | 18.70 | 18.90 | 18.20 | 0.67 |
| ABS/HDTMS-Silica2 0.5 wt% | 24.50 | 23.90 | 24.50 | 23.00 | 24.00 | 23.98 | 0.55 |
| ABS/HDTMS-Silica2 1.0 wt% | 28.00 | 27.00 | 27.40 | 28.70 | 27.70 | 27.76 | 0.57 |
| ABS/HDTMS-Silica2 2.0 wt% | 30.10 | 29.30 | 29.90 | 30.30 | 29.50 | 29.82 | 0.37 |
| ABS/HDTMS-Silica2 3.0 wt% | 14.90 | 16.00 | 16.30 | 15.00 | 15.30 | 15.50 | 0.55 |
| ABS/HDTMS-Silica2 4.0 wt% | 7.90 | 8.00 | 8.10 | 7.90 | 8.30 | 8.04 | 0.15 |
| ABS/HDTMS-Silica2 5.0 wt% | 7.00 | 6.90 | 6.80 | 7.00 | 6.80 | 6.90 | 0.09 |

Table A- 22 Trial 8; Impact strengths (kg-cm/cm$^2$) of ABS/HDTMS-silica2 at various HDTMS-silica2 loadings

| Sample | 1 | 2 | 3 | 4 | 5 | Average | SD |
|---|---|---|---|---|---|---|---|
| ABS/HDTMS unmod 1.0 wt% | 18.20 | 18.40 | 17.00 | 18.70 | 18.00 | 18.06 | 0.58 |
| ABS/HDTMS-Silica2 0.5 wt% | 22.90 | 22.00 | 24.50 | 24.00 | 24.00 | 23.48 | 0.91 |
| ABS/HDTMS-Silica2 1.0 wt% | 27.00 | 27.60 | 26.90 | 27.80 | 27.70 | 27.40 | 0.37 |
| ABS/HDTMS-Silica2 2.0 wt% | 29.90 | 29.30 | 30.00 | 30.30 | 29.50 | 29.80 | 0.36 |
| ABS/HDTMS-Silica2 3.0 wt% | 15.00 | 16.00 | 16.80 | 15.50 | 15.30 | 15.72 | 0.63 |
| ABS/HDTMS-Silica2 4.0 wt% | 8.10 | 8.50 | 8.00 | 8.30 | 8.20 | 8.22 | 0.17 |
| ABS/HDTMS-Silica2 5.0 wt% | 6.50 | 7.00 | 7.00 | 7.00 | 6.80 | 6.86 | 0.20 |

Table A- 23 Trial 9; Impact strengths (kg-cm/cm$^2$) of ABS/HDTMS-silica2 at various HDTMS-silica2 loadings

| Sample | 1 | 2 | 3 | 4 | 5 | Average | SD |
|---|---|---|---|---|---|---|---|
| ABS/HDTMS unmod 1.0 wt% | 17.50 | 18.40 | 17.00 | 18.70 | 18.90 | 18.10 | 0.73 |
| ABS/HDTMS-Silica2 0.5 wt% | 23.00 | 24.00 | 24.50 | 23.90 | 24.00 | 23.88 | 0.49 |
| ABS/HDTMS-Silica2 1.0 wt% | 28.50 | 27.30 | 27.40 | 28.00 | 27.70 | 27.78 | 0.44 |
| ABS/HDTMS-Silica2 2.0 wt% | 29.90 | 29.30 | 31.00 | 30.30 | 29.90 | 30.08 | 0.56 |
| ABS/HDTMS-Silica2 3.0 wt% | 16.20 | 16.50 | 15.00 | 15.60 | 15.30 | 15.72 | 0.56 |
| ABS/HDTMS-Silica2 4.0 wt% | 8.70 | 8.50 | 8.00 | 8.20 | 8.30 | 8.34 | 0.24 |
| ABS/HDTMS-Silica2 5.0 wt% | 7.10 | 8.00 | 6.80 | 7.30 | 6.80 | 7.20 | 0.44 |

Table A- 24 Trial 10; Impact strengths (kg-cm/cm$^2$) of ABS/HDTMS-silica2 at various HDTMS-silica2 loadings

| Sample | 1 | 2 | 3 | 4 | 5 | Average | SD |
|---|---|---|---|---|---|---|---|
| ABS/HDTMS unmod 1.0 wt% | 17.90 | 18.60 | 18.60 | 18.00 | 18.70 | 18.36 | 0.34 |
| ABS/HDTMS-Silica2 0.5 wt% | 23.90 | 23.90 | 25.00 | 24.20 | 24.40 | 24.28 | 0.41 |
| ABS/HDTMS-Silica2 1.0 wt% | 28.00 | 27.60 | 28.80 | 27.80 | 27.70 | 27.98 | 0.43 |
| ABS/HDTMS-Silica2 2.0 wt% | 30.10 | 29.30 | 30.10 | 30.00 | 29.50 | 29.80 | 0.33 |
| ABS/HDTMS-Silica2 3.0 wt% | 16.00 | 17.10 | 15.00 | 15.00 | 15.30 | 15.68 | 0.80 |
| ABS/HDTMS-Silica2 4.0 wt% | 8.00 | 8.50 | 8.30 | 8.30 | 8.00 | 8.22 | 0.19 |
| ABS/HDTMS-Silica2 5.0 wt% | 9.00 | 7.00 | 6.10 | 7.10 | 6.00 | 7.04 | 1.08 |

Table A- 25 Trial 11; Impact strengths (kg-cm/cm$^2$) of ABS/HDTMS-silica2 at various HDTMS-silica2 loadings

| Sample | 1 | 2 | 3 | 4 | 5 | Average | SD |
|---|---|---|---|---|---|---|---|
| ABS/HDTMS unmod 1.0 wt% | 18.00 | 18.40 | 17.90 | 18.70 | 18.00 | 18.20 | 0.30 |
| ABS/HDTMS-Silica2 0.5 wt% | 23.30 | 23.90 | 24.00 | 24.20 | 24.50 | 23.98 | 0.40 |
| ABS/HDTMS-Silica2 1.0 wt% | 28.00 | 27.00 | 27.40 | 28.00 | 27.70 | 27.62 | 0.38 |
| ABS/HDTMS-Silica2 2.0 wt% | 29.50 | 30.00 | 30.10 | 30.00 | 29.50 | 29.82 | 0.26 |
| ABS/HDTMS-Silica2 3.0 wt% | 16.00 | 16.00 | 16.00 | 15.50 | 14.90 | 15.68 | 0.44 |
| ABS/HDTMS-Silica2 4.0 wt% | 8.30 | 8.50 | 8.10 | 8.30 | 8.30 | 8.30 | 0.13 |
| ABS/HDTMS-Silica2 5.0 wt% | 7.00 | 7.00 | 7.50 | 7.10 | 6.80 | 7.08 | 0.23 |

Table A- 26 Trial 12; Impact strengths (kg-cm/cm$^2$) of ABS/HDTMS-silica2 at various HDTMS-silica2 loadings

| Sample | 1 | 2 | 3 | 4 | 5 | Average | SD |
|---|---|---|---|---|---|---|---|
| ABS/HDTMS unmod 1.0 wt% | 18.00 | 17.90 | 18.60 | 18.00 | 18.90 | 18.28 | 0.40 |
| ABS/HDTMS-Silica2 0.5 wt% | 24.20 | 23.00 | 24.50 | 23.50 | 24.00 | 23.84 | 0.53 |
| ABS/HDTMS-Silica2 1.0 wt% | 28.00 | 26.50 | 27.40 | 28.00 | 27.70 | 27.52 | 0.56 |
| ABS/HDTMS-Silica2 2.0 wt% | 30.20 | 28.00 | 30.10 | 31.00 | 29.50 | 29.76 | 1.00 |
| ABS/HDTMS-Silica2 3.0 wt% | 14.00 | 16.50 | 15.00 | 16.00 | 15.30 | 15.36 | 0.86 |
| ABS/HDTMS-Silica2 4.0 wt% | 7.90 | 8.50 | 8.00 | 8.30 | 8.20 | 8.18 | 0.21 |
| ABS/HDTMS-Silica2 5.0 wt% | 6.30 | 7.10 | 6.80 | 7.00 | 6.80 | 6.80 | 0.28 |

Table A- 27 Trial 13; Impact strengths (kg-cm/cm$^2$) of ABS/HDTMS-silica2 at various HDTMS-silica2 loadings

| Sample | 1 | 2 | 3 | 4 | 5 | Average | SD |
|---|---|---|---|---|---|---|---|
| ABS/HDTMS unmod 1.0 wt% | 17.50 | 17.00 | 18.60 | 18.90 | 18.90 | 18.18 | 0.78 |
| ABS/HDTMS-Silica2 0.5 wt% | 22.90 | 23.90 | 24.00 | 24.30 | 24.00 | 23.82 | 0.48 |
| ABS/HDTMS-Silica2 1.0 wt% | 28.10 | 27.00 | 27.40 | 28.00 | 27.70 | 27.64 | 0.40 |
| ABS/HDTMS-Silica2 2.0 wt% | 29.90 | 29.30 | 31.20 | 30.30 | 29.50 | 30.04 | 0.67 |
| ABS/HDTMS-Silica2 3.0 wt% | 16.30 | 17.20 | 15.00 | 15.90 | 15.30 | 15.94 | 0.78 |
| ABS/HDTMS-Silica2 4.0 wt% | 8.30 | 8.00 | 8.10 | 8.40 | 8.30 | 8.22 | 0.15 |
| ABS/HDTMS-Silica2 5.0 wt% | 6.90 | 7.10 | 6.80 | 7.00 | 6.80 | 6.92 | 0.12 |

Table A- 28 Trial 14; Impact strengths (kg-cm/cm$^2$) of ABS/HDTMS-silica2 at various HDTMS-silica2 loadings

| Sample | 1 | 2 | 3 | 4 | 5 | Average | SD |
|---|---|---|---|---|---|---|---|
| ABS/HDTMS unmod 1.0 wt% | 18.00 | 18.40 | 17.00 | 18.70 | 18.90 | 18.20 | 0.67 |
| ABS/HDTMS-Silica2 0.5 wt% | 23.10 | 23.00 | 24.00 | 24.20 | 24.30 | 23.72 | 0.56 |
| ABS/HDTMS-Silica2 1.0 wt% | 28.00 | 27.30 | 27.40 | 28.00 | 27.70 | 27.68 | 0.29 |
| ABS/HDTMS-Silica2 2.0 wt% | 29.20 | 29.30 | 31.00 | 30.30 | 30.00 | 29.96 | 0.67 |
| ABS/HDTMS-Silica2 3.0 wt% | 15.20 | 16.00 | 15.90 | 15.50 | 15.30 | 15.58 | 0.32 |
| ABS/HDTMS-Silica2 4.0 wt% | 8.00 | 8.00 | 8.90 | 8.30 | 8.30 | 8.30 | 0.33 |
| ABS/HDTMS-Silica2 5.0 wt% | 7.00 | 7.20 | 6.80 | 8.00 | 6.80 | 7.16 | 0.45 |

Table A- 29 Trial 15; Impact strengths (kg-cm/cm$^2$) of ABS/HDTMS-silica2 at various HDTMS-silica2 loadings

| Sample | 1 | 2 | 3 | 4 | 5 | Average | SD |
|---|---|---|---|---|---|---|---|
| ABS/HDTMS unmod 1.0 wt% | 18.10 | 18.00 | 17.90 | 18.70 | 18.00 | 18.14 | 0.29 |
| ABS/HDTMS-Silica2 0.5 wt% | 22.90 | 23.00 | 23.90 | 24.20 | 25.10 | 23.82 | 0.81 |
| ABS/HDTMS-Silica2 1.0 wt% | 26.80 | 27.60 | 28.00 | 27.80 | 27.90 | 27.62 | 0.43 |
| ABS/HDTMS-Silica2 2.0 wt% | 29.30 | 30.00 | 30.10 | 30.30 | 29.50 | 29.84 | 0.38 |
| ABS/HDTMS-Silica2 3.0 wt% | 15.00 | 16.30 | 16.10 | 15.50 | 15.00 | 15.58 | 0.54 |
| ABS/HDTMS-Silica2 4.0 wt% | 7.90 | 8.50 | 8.00 | 8.30 | 7.80 | 8.10 | 0.26 |
| ABS/HDTMS-Silica2 5.0 wt% | 6.90 | 7.00 | 7.00 | 7.10 | 7.30 | 7.06 | 0.14 |

Table A- 30 Trial 16; Impact strengths (kg-cm/cm$^2$) of ABS/HDTMS-silica2 at various HDTMS-silica2 loadings

| Sample | 1 | 2 | 3 | 4 | 5 | Average | SD |
|---|---|---|---|---|---|---|---|
| ABS/HDTMS unmod 1.0 wt% | 17.90 | 18.50 | 18.60 | 18.00 | 18.90 | 18.38 | 0.38 |
| ABS/HDTMS-Silica2 0.5 wt% | 24.30 | 23.00 | 24.50 | 23.90 | 24.00 | 23.94 | 0.52 |
| ABS/HDTMS-Silica2 1.0 wt% | 28.20 | 27.00 | 27.40 | 28.00 | 27.70 | 27.66 | 0.43 |
| ABS/HDTMS-Silica2 2.0 wt% | 28.00 | 30.20 | 30.00 | 30.30 | 30.10 | 29.72 | 0.87 |
| ABS/HDTMS-Silica2 3.0 wt% | 16.10 | 15.80 | 15.00 | 14.50 | 15.30 | 15.34 | 0.57 |
| ABS/HDTMS-Silica2 4.0 wt% | 8.90 | 8.50 | 7.90 | 8.30 | 8.00 | 8.32 | 0.36 |
| ABS/HDTMS-Silica2 5.0 wt% | 6.50 | 7.00 | 7.00 | 7.20 | 6.80 | 6.90 | 0.24 |

Table A- 31 Trial 17; Impact strengths (kg-cm/cm$^2$) of ABS/HDTMS-silica2 at various HDTMS-silica2 loadings

| Sample | 1 | 2 | 3 | 4 | 5 | Average | SD |
|---|---|---|---|---|---|---|---|
| ABS/HDTMS unmod 1.0 wt% | 17.50 | 18.20 | 18.00 | 17.50 | 18.00 | 17.84 | 0.29 |
| ABS/HDTMS-Silica2 0.5 wt% | 23.20 | 24.00 | 25.10 | 24.00 | 24.10 | 24.08 | 0.60 |
| ABS/HDTMS-Silica2 1.0 wt% | 28.10 | 27.00 | 26.90 | 27.00 | 27.70 | 27.34 | 0.48 |
| ABS/HDTMS-Silica2 2.0 wt% | 29.20 | 28.50 | 30.00 | 32.10 | 31.00 | 30.16 | 1.28 |
| ABS/HDTMS-Silica2 3.0 wt% | 16.20 | 15.60 | 16.10 | 15.50 | 15.00 | 15.68 | 0.44 |
| ABS/HDTMS-Silica2 4.0 wt% | 7.50 | 8.20 | 8.90 | 8.00 | 8.10 | 8.14 | 0.45 |
| ABS/HDTMS-Silica2 5.0 wt% | 6.30 | 6.60 | 6.50 | 7.00 | 7.30 | 6.74 | 0.36 |

Table A- 32 Trial 18; Impact strengths (kg-cm/cm$^2$) of ABS/HDTMS-silica2 at various HDTMS-silica2 loadings

| Sample | 1 | 2 | 3 | 4 | 5 | Average | SD |
|---|---|---|---|---|---|---|---|
| ABS/HDTMS unmod 1.0 wt% | 17.30 | 18.90 | 18.00 | 18.70 | 19.00 | 18.38 | 0.64 |
| ABS/HDTMS-Silica2 0.5 wt% | 24.00 | 23.20 | 25.00 | 24.00 | 24.10 | 24.06 | 0.57 |
| ABS/HDTMS-Silica2 1.0 wt% | 27.10 | 28.00 | 27.80 | 28.00 | 27.50 | 27.68 | 0.34 |
| ABS/HDTMS-Silica2 2.0 wt% | 29.30 | 28.90 | 31.20 | 31.10 | 30.00 | 30.10 | 0.93 |
| ABS/HDTMS-Silica2 3.0 wt% | 16.10 | 15.20 | 15.00 | 16.30 | 15.40 | 15.60 | 0.51 |
| ABS/HDTMS-Silica2 4.0 wt% | 7.80 | 8.90 | 8.00 | 7.90 | 8.00 | 8.12 | 0.40 |
| ABS/HDTMS-Silica2 5.0 wt% | 6.30 | 7.20 | 7.00 | 7.30 | 6.90 | 6.94 | 0.35 |

Table A- 33 Trial 19; Impact strengths (kg-cm/cm$^2$) of ABS/HDTMS-silica2 at various HDTMS-silica2 loadings

| Sample | 1 | 2 | 3 | 4 | 5 | Average | SD |
|---|---|---|---|---|---|---|---|
| ABS/HDTMS unmod 1.0 wt% | 16.50 | 18.00 | 17.90 | 18.00 | 18.30 | 17.74 | 0.63 |
| ABS/HDTMS-Silica2 0.5 wt% | 24.10 | 23.40 | 23.90 | 24.00 | 24.30 | 23.94 | 0.30 |
| ABS/HDTMS-Silica2 1.0 wt% | 27.50 | 27.00 | 26.90 | 27.20 | 26.90 | 27.10 | 0.23 |
| ABS/HDTMS-Silica2 2.0 wt% | 28.00 | 31.20 | 30.90 | 31.10 | 29.00 | 30.04 | 1.30 |
| ABS/HDTMS-Silica2 3.0 wt% | 15.20 | 17.00 | 16.30 | 15.40 | 15.00 | 15.78 | 0.75 |
| ABS/HDTMS-Silica2 4.0 wt% | 8.00 | 8.30 | 8.20 | 7.90 | 8.00 | 8.08 | 0.15 |
| ABS/HDTMS-Silica2 5.0 wt% | 6.00 | 7.10 | 6.20 | 7.90 | 6.30 | 6.70 | 0.71 |

Table A- 34 Trial 20; Impact strengths (kg-cm/cm$^2$) of ABS/HDTMS-silica2 at various HDTMS-silica2 loadings

| Sample | 1 | 2 | 3 | 4 | 5 | Average | SD |
|---|---|---|---|---|---|---|---|
| ABS/HDTMS unmod 1.0 wt% | 17.20 | 18.30 | 17.90 | 18.00 | 17.80 | 17.84 | 0.36 |
| ABS/HDTMS-Silica2 0.5 wt% | 23.00 | 23.10 | 25.00 | 24.10 | 23.00 | 23.64 | 0.80 |
| ABS/HDTMS-Silica2 1.0 wt% | 26.90 | 28.00 | 27.10 | 27.30 | 26.00 | 27.06 | 0.65 |
| ABS/HDTMS-Silica2 2.0 wt% | 30.10 | 31.20 | 31.00 | 29.80 | 29.00 | 30.22 | 0.81 |
| ABS/HDTMS-Silica2 3.0 wt% | 14.80 | 16.90 | 15.20 | 15.30 | 14.90 | 15.42 | 0.76 |
| ABS/HDTMS-Silica2 4.0 wt% | 8.00 | 7.50 | 8.20 | 8.50 | 9.00 | 8.24 | 0.50 |
| ABS/HDTMS-Silica2 5.0 wt% | 6.30 | 7.10 | 6.50 | 7.00 | 7.30 | 6.84 | 0.38 |

*Table A- 35 Trial 1;* Impact strengths (kg-cm/cm$^2$) of ABS/HDTMS-$SiO_2$ at various HDTMS-$SiO_2$ loadings

| Sample | 1 | 2 | 3 | 4 | 5 | Average | SD |
|---|---|---|---|---|---|---|---|
| ABS/HDTMS-$SiO_2$ 0.5 wt% | 29.00 | 28.00 | 29.10 | 28.00 | 28.10 | 28.44 | 0.50 |
| ABS/HDTMS-$SiO_2$ 1.0 wt% | 32.80 | 32.60 | 31.00 | 32.10 | 33.00 | 32.30 | 0.72 |
| ABS/HDTMS-$SiO_2$ 2.0 wt% | 29.00 | 29.90 | 30.00 | 31.10 | 31.00 | 30.20 | 0.78 |
| ABS/HDTMS-$SiO_2$ 3.0 wt% | 15.10 | 14.00 | 13.90 | 14.00 | 14.50 | 14.30 | 0.45 |
| ABS/HDTMS-$SiO_2$ 4.0 wt% | 13.50 | 14.00 | 15.10 | 16.00 | 15.20 | 14.76 | 0.90 |
| ABS/HDTMS-$SiO_2$ 5.0 wt% | 6.80 | 6.30 | 6.00 | 6.20 | 7.00 | 6.46 | 0.38 |

Table A- 36 Trial 2; Impact strengths (kg-cm/cm$^2$) of ABS/HDTMS-$SiO_2$ at various HDTMS-$SiO_2$ loadings

| Sample | 1 | 2 | 3 | 4 | 5 | Average | SD |
|---|---|---|---|---|---|---|---|
| ABS/HDTMS-$SiO_2$ 0.5 wt% | 28.00 | 27.50 | 26.90 | 28.90 | 29.10 | 28.08 | 0.83 |
| ABS/HDTMS-$SiO_2$ 1.0 wt% | 31.80 | 33.10 | 32.90 | 31.20 | 33.00 | 32.40 | 0.76 |
| ABS/HDTMS-$SiO_2$ 2.0 wt% | 29.50 | 29.20 | 31.00 | 31.20 | 29.50 | 30.08 | 0.84 |
| ABS/HDTMS-$SiO_2$ 3.0 wt% | 14.00 | 15.90 | 13.20 | 13.20 | 14.00 | 14.06 | 0.99 |
| ABS/HDTMS-$SiO_2$ 4.0 wt% | 13.40 | 14.20 | 14.00 | 15.60 | 16.10 | 14.66 | 1.02 |
| ABS/HDTMS-$SiO_2$ 5.0 wt% | 6.30 | 7.00 | 6.90 | 6.50 | 7.10 | 6.76 | 0.31 |

Table A- 37 Trial 3; Impact strengths (kg-cm/cm$^2$) of ABS/HDTMS-$SiO_2$ at various HDTMS-$SiO_2$ loadings

| Sample | 1 | 2 | 3 | 4 | 5 | Average | SD |
|---|---|---|---|---|---|---|---|
| ABS/HDTMS-$SiO_2$ 0.5 wt% | 26.30 | 27.00 | 26.20 | 27.50 | 28.00 | 27.00 | 0.69 |
| ABS/HDTMS-$SiO_2$ 1.0 wt% | 32.40 | 32.00 | 31.90 | 31.00 | 33.50 | 32.16 | 0.81 |
| ABS/HDTMS-$SiO_2$ 2.0 wt% | 29.00 | 29.80 | 30.00 | 28.90 | 29.00 | 29.34 | 0.46 |
| ABS/HDTMS-$SiO_2$ 3.0 wt% | 14.30 | 15.20 | 13.90 | 15.00 | 14.20 | 14.52 | 0.50 |
| ABS/HDTMS-$SiO_2$ 4.0 wt% | 13.20 | 14.00 | 15.20 | 13.90 | 14.00 | 14.06 | 0.64 |
| ABS/HDTMS-$SiO_2$ 5.0 wt% | 7.20 | 6.90 | 6.00 | 7.10 | 7.00 | 6.84 | 0.43 |

Table A- 38 Trial 4; Impact strengths (kg-cm/cm$^2$) of ABS/HDTMS-$SiO_2$ at various HDTMS-$SiO_2$ loadings

| Sample | 1 | 2 | 3 | 4 | 5 | Average | SD |
|---|---|---|---|---|---|---|---|
| ABS/HDTMS-$SiO_2$ 0.5 wt% | 27.90 | 27.50 | 25.00 | 27.30 | 28.00 | 27.14 | 1.10 |
| ABS/HDTMS-$SiO_2$ 1.0 wt% | 32.00 | 32.90 | 32.10 | 32.00 | 32.90 | 32.38 | 0.43 |
| ABS/HDTMS-$SiO_2$ 2.0 wt% | 28.00 | 28.90 | 29.90 | 30.00 | 28.90 | 29.14 | 0.74 |
| ABS/HDTMS-$SiO_2$ 3.0 wt% | 15.20 | 16.00 | 14.80 | 14.20 | 14.10 | 14.86 | 0.70 |
| ABS/HDTMS-$SiO_2$ 4.0 wt% | 13.90 | 13.80 | 14.10 | 14.00 | 15.70 | 14.30 | 0.71 |
| ABS/HDTMS-$SiO_2$ 5.0 wt% | 7.00 | 6.30 | 6.50 | 6.30 | 7.00 | 6.62 | 0.32 |

Table A- 39 Trial 5; Impact strengths (kg-cm/cm$^2$) of ABS/HDTMS-$SiO_2$ at various HDTMS-$SiO_2$ loadings

| Sample | 1 | 2 | 3 | 4 | 5 | Average | SD |
|---|---|---|---|---|---|---|---|
| ABS/HDTMS-$SiO_2$ 0.5 wt% | 28.10 | 27.00 | 28.30 | 28.00 | 28.90 | 28.06 | 0.62 |
| ABS/HDTMS-$SiO_2$ 1.0 wt% | 32.10 | 33.20 | 32.10 | 32.00 | 32.90 | 32.46 | 0.49 |
| ABS/HDTMS-$SiO_2$ 2.0 wt% | 29.90 | 28.50 | 31.20 | 30.00 | 29.80 | 29.88 | 0.86 |
| ABS/HDTMS-$SiO_2$ 3.0 wt% | 14.50 | 14.80 | 14.30 | 14.60 | 14.20 | 14.48 | 0.21 |
| ABS/HDTMS-$SiO_2$ 4.0 wt% | 13.00 | 13.70 | 14.20 | 15.00 | 13.20 | 13.82 | 0.72 |
| ABS/HDTMS-$SiO_2$ 5.0 wt% | 6.00 | 6.30 | 6.50 | 6.20 | 6.10 | 6.22 | 0.17 |

Table A- 40 Trial 6; Impact strengths (kg-cm/cm$^2$) of ABS/HDTMS-$SiO_2$ at various HDTMS-$SiO_2$ loadings

| Sample | 1 | 2 | 3 | 4 | 5 | Average | SD |
|---|---|---|---|---|---|---|---|
| ABS/HDTMS-$SiO_2$ 0.5 wt% | 27.50 | 27.00 | 27.30 | 28.00 | 29.00 | 27.76 | 0.70 |
| ABS/HDTMS-$SiO_2$ 1.0 wt% | 32.90 | 33.50 | 33.70 | 33.10 | 33.20 | 33.28 | 0.29 |
| ABS/HDTMS-$SiO_2$ 2.0 wt% | 29.80 | 29.00 | 30.50 | 30.20 | 29.80 | 29.86 | 0.50 |
| ABS/HDTMS-$SiO_2$ 3.0 wt% | 14.10 | 14.80 | 14.20 | 14.50 | 14.20 | 14.36 | 0.26 |
| ABS/HDTMS-$SiO_2$ 4.0 wt% | 13.00 | 13.90 | 14.20 | 14.10 | 14.00 | 13.84 | 0.43 |
| ABS/HDTMS-$SiO_2$ 5.0 wt% | 6.90 | 6.30 | 6.20 | 6.60 | 7.00 | 6.60 | 0.32 |

Table A- 41 Trial 7; Impact strengths (kg-cm/cm$^2$) of ABS/HDTMS-$SiO_2$ at various HDTMS-$SiO_2$ loadings

| Sample | 1 | 2 | 3 | 4 | 5 | Average | SD |
|---|---|---|---|---|---|---|---|
| ABS/HDTMS-$SiO_2$ 0.5 wt% | 28.30 | 27.00 | 27.50 | 28.00 | 29.30 | 28.02 | 0.78 |
| ABS/HDTMS-$SiO_2$ 1.0 wt% | 33.00 | 33.50 | 32.90 | 33.00 | 33.10 | 33.10 | 0.21 |
| ABS/HDTMS-$SiO_2$ 2.0 wt% | 29.00 | 29.70 | 29.50 | 31.50 | 29.80 | 29.90 | 0.85 |
| ABS/HDTMS-$SiO_2$ 3.0 wt% | 14.30 | 14.90 | 14.20 | 14.60 | 14.30 | 14.46 | 0.26 |
| ABS/HDTMS-$SiO_2$ 4.0 wt% | 14.00 | 13.80 | 13.50 | 14.50 | 14.90 | 14.14 | 0.50 |
| ABS/HDTMS-$SiO_2$ 5.0 wt% | 7.10 | 6.30 | 6.70 | 6.90 | 7.00 | 6.80 | 0.28 |

Table A- 42 Trial 8; Impact strengths (kg-cm/cm$^2$) of ABS/HDTMS-$SiO_2$ at various HDTMS-$SiO_2$ loadings

| Sample | 1 | 2 | 3 | 4 | 5 | Average | SD |
|---|---|---|---|---|---|---|---|
| ABS/HDTMS-$SiO_2$ 0.5 wt% | 28.30 | 28.00 | 26.80 | 28.90 | 28.70 | 28.14 | 0.74 |
| ABS/HDTMS-$SiO_2$ 1.0 wt% | 33.60 | 32.80 | 33.10 | 33.00 | 33.20 | 33.14 | 0.27 |
| ABS/HDTMS-$SiO_2$ 2.0 wt% | 29.10 | 29.30 | 29.70 | 30.50 | 29.00 | 29.52 | 0.55 |
| ABS/HDTMS-$SiO_2$ 3.0 wt% | 13.00 | 13.90 | 15.20 | 14.30 | 14.60 | 14.20 | 0.73 |
| ABS/HDTMS-$SiO_2$ 4.0 wt% | 13.20 | 13.60 | 14.00 | 13.90 | 14.10 | 13.76 | 0.33 |
| ABS/HDTMS-$SiO_2$ 5.0 wt% | 6.90 | 7.00 | 6.30 | 7.10 | 7.20 | 6.90 | 0.32 |

Table A- 43 Trial 9; Impact strengths (kg-cm/cm$^2$) of ABS/HDTMS-$SiO_2$ at various HDTMS-$SiO_2$ loadings

| Sample | 1 | 2 | 3 | 4 | 5 | Average | SD |
|---|---|---|---|---|---|---|---|
| ABS/HDTMS-$SiO_2$ 0.5 wt% | 27.80 | 27.00 | 27.50 | 27.10 | 28.00 | 27.48 | 0.39 |
| ABS/HDTMS-$SiO_2$ 1.0 wt% | 32.00 | 33.50 | 32.80 | 32.00 | 33.50 | 32.76 | 0.67 |
| ABS/HDTMS-$SiO_2$ 2.0 wt% | 30.00 | 28.70 | 29.90 | 31.00 | 31.10 | 30.14 | 0.87 |
| ABS/HDTMS-$SiO_2$ 3.0 wt% | 15.10 | 14.50 | 13.90 | 14.10 | 14.20 | 14.36 | 0.42 |
| ABS/HDTMS-$SiO_2$ 4.0 wt% | 14.20 | 13.60 | 13.00 | 13.50 | 14.80 | 13.82 | 0.62 |
| ABS/HDTMS-$SiO_2$ 5.0 wt% | 6.00 | 6.30 | 7.50 | 7.20 | 6.30 | 6.66 | 0.58 |

Table A- 44 Trial 10; Impact strengths (kg-cm/cm$^2$) of ABS/HDTMS-$SiO_2$ at various HDTMS-$SiO_2$ loadings

| Sample | 1 | 2 | 3 | 4 | 5 | Average | SD |
|---|---|---|---|---|---|---|---|
| ABS/HDTMS-$SiO_2$ 0.5 wt% | 28.10 | 28.20 | 27.90 | 28.00 | 28.30 | 28.10 | 0.14 |
| ABS/HDTMS-$SiO_2$ 1.0 wt% | 32.80 | 32.40 | 33.10 | 33.00 | 33.50 | 32.96 | 0.36 |
| ABS/HDTMS-$SiO_2$ 2.0 wt% | 29.00 | 29.90 | 30.10 | 32.00 | 30.90 | 30.38 | 1.01 |
| ABS/HDTMS-$SiO_2$ 3.0 wt% | 13.80 | 14.90 | 14.50 | 13.00 | 13.80 | 14.00 | 0.65 |
| ABS/HDTMS-$SiO_2$ 4.0 wt% | 13.00 | 13.50 | 13.10 | 13.80 | 14.00 | 13.48 | 0.39 |
| ABS/HDTMS-$SiO_2$ 5.0 wt% | 6.50 | 7.00 | 6.90 | 7.00 | 7.30 | 6.94 | 0.26 |

# VITA

Mr. Charungkit Chaikeaw was born on March 28, 1972 in Chiang Mai, Thailand. He graduated with Bachelor's Degree of Science (Chemistry) from Ramkamhaeng University in 1996. Since, he has joined the Production of ABS plant and continued to join R&D Department, IRPC Public Company Limited. He was accepted as a graduate student in the M.Sc. course in Petrochemistry and Polymer Science Program, Faculty of Science, Chulalongkorn University. He received a Master's degree of Science in Polymer Science, in April 2011. During working in IRPC, he decided to study in Doctoral degree program in Materials Science, department of Materials Science, Faculty of Science, Chulalongkorn University in 2012 and graduated in 2017.

Presentations:

1. 2010 : Poster Presentation "Reactive Melt Grafting of High-Density Polyethylene-g-Maleic Anhydride Compatibilizer by Twin Screw Extruder" 1st Polymer Conference of Thailand at the Convention Center, Chulabhorn Research Institute, Bangkok, Thailand.

Publications:

1. Chaikeaw, C. and Srikulkit, K., In situ synthesis of ABS containing hydrophobic silica nanoparticles and their effects on mechanical properties. Journal of Sol-Gel Science and Technology (2017) 81:774–781.

2. Chaikeaw, C. and Srikulkit, K., Preparation and Properties of Poly(lactic Acid)/PLA-g-ABS Blends. Fibers and Polymers, 2018 (In press).

Work Experience:

1997-2010 : Boardman operation control, ABS plant, IRPC Public Company Limited, Thailand.

2010-present : Researcher, R&D department, IRPC Public Company Limited, Thailand.